

**Spectroscopic characterization of Dy³⁺ ions doped
phosphate glasses for epoxy-free white LED applications**

A thesis submitted in partial fulfillment of the requirements for the award of the degree of

Master of Science

In

Physics

By

Ankita

(2K20/MSCPHY/04)

&

Vidhi

(2K20/MSCPHY/33)

Under the supervision of

Prof. A.S. Rao

Department of Applied Physics



Delhi Technological University

(Formerly Delhi College of Engineering)

Bawana Road, Delhi-110042

May-2022

DECLARATION

We/I hereby certify that the work which is presented in the Major Project-II/Research Work entitled Spectroscopic characterization of Dy³⁺ ions doped phosphate glasses for epoxy-free white LED applications in fulfilment of the requirement for the award of the Degree of Bachelor/Master of Technology in Physics and submitted to the Department of Applied Physics, Delhi Technological University, Delhi is an authentic record of my/our own, carried out during a period from Aug 2021-May 2022 under the supervision of Prof. A.S. Rao.

The matter presented in this report/thesis has not been submitted by us/me for the award of any other degree of this or any other Institute/University. The work has been published/accepted/communicated in SCI/SCI expanded/SSCI/Scopus indexed journal OR peer reviewed Scopus indexed conference with the following details:

Title of the Paper: Spectroscopic characterization of Dy³⁺ ions doped phosphate glasses for epoxy-free white LED applications

Author names (in sequence as per research paper): Vidhi Kundu, Ankita Wadhwa, A.S. Rao

Name of Conference/Journal: ICAPIE '22

Conference Dates with venue (if applicable): 11-12 June 2022

Have you registered for the conference (Yes/No)? YES

Status of paper (Accepted/Published/Communicated): Accepted

Date of paper communication: 7th May 2022

Date of paper acceptance: 10th May 2022

Date of paper publication:

2K20/MSCPHY/04, Ankita,



2K20/MSCPHY/33, Vidhi,



Student(s) Roll No., Name and Signature

SUPERVISOR CERTIFICATE

To the best of my knowledge, the above work has not been submitted in part or full for any Degree or Diploma to this University or elsewhere. I, further certify that the publication and indexing information given by the students is correct.

Prof. A.S. Rao



Supervisor Name and Signature

Place: New Delhi

Date: 10th May 2022

NOTE: PLEASE ENCLOSE RESEARCH PAPER ACCEPTANCE/PUBLICATION/COMMUNICATION PROOF ALONG WITH SCOPUS INDEXING PROOF (Conference Website OR Science Direct in case of Journal Publication).



DELHI TECHNOLOGICAL UNIVERSITY


(Formerly Delhi College of Engineering)

Bawana Road, Delhi – 110042


CERTIFICATE


This is to certify that the dissertation titled as “**Spectroscopic characterization of Dy³⁺ ions doped phosphate glasses for epoxy-free white LED applications**” submitted to Delhi Technological University (Formerly Delhi College of Engineering) by **Ankita (2K20/MSCPHY/04) & Vidhi (2K20/MSCPHY/33)** in the partial fulfillment of the requirements for the award of the degree of **Master of Science in Physics (Department of applied Physics)** is a bona fide record of the candidates’ own work carried out under the supervision of **Prof. A.S. Rao**. The information and data enclosed in thesis is original and has not been submitted elsewhere for honoring any other degree/diploma.

1. 
.....
Signature of Candidate

2. 
.....
Signature of Candidate

This is to certify that the above statement made by the candidates is correct to the best of our knowledge.


(Prof. A.S. Rao)
Project Supervisor
Department of Applied Physics
Delhi Technological University
Delhi – 110042


(Prof. Rinku Sharma)
10th May 2022
Head of the Department
Department of Applied Physics
Delhi Technological University
Delhi – 110042



DELHI TECHNOLOGICAL UNIVERSITY

(Formerly Delhi College of Engineering)

Bawana Road, Delhi – 110042

CANDIDATES DECLARATION

We, Ankita (2K20/MSCPHY/04) & Vidhi (2K20/MSCPHY/33), the students of M.Sc. Physics, hereby declare that the work is being presented in this thesis titled as “Spectroscopic characterization of Dy³⁺ ions doped phosphate glasses for epoxy-free white LED applications” is our own work carried out under the supervision of Prof. A.S. Rao, Department of Applied Physics, Delhi Technological University, Delhi. We further declare that the matter embodied in this dissertation has not been submitted for the award of any other degree or diploma.

Date: 10.05.22

Place: New Delhi

Ankita

(2K20/MSCPHY/04)

Signature.....

Vidhi

(2K20/MSCPHY/33)

Signature.....



Prof. A.S. Rao
(Project Supervisor)

ACKNOWLEDGEMENTS

First and foremost, we would like to express our sincere gratitude to our project supervisor, Prof. A.S. Rao, for his invaluable guidance, motivation and support throughout the entire project. We have benefitted immensely from his wealth of knowledge. His work ethics would continue to inspire us throughout our career in research.

We extend our gratitude to our PhD scholar Mr. Rajat Bajaj and MS. Anu for being the constant support throughout and for providing us with the technical support during the characterization techniques that needed to be performed.

A special thanks to Delhi Technological University (formerly Delhi College of Engineering) for giving us the opportunity to undertake this research project.

We would like to thank our family and friends Anne and Gaurang for creating a motivational and enjoyable environment throughout this journey.

This opportunity will be a significant milestone in our careers' progression and we will strive to utilize the gained skills and knowledge in the best possible way.

Ankita

(2K20/MSCPHY/04)

Department of Applied Physics

Delhi Technological University

Delhi – 110042

Vidhi

(2K20/MSCPHY/33)

Department of Applied Physics

Delhi Technological University

Delhi – 110042

CONTENTS

Certificate	ii
Candidate Declaration	iii
Acknowledgements	iv
Contents	v
List of tables	vi
List of figures	vii
Abstract	viii
Chapter 1: Introduction	1
1.1 Light Emitting Diodes	1
1.2 Literature review	3
Chapter 2: Theoretical Framework	8
2.1 Photoluminescence of materials	8
2.2 Difference between fluorescence, phosphorescence and chemiluminescence	8
2.3 Rare earth (RE) materials	9
2.4 Rare earth elements in glass synthesis	10
2.5 White LEDs	11
Chapter 3: Experimental Techniques	12
3.1 Materials & Methods	12
3.2 Characterization Techniques	14
Chapter 4: Results	24
4.1 Structural analysis	24
4.2 Thermal analysis using DSC-TGA	28
4.3 Absorption spectral study	30
4.4 PL spectral analysis	37
4.5 PL decay analysis	41
4.6 Colorimetric analysis	42
4.7 Temperature-dependent PL (TD-PL) studies and activation-energy estimation ..	44
Chapter 5: Summary & Future scope	51

LIST OF TABLES

Table No.	Description	Page No.
1.	Types of luminescence and their origin	8
2.	Assignment of identified FT-IR bands for Dy ³⁺ ions doped ZnAlNaP glasses.	26
3.	The assignments of Raman bands for Dy ³⁺ ions doped ZnAlNaP glasses.	28
4.	Nephelauxetic ratio (β), bonding parameter (δ), band gap (eV) and Urbach energy (eV) for Dy ³⁺ ions doped ZnAlNaP glasses.	32
5.	Physical properties of Dy ³⁺ ions doped ZnAlNaP glasses.	36
6.	Comparison of CIE color chromaticity co-ordinates and Y/B ratio of ZnAlNaPDy1.5 glass with some reported data.	40
7.	Comparison of τ_{exp} of ZnAlNaPDy1.0 glass with some reported data.	42
8.	CIE Co-ordinates, yellow to Blue (Y/B) intensity ratio and experimental lifetime (τ_{exp} (ms)) of Dy ³⁺ ions doped ZnAlNaP glasses.	44

LIST OF FIGURES

Figure No.	Description	Page No.
1.	White LED	2
2.	Location of Rare Earth elements in the periodic table	10
3.	Furnace used for melt quenching	13
4.	Flow chart of the steps involved in the synthesis process of glasses using melt-quenching method.	13
5.	A demonstration of X-rays being scattered by the sample	15
6.	Experimental setup for XRD analysis	15
7.	Diagram showing the incident & diffracted x-rays from crystal	16
8.	The Spectrophotometer used for Absorption spectroscopy	17
9.	Phenomenon of Photoluminescence	18
10.	Parts of an FT-IR spectrometer with source, interferometer & detector	19
11.	Different cases of scattering	21
12.	Phenomenon of Raman Scattering	22
13.	XRD pattern of undoped ZnAlNaPDy glass	24
14.	FT-IR spectrum of un-doped ZnAlNaP glass.	25
15.	Raman spectrum of 1.0 mol% Dy ³⁺ doped ZnAlNaP glass.	27
16.	DSC of the un-doped ZnAlNaP glass	29
17.	TGA of the un-doped ZnAlNaP glass.	30
18.	Absorption spectra of Dy ³⁺ doped ZnAlNaP glasses for different concentrations.	31
19.	Tauc plot for optical band gap of Dy ³⁺ doped ZnAlNaP glasses for different concentrations.	34
20.	Variation of physical parameters as a function of Dy ³⁺ ion concentration in ZnAlNaP glasses.	36
21.	PL Excitation and PL emission spectrum of 2.0 mol% Dy ³⁺ ion doped ZnAlNaP glass	37
22.	PL emission spectra of Dy ³⁺ ions doped ZnAlNaP glasses at $\lambda_{ex} = 350$ nm.	38
23.	Energy level diagram for Dy ³⁺ doped ZnAlNaP glasses.	39
24.	Decay profile of Dy ³⁺ ions in ZnAlNaP glasses.	41
25.	CIE chromaticity diagram of Dy ³⁺ doped ZnAlNaPDy1.5 glasses at $\lambda_{ex} = 350$ nm.	43
26.	Temperature dependent PL emission intensity variation of ZnAlNaPDy1.0 glass	45
27.	Linear fitted curve of $\ln[(I_0/I_T) - 1]$ versus $1/K_B T$.	46

ABSTRACT

The present work illustrates a detailed spectroscopic analysis carried out on dysprosium ions doped Zinc Alumino Sodium Phosphate (ZnAlNaP) glasses with a chemical composition of $(10-x) \text{ZnO} \cdot 20\text{Al}_2\text{O}_3 \cdot 10\text{Na}_2\text{O} \cdot 60\text{P}_2\text{O}_5 \cdot x\text{Dy}_2\text{O}_3$ ($x = 0.1$ to 2.0 mol%). The XRD spectrum recorded for an un-doped ZnAlNaP glass demonstrates a broad hump confirming its non-crystalline nature. The FT-IR and Raman spectrum recorded for an un-doped ZnAlNaP and ZnAlNaPDy1.0 glass elucidates various functional groups and vibrational modes involved. The DSC & TGA studies conducted on an un-doped ZnAlNaP glass revealed its overall weight loss and thermal stability. The absorption spectra recorded were used to calculate the optical bandgap for the titled glasses and were found to be in the range from 4.52 to 4.81 eV. To understand the applicability of the titled glasses for epoxy-free solid-state lighting devices, photoluminescence (excitation, emission, and decay) spectra were recorded and analysed. The photoluminescence (PL) emission recorded under 350 nm excitation show two significant bands, ${}^4\text{F}_{9/2} \rightarrow {}^6\text{H}_{15/2}$ (blue) and ${}^4\text{F}_{9/2} \rightarrow {}^6\text{H}_{13/2}$ (yellow) at 484 nm and 573 nm respectively. Temperature-dependent PL studies conducted on 1.0 mol% of the Dy^{3+} ions in ZnAlNaP glasses revealed activation energy of 0.212 eV with a percentage of loss 25.6% in PL intensity. The CIE-chromaticity coordinates and color correlated temperature (CCT) were evaluated from the PL spectral characteristics. All the spectroscopic investigations conducted on the titled glasses finally reveal their superior nature in fabricating epoxy-free white light-emitting diodes and other related optoelectronic devices.

Chapter 1: Introduction

1.1 Light Emitting Diodes

Since the beginning of mankind, people have always tried to invent, innovate, and discover new things that can benefit human civilization. Therefore, it should not come as a surprise, but at the same time, we can admit these commendable advancements made by researchers, which are useful for lighting applications in day-to-day life. One of the most remarkable innovations of the twentieth century was light-emitting diodes (LEDs). These devices are a great source of artificial lighting and at the same time eco-friendly.

Today, white- LEDs (w-LEDs) have become fourth-generation solid-state lighting (SSL) gadgets due to the wide range of benefits, such as power saving, higher dependability, brilliant productivity, life span, luminous efficiency and earth-friendly. The w-LEDs are now made with optical excitation sources that have a single or many layers of phosphors [1,2]. The concentration of epoxy resin placed on the phosphor has a significant impact on the emission of phosphor converted (pc) w-LEDs. The sealant used in pc w-LEDs gets degraded at high temperatures, which considerably affects its characteristics such as luminous efficiency and color rendering index [3–6].

The research in rare earth (RE) doped luminescent materials has taken a quantum leap due to impressive advancements in SSL technologies. RE doped glasses have proven to be more advantageous than phosphors due to their unique properties including broader non-homogeneous bandwidths, large doping capacity, and improved thermal stability. RE doped glasses are used in optical devices such as fibre optic amplifiers, lasers, pharmaceuticals, photovoltaics, telecommunications, and civil-military purposes for instance infrared detectors, infrared fairings, nuclear imaging and surveillance [7–11]. The above-mentioned applications of RE doped glasses are possible only if it is chemically & thermally stable, has relatively minimal phonon energies, have better RE³⁺ solubility with excellent transparency. The host glass's structure and ligand field environment affect the bandwidths of emission bands and decides the photoluminescence (PL) adequacy of RE³⁺. Thus, selecting a host material with relatively lower phonon energies is very important [6,12].



Fig. 1. White LED

Phosphate glasses, in contrast to commonly used glass formers such as silicate, borate, and others, are known to have good mechanical and thermal stability, excellent transparency, better RE^{3+} solubility, low melting point (compared to silicate glass), eco-friendly and isotropic refractive index [13–17]. Nonetheless, pure phosphorus pentoxide (P_2O_5), a chemically unstable oxide is a compound that comes in the category of glass formers. P_2O_5 is immensely hygroscopic in nature when it comes to moisture-induced hydrolysis of the P–O–P bonds. As a result, its usage as a substitute for silicate glasses is frequently limited to a narrow range of technological applications. Despite this, the high solubility of P_2O_5 glasses makes them useful in synthesizing bioactive materials [18–21].

The morphology of glass is decided by two main components, the network former and the network modifier. Network formers are considered to be an integral component in the construction of any glass matrix. It can be a metal oxide and one such case is that of Al_2O_3 which we have also used in the composition of our glass. Al_2O_3 conjugation in phosphate glass can act as a network former as well as a network modifier. Al_2O_3 increases the crosslinks with PO_4 tetrahedra in the glass. It gives the phosphate glass moisture resistance and thermal stability, as well as a lower thermal coefficient of expansion, which makes it suitable for ion exchange planar waveguide devices. Aluminium oxide in phosphate glass can improve the host glass's physical and chemical stability [22–24].

The addition of network modifiers in the host matrix modifies its internal structure and simultaneously builds an integrated environment for the RE^{3+} , allowing them to maintain a high luminescence efficiency [25]. The glass modifiers that we have used in our study are zinc oxide (ZnO) and sodium oxide (Na_2O). We can improve the noble features of phosphate glass by adding

divalent metal oxides like zinc oxide (ZnO) to it, such as lower glass transition temperatures and higher chemical stability. Furthermore, glasses containing ZnO are less hygroscopic and toxic, making them more efficient for developing optoelectronic devices [6,12,24,26]. In glasses, alkaline metal oxides like sodium oxide (Na₂O) can influence and regulate their optical properties. Adding Na₂O to the phosphate glass matrix as a network modifier promotes the formation of non-branching oxygen atoms. Also, it improves the solubility of RE ions, making it suitable for higher concentration of dopants in the glass and also useful for short-length optical amplifiers [27,28].

Doping RE³⁺ in phosphate glasses has several advantages, including lower propagation losses, a high number of intra-configuration transition channels for RE³⁺, an isotropic refractive index, and the ability to produce them more easily. The outer 5s and 5p shells shield the RE³⁺ surroundings, affecting the 4f-4f transitions in RE³⁺, resulting in intense and narrow emissions [3]. From the existing seventeen RE ions, Dy³⁺ ions when used as a dopant in glass, makes it quite suitable for producing white light due to two major bands of emission corresponding to the ⁴F_{9/2}→⁶H_{15/2} transition which is a magnetic dipole and ⁴F_{9/2}→⁶H_{13/2} transition which is an electric dipole pertaining to 480-500 nm and 580-600 nm ascribing to the blue and yellow part of the visible spectrum, respectively [29,30]. The yellow band is more susceptible to the nature of the host's material and is heavily dependent on it, whereas the blue band is less susceptible to the host material. As a result, Dy³⁺ doped glasses with an acceptable yellow and blue transitions ratio can create white light [31].

Apart from being a single-phase white light source, Dy³⁺ doped glasses have a wide range of applications, including luminescence lamps that are free of mercury and light generating materials when mixed RE ions are added. All of the aforementioned advantages of the constituent chemical species like P₂O₅, Al₂O₃, ZnO, Na₂O and Dy₂O₃ gave us an incentive to prepare a series of phosphate glasses by name zinc alumino sodium phosphate (ZnAlNaP) glasses.

1.2 Literature review

H. George et. al. conducted spectroscopic investigation by evaluating the CCT values for the Dy³⁺ doped NaBiSrP glasses which lie in the neutral white zone under n-UV excitation [32]. The structural, thermal and optical studies of Dy³⁺ doped B₂O₃-WO₃-ZnO-Li₂O-Na₂O glasses were performed by G. Lakshminarayana et al [33]. The PL studies performed on the aforementioned glasses show strong peaks at blue and yellow emission bands when observed using UV excitation

and the Y/B values show relatively higher values, making this combination a suitable candidate for white light generation [33]. The optical and radiative properties of dysprosium doped sodium aluminum phosphate (NAP) glasses were investigated by A. Amarnath Reddy et al [34]. The Y/B ratios found in visible emission imply the prominent nature of covalency and asymmetry effects in the aforementioned glasses, and the Y/B intensity ratios observed in visible emission showing the ease of producing white light in the Dy³⁺ doped NAP glass [34].

All of above-mentioned researchers motivated us to work in this field utilizing Dy³⁺ doped phosphate glasses that can be suitably significant for white light applications in photonic devices. In the present work, we have investigated the glassy nature, structural aspects, thermal stability and spectroscopic features of the as-prepared glasses using various characterization techniques like XRD, FT-IR, Raman, DSC-TGA, optical absorption, PL (excitation, emission and decay) and temperature dependent PL (TD-PL).

References:

1. T.A. Lodi, N.F. Dantas, T.S. Goncalves, A.S.S. de Camargo, F. Pedrochi, A. Steimacher, Dy³⁺ doped calcium boroaluminate glasses and Blue Led for smart white light generation, *Journal of Luminescence*. 207 (2019) 378–385. <https://doi.org/10.1016/J.JLUMIN.2018.11.045>.
2. S. Damodaraiah, Y.C. Ratnakaram, Energy transfer studies and neutral to warm white light generation in Dy³⁺-Sm³⁺ co-doped bismuth phosphate glasses for lighting applications, *Journal of Luminescence*. 207 (2019) 553–560. <https://doi.org/10.1016/J.JLUMIN.2018.12.002>.
3. N. Deopa, A.S. Rao, Spectroscopic studies of Sm³⁺ ions activated lithium lead alumino borate glasses for visible luminescent device applications, *Optical Materials*. 72 (2017) 31–39. <https://doi.org/10.1016/J.OPTMAT.2017.04.067>.
4. A.N. Meza-Rocha, I. Camarillo, R. Lozada-Morales, U. Caldino, Reddish-orange and neutral/warm white light emitting phosphors: Eu³⁺, Dy³⁺ and Dy³⁺/Eu³⁺ in potassium-zinc phosphate glasses, *Journal of Luminescence*. 183 (2017) 341–347. <https://doi.org/10.1016/J.JLUMIN.2016.11.068>.
5. S. Kaur, A.K. Vishwakarma, N. Deopa, A. Prasad, M. Jayasimhadri, A.S. Rao, Spectroscopic Studies of Dy³⁺ doped Borate Glasses for Cool White Light Generation, *Materials Research Bulletin*. 104 (2018) 77–82. <https://doi.org/10.1016/j.materresbull.2018.04.002>.
6. S. Mahamuda, K. Swapna, M. Venkateswarlu, A. Srinivasa Rao, S. Shakya, G. Vijaya Prakash, Spectral characterisation of Sm³⁺ ions doped Oxy-fluoroborate glasses for visible

- orange luminescent applications, *Journal of Luminescence*. 154 (2014) 410–424. <https://doi.org/10.1016/j.jlumin.2014.05.017>.
7. S.F. Wang, Y.F. Hsu, H.C. Lug, S.C. Lo, C.S. Chen, B₂O₃-free SiO₂-Al₂O₃-SrO-La₂O₃-ZnO-TiO₂ glass sealants for intermediate temperature solid oxide fuel cell applications, *International Journal of Hydrogen Energy*. 37 (2012) 5901–5913. <https://doi.org/10.1016/J.IJHYDENE.2011.12.121>.
 8. H. Gui, C. Li, C. Lin, Q. Zhang, Z. Luo, L. Han, J. Liu, T. Liu, A. Lu, Glass forming, crystallization, and physical properties of MgO-Al₂O₃-SiO₂-B₂O₃ glass-ceramics modified by ZnO replacing MgO, *Journal of the European Ceramic Society*. 39 (2019) 1397–1410. <https://doi.org/10.1016/j.jeurceramsoc.2018.10.002>.
 9. K. Annapoorani, K. Marimuthu, Spectroscopic properties of Eu³⁺ ions doped Barium telluro borate glasses for red laser applications, *Journal of Non-Crystalline Solids*. 463 (2017) 148–157. <https://doi.org/10.1016/j.jnoncrysol.2017.03.004>.
 10. A. Askın, Evaluation of the radiation shielding capabilities of the Na₂B₄O₇-SiO₂-MoO₃-Dy₂O₃ glass quaternary using Geant4 simulation code and Phy-X/PSD database, *Ceramics International*. 46 (2020) 9096–9102. <https://doi.org/10.1016/j.ceramint.2019.12.158>.
 11. T. Liu, C. Lib, Q. Huang, C. Liu, C. Lin, Q. Zhang, Z. Luo, L. Zhu, A. Lu, Characterization of structure and properties of MgO-Al₂O₃-SiO₂-B₂O₃-Cr₂O₃ glass ceramics, *Journal of Non-Crystalline Solids*. 543 (2020). <https://doi.org/10.1016/j.jnoncrysol.2020.120154>.
 12. S. Mahamuda, K. Swapna, A. Srinivasa Rao, T. Sasikala, L. Rama Moorthy, Reddish orange emission from Pr³⁺ doped zinc alumino bismuth borate glasses, *Physica B Condensed Matter*. 428 (2013) 36–42. <https://doi.org/10.1016/j.physb.2013.07.010>.
 13. H. Aboud, R. Amjad, SnO₂ nanoparticles concentration dependent structural and luminescence characteristics of Er³⁺ doped zinc-lead-phosphate glass, *Journal of Non-Crystalline Solids*. 471 (2017) 1–5. <https://doi.org/10.1016/j.jnoncrysol.2017.03.018>.
 14. L. Mariscal-Becerra, S. Carmona-Téllez, G. Arredondo-Martínez, S. Salas-Mariscal, J. Hernández-Sánchez, C. Falcony, Yttrium-europium oxide doped zinc phosphate glasses, a luminescence study, *Journal of Non-Crystalline Solids*. 471 (2017) 268–273. <https://doi.org/10.1016/j.jnoncrysol.2017.06.003>.
 15. T. Srihari, C.K. Jayasankar, Fluorescence properties and white light generation from Dy³⁺-doped niobium phosphate glasses, *Optical Materials*. 69 (2017) 87–95. <https://doi.org/10.1016/j.optmat.2017.03.018>.
 16. K. Anil Kumar, S. Babu, V. Reddy Prasad, S. Damodaraiah, Y. Ratnakaram, Optical response and luminescence characteristics of Sm³⁺ and Tb³⁺/Sm³⁺ co-doped potassium-fluoro-phosphate glasses for reddish-orange lighting applications, *Materials Research Bulletin*. 90 (2017) 31–40. <https://doi.org/10.1016/j.materresbull.2017.01.046>.

17. M. Saad, W. Stambouli, S.A. Mohamed, H. Elhouichet, Ag nanoparticles induced luminescence enhancement of Eu³⁺ doped phosphate glasses, *Journal of Alloys and Compounds*. 705 (2017) 550–558. <https://doi.org/10.1016/J.JALLCOM.2016.12.410>.
18. M.R. Reidmeyer, M. Rajaram, D.E. Day, Preparation of phosphorus oxynitride glasses, *Journal of Non-Crystalline Solids*. 85 (1986) 186–203. [https://doi.org/10.1016/0022-3093\(86\)90090-6](https://doi.org/10.1016/0022-3093(86)90090-6).
19. M. Erol, A. Özyüğüran, Ö. Özarpat, S. Küçükbayrak, 3D Composite scaffolds using strontium containing bioactive glasses, *Journal of the European Ceramic Society*. 32 (2012) 2747–2755. <https://doi.org/10.1016/J.JEURCERAMSOC.2012.01.015>.
20. A. Goel, R.R. Rajagopal, J.M.F. Ferreira, Influence of strontium on structure, sintering and biodegradation behaviour of CaO–MgO–SrO–SiO₂–P₂O₅–CaF₂ glasses, *Acta Biomaterialia*. 7 (2011) 4071–4080. <https://doi.org/10.1016/J.ACTBIO.2011.06.047>.
21. M.D. O’Donnell, R.G. Hill, Influence of strontium and the importance of glass chemistry and structure when designing bioactive glasses for bone regeneration, *Acta Biomaterialia*. 6 (2010) 2382–2385. <https://doi.org/10.1016/J.ACTBIO.2010.01.006>.
22. N. Deopa, A.S. Rao, Spectroscopic studies of single near ultraviolet pumped Tb³⁺ doped Lithium Lead Alumino Borate glasses for green lasers and tricolour w-LEDs, *Journal of Luminescence*. 194 (2018) 56–63. <https://doi.org/10.1016/J.JLUMIN.2017.09.057>.
23. J. Cao, Z. He, W. Guo, C. Li, L. Gai, J. Qi, Joining of Al₂O₃ to ZTA using a B₂O₃–Al₂O₃–SiO₂ glass with in-situ precipitated whiskers, *Ceramics International*. 47 (2021) 25541–25550. <https://doi.org/10.1016/J.CERAMINT.2021.05.278>.
24. K. Swapna, S. Mahamuda, A.S. Rao, T. Sasikala, P. Packiyaraj, L.R. Moorthy, G.V. Prakash, Luminescence characterization of Eu³⁺ doped Zinc Alumino Bismuth Borate glasses for visible red emission applications, *Journal of Luminescence*. 156 (2014) 80–86. <https://doi.org/10.1016/J.JLUMIN.2014.07.022>.
25. M.A. Algradee, A.E.B. Alwany, M. Sultan, M. Elgoshimy, Q. Almoraisy, Physical and optical properties for Nd₂O₃ doped lithium-zinc-phosphate glasses, *Optik*. 142 (2017) 13–22. <https://doi.org/10.1016/J.IJLEO.2017.05.065>.
26. S. Kaur, N. Deopa, A. Prasad, R. Bajaj, A.S. Rao, Intense green emission from Tb³⁺ ions doped zinc lead alumino borate glasses for laser and w-LEDs applications, *Optical Materials*. 84 (2018) 318–323. <https://doi.org/10.1016/J.OPTMAT.2018.07.020>.
27. L. Ma, R.K. Brow, A. Choudhury, Structural study of Na₂O–FeO–Fe₂O₃–P₂O₅ glasses by Raman and Mössbauer spectroscopy, *Journal of Non-Crystalline Solids*. 402 (2014) 64–73. <https://doi.org/10.1016/J.JNONCRY SOL.2014.05.013>.
28. G. Lakshminarayana, J. Qiu, M.G. Brik, G.A. Kumar, I. v Kityk, Spectral analysis of Er³⁺-, Er³⁺/Yb³⁺- and Er³⁺/Tm³⁺/Yb³⁺-doped TeO₂–ZnO–WO₃–TiO₂–Na₂O glasses, *Journal of Physics: Condensed Matter*. 20 (2008) 375101. <https://doi.org/10.1088/0953-8984/20/37/375101>.

29. F. Huang, Y. Tian, D. Chen, S. Xu, J. Zhang, Spectroscopic properties and energy transfer mechanism in Dy³⁺/Tm³⁺ codoped fluoroaluminate glasses modified by TeO₂, *Ceramics International*. 42 (2016) 132–137.
30. S.A. Saleem, B.C. Jamalaiah, M. Jayasimhadri, A.S. Rao, K. Jang, L.R. Moorthy, Luminescent studies of Dy³⁺ ion in alkali lead tellurofluoroborate glasses, *Journal of Quantitative Spectroscopy & Radiative Transfer*. 112 (2011) 78–84.
31. K. Linganna, C.S. Rao, C.K. Jayasankar, Optical properties and generation of white light in Dy³⁺-doped lead phosphate glasses, *Journal of Quantitative Spectroscopy and Radiative Transfer*. 118 (2013) 40–48. <https://doi.org/10.1016/J.JQSRT.2012.12.002>.
32. H. George, N. Deopa, S. Kaur, A. Prasad, M. Sreenivasulu, M. Jayasimhadri, A.S. Rao, Judd-Ofelt parametrization and radiative analysis of Dy³⁺ ions doped Sodium Bismuth Strontium Phosphate glasses, *Journal of Luminescence*. 215 (2019) 116693. <https://doi.org/10.1016/J.JLUMIN.2019.116693>.
33. G. Lakshminarayana, S.O. Baki, A. Lira, I. v Kityk, U. Caldiño, K.M. Kaky, M.A. Mahdi, Structural, thermal and optical investigations of Dy³⁺-doped B₂O₃–WO₃–ZnO–Li₂O–Na₂O glasses for warm white light emitting applications, *Journal of Luminescence*. 186 (2017) 283–300. <https://doi.org/10.1016/J.JLUMIN.2017.02.049>.
34. [34] A. Amarnath Reddy, M. Chandra Sekhar, K. Pradeesh, S. Surendra Babu, G. Vijaya Prakash, Optical properties of Dy³⁺-doped sodium–aluminum–phosphate glasses, *Journal of Materials Science*. 46 (2011) 2018–2023. <https://doi.org/10.1007/s10853-010-4851-3>.

Chapter 2: Theoretical Framework

2.1 Photoluminescence of materials:

Luminescent materials are substances that, in addition to black-body emission, transform an incident energy source into electromagnetic wave output in the ultraviolet (UV), visible, or infrared regions of the spectra. Luminescence can be classified on the basis of the simulation that is provided and the Table 1 given below summarizes it [1].

Table 1: Types of luminescence and their origin

DESIGNATION	STIMULATED BY	TRIGGER	ACRONYM
PHOTOLUMINESCENCE	UV, Visible Photons	-	PL
RADIOLUMINESCENCE	X-Ray, Gamma Rays, Charged Particles	-	RL
CATHODOLUMINESCENCE	Energetic Electrons	-	CL
ELECTROLUMINESCENCE	Collisional excitation of internal electrons accelerated	Applied Electric Field	EL
THERMOLUMINESCENCE	Photons, Charged Particles	Heat	TSL

2.2 Difference between fluorescence, phosphorescence and chemiluminescence:

- Photoluminescence is classified into fluorescence and phosphorescence. If the substance's glow is triggered by light, then it is photoluminescence, whereas if the glow is caused by a chemical reaction, then it is chemiluminescence.
- Fluorescence and phosphorescence are both caused by a substance's capacity to absorb the light and subsequently release the light with a longer wavelength and consequently less energy.

- The basic difference between these two phenomena is the time taken to complete the process. In the case of fluorescence, the emission occurs immediately, so it can be observed only when the light source is kept on (for example, UV lights); however, in the case of phosphorescence, the absorbed light energy can be stored for a period of time and then released later, as a result, even after the light source has been switched off, there is an afterglow.
- To conclude, if it fades away quickly, it is fluorescence; if it lasts longer, it is phosphorescence. It's chemiluminescence if it requires some type of activation.
- A good example of it can be considered if we imagine a scenario at the nightclub: Teeth, eyes and fabric glowing under the black light are considered fluorescent, the emergency exit sign is phosphorescent and the glow sticks are chemiluminescent [1].

2.3 Rare earth (RE) materials:

- There are 17 RE elements in periodic table. Scandium, Yttrium and some 15 other lanthanide series elements come under this category.
- Since, all RE elements are metals, therefore they are sometimes known as the "Rare Earth metals".
- They are also called "Rare Earth oxides" since most of them are available in the market as oxide compounds.
- Rare earth elements are commonly employed as catalysts, phosphors, and polishing agents. In air pollution management, illuminated screens in electronic devices, and a variety of other applications rare earth elements are commonly used [2].

Rare Earth Elements
by Geology.com

H																	He
Li	Be											B	C	N	O	F	Ne
Na	Mg											Al	Si	P	S	Cl	Ar
K	Ca	Sc	Ti	V	Cr	Mn	Fe	Co	Ni	Cu	Zn	Ga	Ge	As	Se	Br	Kr
Rb	Sr	Y	Zr	Nb	Mo	Tc	Ru	Rh	Pd	Ag	Cd	In	Sn	Sb	Te	I	Xe
Cs	Ba	La-Lu	Hf	Ta	W	Re	Os	Ir	Pt	Au	Hg	Tl	Pb	Bi	Po	At	Rn
Fr	Ra	Ac-Lr	Rf	Db	Sg	Bh	Hs	Mt									
Lanthanides																	
La Ce Pr Nd Pm Sm Eu Gd Tb Dy Ho Er Tm Yb Lu																	
Actinides																	
Ac Th Pa U Np Pu Am Cm Bk Cf Es Fm Md No Lr																	

Fig. 2. Location of Rare Earth elements in the periodic table

- Actually, rare earth elements are not "rare" as the name suggests. For example, the two least abundant rare earth elements are Thulium and Lutetium but each of them has an average crustal abundance approximately 200 times more than that of the gold. Although these metals are not rare but are quite tough to mine as it is uncommon to obtain these metals in enough concentrations for economical extraction.
- Yttrium, cerium, lanthanum and neodymium come under the category of the most abundant rare earth elements. The average crustal abundances for these elements are similar to some of the most frequently used industrial metals for instance chromium (Cr), nickel (Ni), zinc (Zn), and lead (Pb) etc. But again, they can rarely be found in extractable concentrations [2].

2.4 Rare earth elements in glass synthesis:

- Researchers have been studying rare earth oxides for a long time now, especially how the addition of rare earth oxides can change the properties of the glass. It was for the first time in the 1800s that Drossbach, a German scientist patented his work of manufacturing a mixture of rare earth oxides to decolorize the glass. It is said to be cerium is firstly commercially used although it is in their raw form combining with other RE oxides. Later in 1912, Crookes from England discovered cerium's excellent properties for ultraviolet absorption without giving any color hence making it quite useful in making protective eyeglasses.

- Some of the most commonly used Rare Earth Elements in glass are erbium, ytterbium, and neodymium. Some of the uses are: Erbium-doped silica fiber is widely used for optical communication; ytterbium-doped silica fiber is used in manufacturing some engineering materials, and neodymium-doped is useful in making glass lasers. Addition of rare earth oxides in glass have the ability to change the fluorescent properties of the glass [3].

2.5 White LEDs:

- One of the most remarkable innovations of the twentieth century was that of the light-emitting diodes (LEDs). These devices are a great source of artificial lighting and at the same time eco-friendly. Today, white- LEDs or w-LEDs have become fourth generation solid-state lighting (SSL) gadgets due to the wide range of benefits that they offer, such as power saving, higher dependability, brilliant productivity, life span, luminous efficiency and earth friendly.
- At present, w-LEDs are fabricated using optical excitation sources with a coating of one or many phosphors. In the case of phosphor converted (pc) w-LEDs, the resulting emitted light is immensely affected due to concentration of epoxy-resin coated on phosphor. The sealant used in pc w-LEDs, gets degraded at high temperatures which in turn considerably affect its characteristics such as, luminous efficiency and color rendering index.
- The research in the field of rare earth (RE) doped luminescent materials have taken a quantum leap due to impressive advancements in SSL technologies. Owing to their peculiar qualities such as high doping capacity, broad inhomogeneous bandwidths and better thermal stability, rare earth doped glasses have proved to be more advantageous over phosphors [4].

References:

1. <https://www.sciencedirect.com/topics/materials-science/luminescent-material>
2. <https://www.sciencedirect.com/topics/earth-and-planetary-sciences/rare-earth-element>
3. B.Locardi , E.Guadagnino, “*Rare earths in glass technology*” , Materials Chemistry and Physics, Volume 31, Issues 1–2, March–April 1992, Pages 45-49.
4. Yulei Zhao, et.al., “*Luminescent properties of Tm³⁺-Dy³⁺ co-doped P₂O₅-SrO-BaO-B₂O₃-ZnO glasses for white LED applications*”, Journal of Non-Crystalline Solids, Volume 573, December2021, 121121, ISSN 0022-3093.

Chapter 3: Experimental Techniques

3.1 Materials & Methods:

A. Preparation: The most common methods to prepare a glass are melt quenching method, Chemical vapor deposition and sol-gel method. Out of these three techniques, melt quenching has been the most popular and quite feasible so far in the research field. The key feature of this melt quenching technique is that it is widely applicable to prepare all kinds of compositions of glasses like borate, phosphate, silicate, oxide or non-oxide systems. We have all kinds of options available as dopants and co-dopants to give a variety to our glass system which becomes quite easy using this technique. There are minor chances of the sample being prone to some kind of impurities but that can be avoided using the crucibles made of noble metals like Gold, Platinum, etc. [1].

B. Melt-quenching Technique: We have prepared a phosphate glass for our research work and the Rare Earth ion that has been used as a dopant is Dysprosium (Dy^{3+}). The high purity analytical grade oxides or salts were taken as precursors. Powders such as zinc oxide (ZnO), sodium oxide (Na_2O), aluminum oxide (Al_2O_3), di-ammonium hydrogen orthophosphate ($(NH_4)_2 HPO_4$) and the dopant dysprosium oxide (Dy_2O_3) were weighed in required quantities using a high-accuracy electronic balance. Then using acetone as the dispersing medium, the components were then grinded in an agate mortar for about 45 minutes until the mixture was a soft powder. The so-obtained fine powder was then transferred to a silica crucible and a constant heat of 1270 °C was applied in a programmable furnace for two hours. Thereafter, the as obtained melt was cast into a coin shaped glass by pressing it between two pre-heated brass plates. This process is known as quenching and since the melt was quenched into a coin shape, this is why we call it the melt quenching technique. The coin shaped glasses were then immediately transferred to an annealing furnace at 350 °C for 2 hours to eradicate the internal stresses, air bubbles and to maintain the stability of the internal glass structure [1, 6].

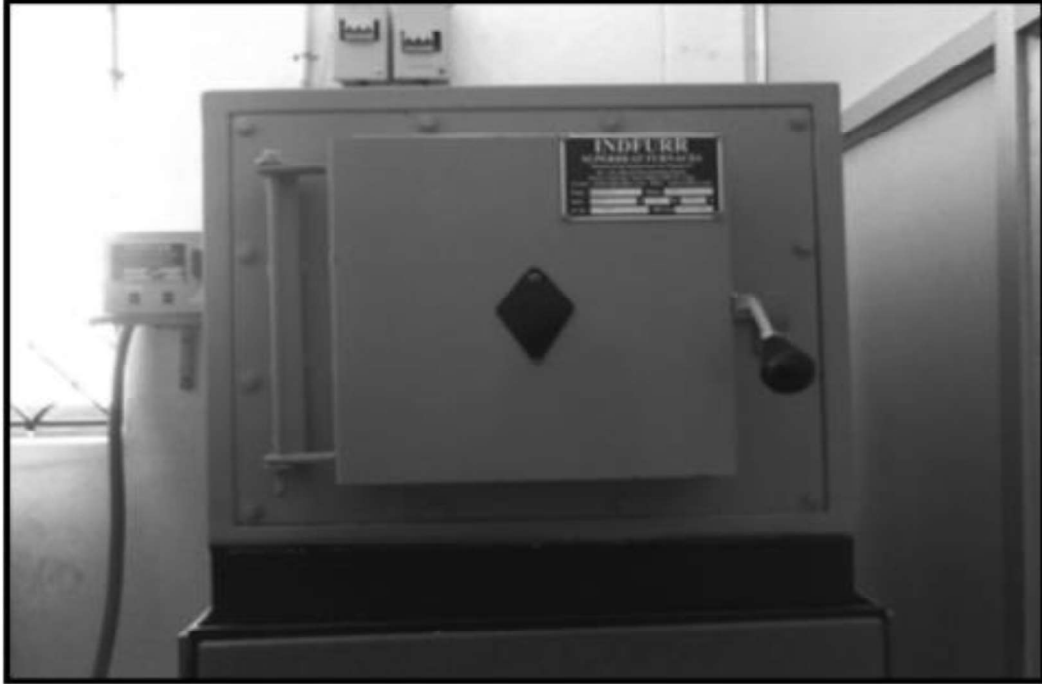


Fig. 3. Furnace used for melt quenching

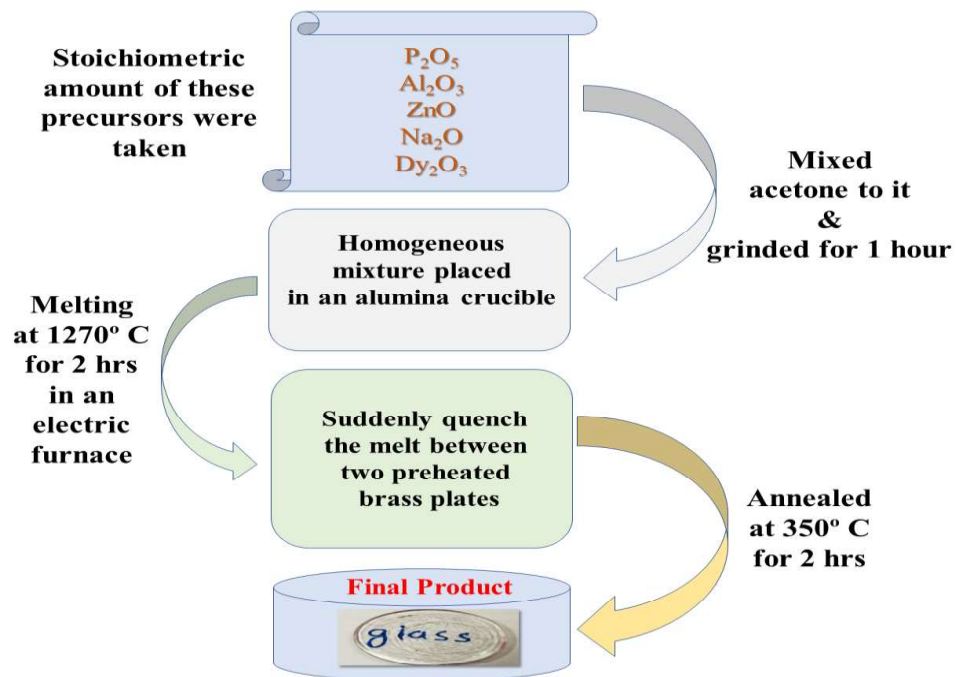


Fig. 4. Flow chart of various steps involved in the synthesis process of glasses using melt-quenching method.

Using a Bruker D8 Advance Diffractometer with nickel filtered Cu-K α radiation ($\lambda = 1.5406 \text{ \AA}$) and diffraction angles ranging from $10^\circ \leq 2\theta \leq 80^\circ$, the XRD spectrum of an un-doped ZnAlNaP glass sample was obtained. Perkin Elmer's Frontier Spectrometer ($450\text{--}4000 \text{ cm}^{-1}$) was used to measure the FT-IR spectrum of the identical sample utilizing the KBr-disk method. Raman spectroscopy was performed using a Renishaw model Invia Reflex Raman microscope. The optical absorption studies were done using a Jasco V-770 Spectrophotometer. A JASCO made (FP-8300) spectrofluorophotometer (resolution of 1.0 nm) with a Xenon flash lamp as an excitation source was used to make the spectral recordings of PL excitation, PL emission and PL decay. All measurements were recorded at an ambient temperature. TDPL studies were conducted on FLMS15147 Spectrometer.

3.2 Characterization Techniques:

a. XRD: Diffraction of light refers to the bending of light around the corners of an obstacle. It is the required condition for diffraction to occur. The size of the obstacle needs to be almost equivalent to the frequency of light being used. X-ray, as other EM rays, can also be diffracted, but for the diffraction of X-ray the size of the obstacle ought to be a couple of angstroms (approx. 1 \AA), which is approximately the frequency of X-rays. The reason behind this is that the atomic spacing in the Crystal is almost a few \AA . The constructive interference of monochromatic x-rays is the basic principle of XRD. X-rays are directed towards the sample under investigation, and sample's crystal structure causes the X-rays to spread in a variety of directions. It is recorded by a detector and further amplified to be analyzed on a monitor screen [7].

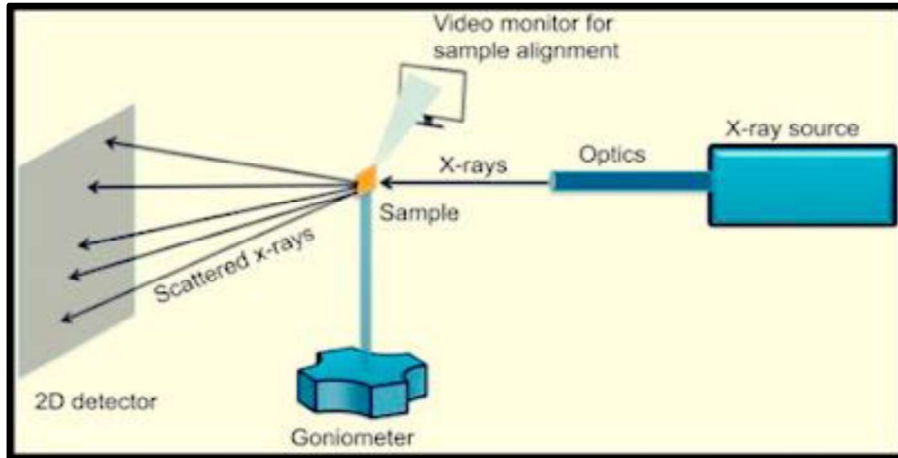


Fig. 5. A demonstration of x-rays being scattered by the sample

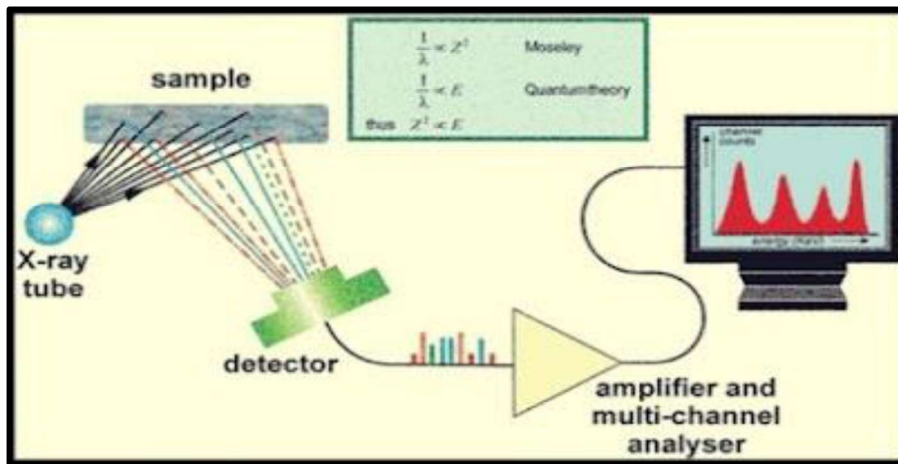


Fig. 6. Experimental setup for XRD analysis

Bragg's Law:

This law implies that if an x-ray is incident at an angle of incidence (θ) onto a crystal surface, then that x-ray reflects at the same angle of scattering (θ). If the path difference (d) is a whole number (n) multiple of wavelength (λ) then an interference pattern can be seen.

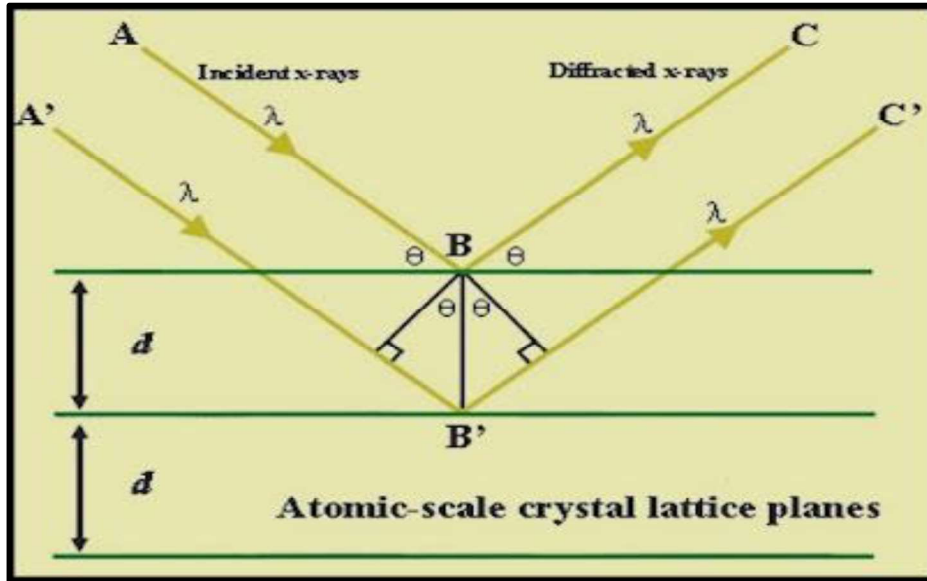


Fig. 7. Diagram showing the incident and diffracted x-rays from the crystal surface

Bragg's Law is:

$$n \lambda = 2d \sin(\theta) \quad (1)$$

here, λ is the incident wavelength of x-rays, d is the spacing between the crystal layers (i.e., path difference), θ is the angle of incidence & n is the diffraction order.

X-Ray Diffraction (XRD) Methods

There are several XRD methods:

1. Laue's Photographic Method
2. Bragg's X-Ray Spectrometer Method
3. Rotating Crystal Method
4. Powder Crystal Method

Since we have used powder method, so elaborating on that:

The sample to be tested is homogenized and ground into a fine powder. The powdered sample is then struck on a hair and mounted vertically in the axis of a cylindrical camera with a piece of gum.

A monochromatic beam is permitted to fall on it, various possibilities exist. A few particles may emerge from the random alignment of tiny crystals. For each set, there is the probability of reflections in different orders. In addition, another proportion of grains will have a different

set of planes in the appropriate positions for reflections to occur [3].

b. ABSORPTION: Absorption spectroscopy of a glass sample is carried out using the radiations lying in the UV-Visible region of Electromagnetic spectrum. The amount of light absorbed by a particular glass sample is observed in the phenomenon. When the radiation of a particular wavelength falls on the glass sample, the electrons in the outermost shells of the compound participate and get excited to the first excited state of the material. The light from a source (usually tungsten lamp or deuterium) after passing through a monochromator falls on the beam splitter and a series of mirrors. Thereafter, the light finally falls on the sample holder where the glass sample is placed. The absorption data corresponding to a particular wavelength range of that particular sample is obtained on a computer screen connected to the spectrophotometer. This data shows how much light of a particular wavelength is absorbed by the sample. The measurements are carried out using a reference sample for which the absorption data is already known. It is to be noted that this process involves relative measurements and not direct measurements. This phenomenon is used to determine the optical properties of the glass sample like optical band gap, refractive index and other such properties [5].



Fig. 8. The Spectrophotometer used for Absorption spectroscopy

c. PHOTOLUMINESCENCE (PL) SPECTROSCOPY: PL spectroscopy is a type of light-emitting spectroscopy in which the emission of light arises due to a process called photo-excitation. As the light is directed to the sample, the electrons inside the material go to the

excited regions (excitation). After releasing energy in non-radiative forms, the electron goes down to an intermediate level called the conduction band. Thereafter, when electrons flow from the conduction band to their ground states, energy can be released in the form of light (called radiative relaxation). This phenomenon is shown in fig. 9. The experimental setup is quite similar to that of Absorption spectroscopy except for the monochromator near the source. PL spectroscopy is beneficial to estimate the electronic structure and assets of the compound as it provides the peak light intensity that objects can emit at a certain wavelength [1].

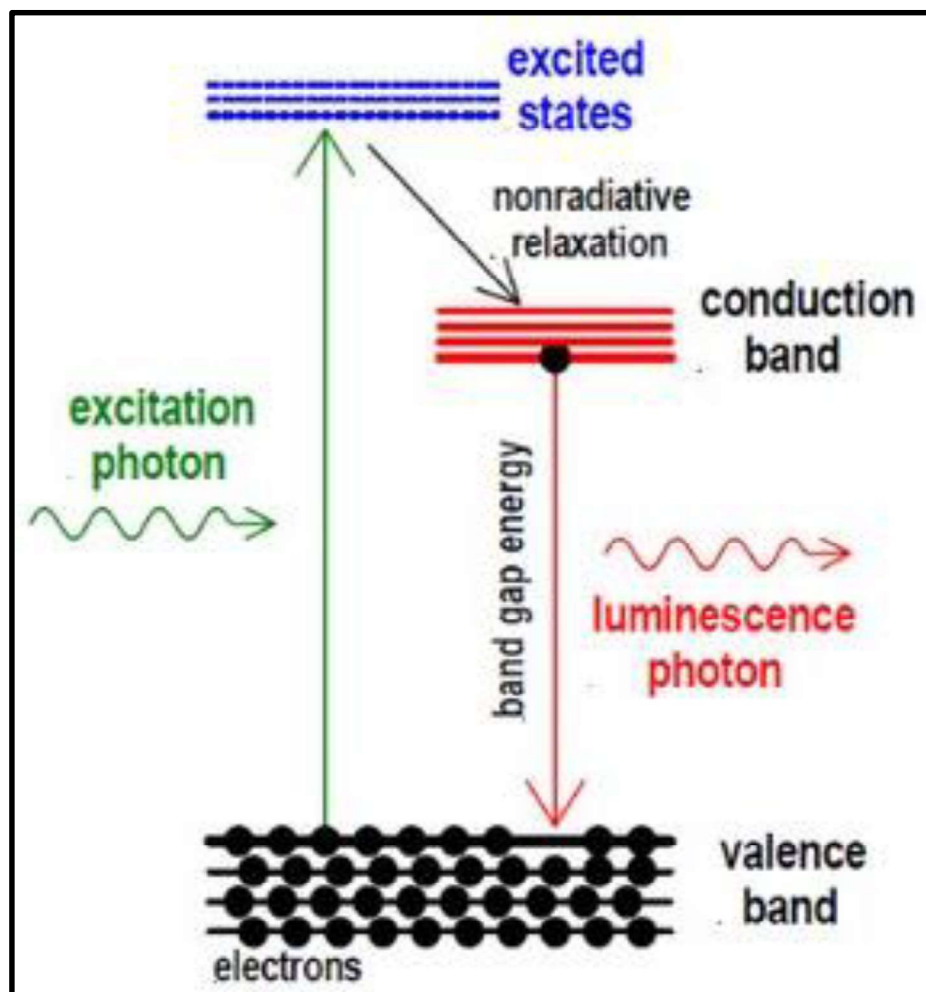


Fig. 9. Phenomenon of Photoluminescence

d. FT-IR: FT-IR Spectroscopy (fourier-transform infrared spectroscopy) is a characterization technique that is concerned with the vibration of molecules. The source, interferometer, and detector are the three important parts of an FT-IR Spectroscopy (fig. 10).

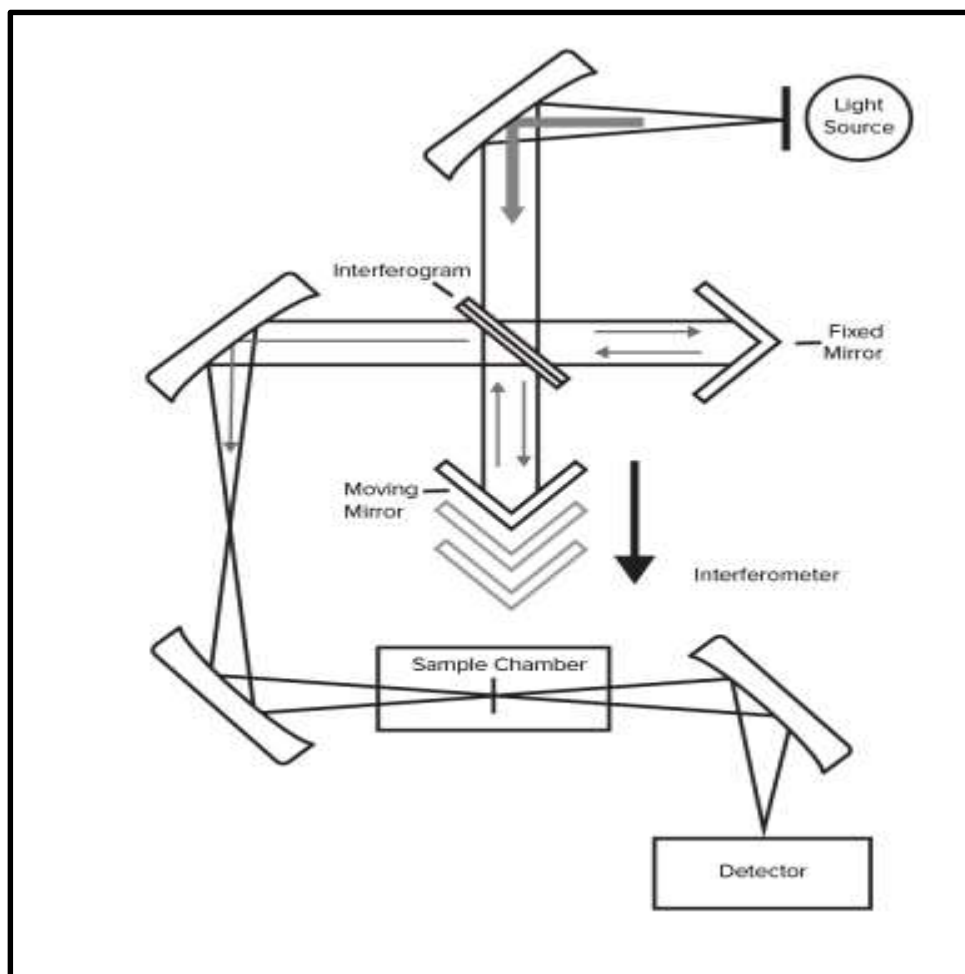


Fig. 10. Parts of an FTIR spectrometer with source, interferometer & detector.

The source energy is directed onto the sample through an interferometer. All source radiation must reach the sample during each scan. The light is then split into two directions at right angles by passing through a beam splitter. One of these beams is directed and sent to a fixed mirror before returning to beam-splitter. Another beam is channeled at a movable mirror. Furthermore, both of these two beams will recombine at the beam-splitter, although difference in path lengths will cause constructive and destructive interference, resulting in interference pattern. The sample is next passed through the earlier recombined beam, which absorbs all of the distinct wavelength's characteristic of its spectrum. The detector records the change in energy and time corresponding to many wavelengths for same time. A laser beam is imposed throughout the procedure to give a reference for instrument operation.

Now, one could think that recording a spectrum in terms of energy vs time is strange, unless one considers the correlation between time and frequency: they are reciprocal. Using the Fourier transform (FT) function, an I-vs-t spectrum can be transformed to an I-vs- ν spectrum. The FT can be given by the expression:

$$A(r) = \sum X(k) \exp(-2\pi \frac{irk}{N}) \quad (2)$$

here, $A(r)$ are the frequency domain & $X(k)$ are the time domain points and N are the total points in the spectrum.

Because each functional group has its own distinct vibrational energy that may be utilized to identify a molecule by combining all of the functional groups, FTIR microscopy is an excellent tool for identifying samples, characterization of multilayer films, and particle analysis. Because each functional group is made up of distinct atoms with variable bond strengths, each of these functional groups, and categories of functional groups, has its own set of vibrations. Because each molecule's collection of vibrational energy bands is distinct, these peaks can be utilized to identify the functional groups involved utilizing literature analyses of large sample datasets [8].

- e. **RAMAN SPECTROSCOPY:** Raman spectroscopy is a method for measuring the vibrational energy modes of a material by means of diffused light. CV Raman, an Indian physicist, was the first to see Raman spectra in 1928, along with his research partner KS Krishnan. Raman spectroscopy may offer both chemical and structural information, as well as material identification via Raman fingerprints. By detecting the Raman Scattering of a material, Raman spectroscopy retrieves this information. Whenever light is scattered by a molecule, the photon's electromagnetic oscillatory field results in the polarization of the electron cloud, leaving the molecule in a high-energy state with the photon energy imparted to it. This results in the production of a virtual state of the molecule, which is an extremely short-lived combination between a photon and a molecule. Like scattered light, this virtual state is unstable, and the photon is expelled almost instantly.

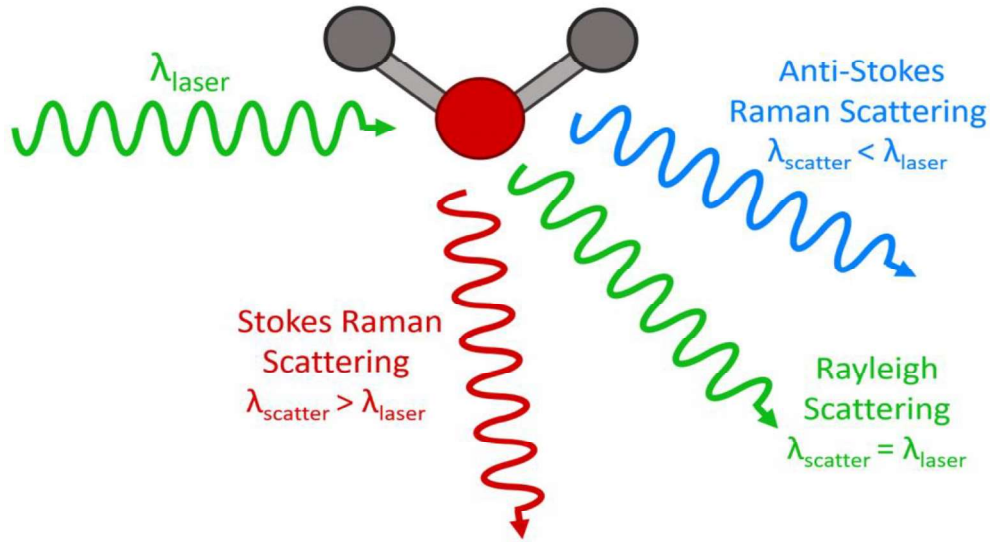


Fig. 11. Different cases of scattering

The energy of a molecule does not vary after interacting with a photon in the most of the scattering and energy, & therefore the wavelength, of the scattering photon is equal to incident photon. This is known as elastic scattering Rayleigh scattering ($\lambda_{\text{scatter}} = \lambda_{\text{laser}}$) and is the most common mechanism.

But to observe Raman scattering, we need to use certain kinds of filters in order to let in only that wavelength which satisfies the conditions for Raman Scattering. The conditions imposed on the wavelength to observe Raman Scattering is that the wavelength of the scattered photon should be either greater than or less than that of the laser used. Former is the case when we get to observe the Stokes Raman Scattering ($\lambda_{\text{scatter}} > \lambda_{\text{laser}}$) and latter is the case when we get to observe the Anti-Stokes Raman Scattering ($\lambda_{\text{scatter}} < \lambda_{\text{laser}}$) [4].

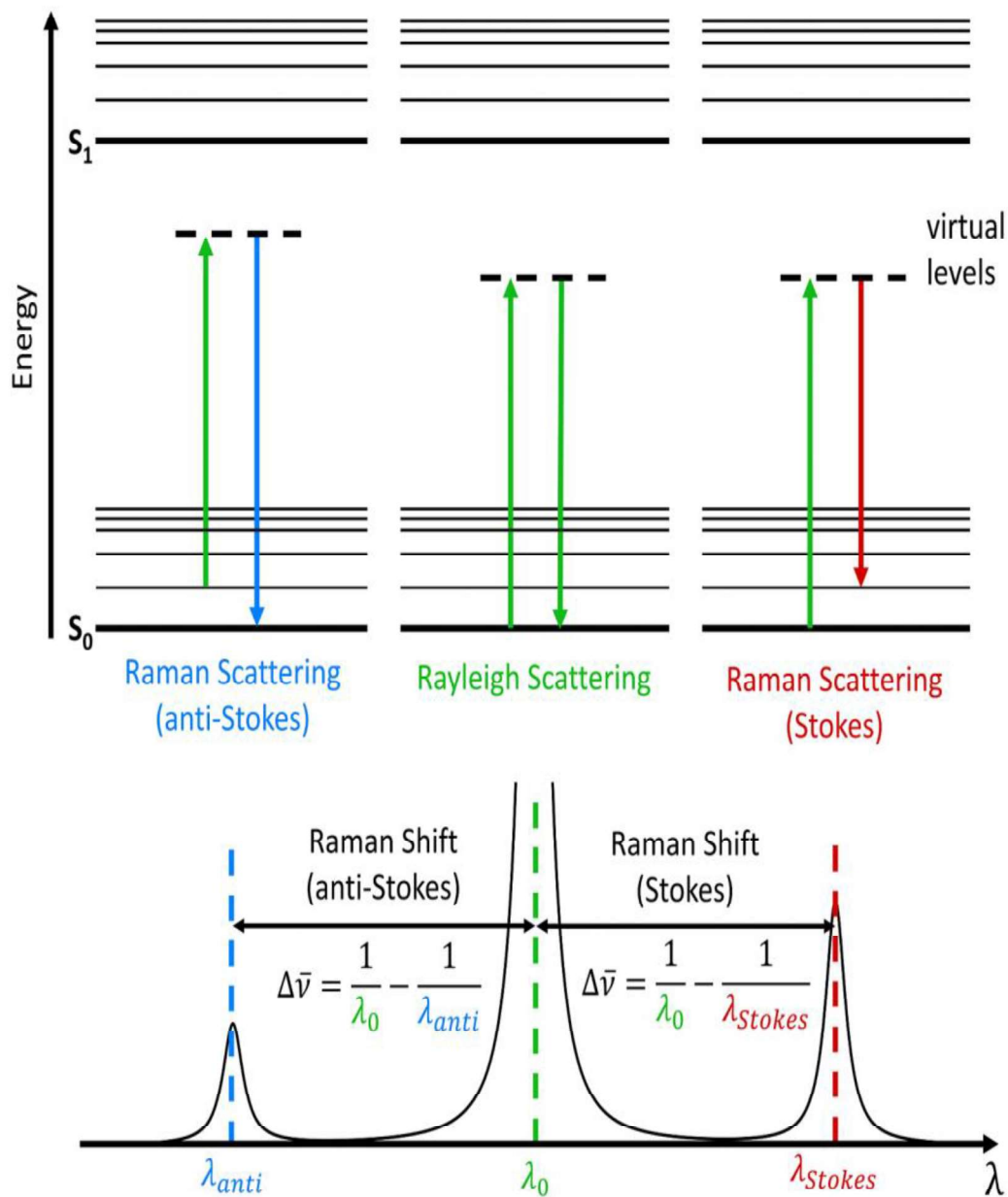


Fig. 12. Phenomenon of Raman Scattering

References:

1. P. Murugasen, S. Sagadevana and D. Shajan, “*Preparation, techniques and tools used for investigating glasses: An overview*”, Int. J. Chem. Sci.: 13(2), 2015, 693-713 ISSN 0972-768X.
2. Renata Reisfeld, “*Future technological applications of rare-earth-doped materials*”, Journal of the Less Common Metals, Volume 93, Issue 2, 1983, Pages 243-251, ISSN 0022-5088.

3. <https://www.sciencedirect.com/topics/materials-science/x-ray-diffraction>
4. Azadeh Kiani, John V. Hanna, Scott P. King, Gregory J. Rees, Mark E. Smith, Nima Roohpour, Vehid Salih, Jonathan C. Knowles, “*Structural characterization and physical properties of P₂O₅–CaO–Na₂O–TiO₂ glasses by Fourier transform infrared, Raman and solid-state magic angle spinning nuclear magnetic resonance spectroscopies*”, Acta Biomaterialia, Volume 8, Issue 1, 2012, Pages 333-340, ISSN 1742-7061.
5. Sk. Mahamuda, M. Venkateswarlu and et.al., “*Spectral characterization of Dy³⁺ ions doped phosphate glasses for yellow laser applications*”, Journal of Non-Crystalline Solids, Volume 555, 2021, 120538, ISSN 0022-3093.
6. Rajat Bajaj, A.S. Rao, G. Vijaya Prakash, “*Photoluminescence down-shifting studies of thermally stable Eu³⁺ ions doped borosilicate glasses for visible red photonic device applications*”, Journal of Non-Crystalline Solids, Volume 575, 2022, 121184, ISSN 0022-3093.

Chapter 4: Spectroscopic Characterization of Dy³⁺ ions doped Phosphate glasses for epoxy free white LED applications

4.1 Structural analysis

4.1.1. XRD spectrum:

Fig. 13 shows the XRD spectrum obtained for an un-doped ZnAlNaP glass in the $10^\circ \leq 2\theta \leq 80^\circ$ spectral region. The existence of a large hump in the recorded XRD spectrum in absence of intense peaks indicates the non-crystalline behavior of the as-prepared glass, which is a sign of long-range structural instability.

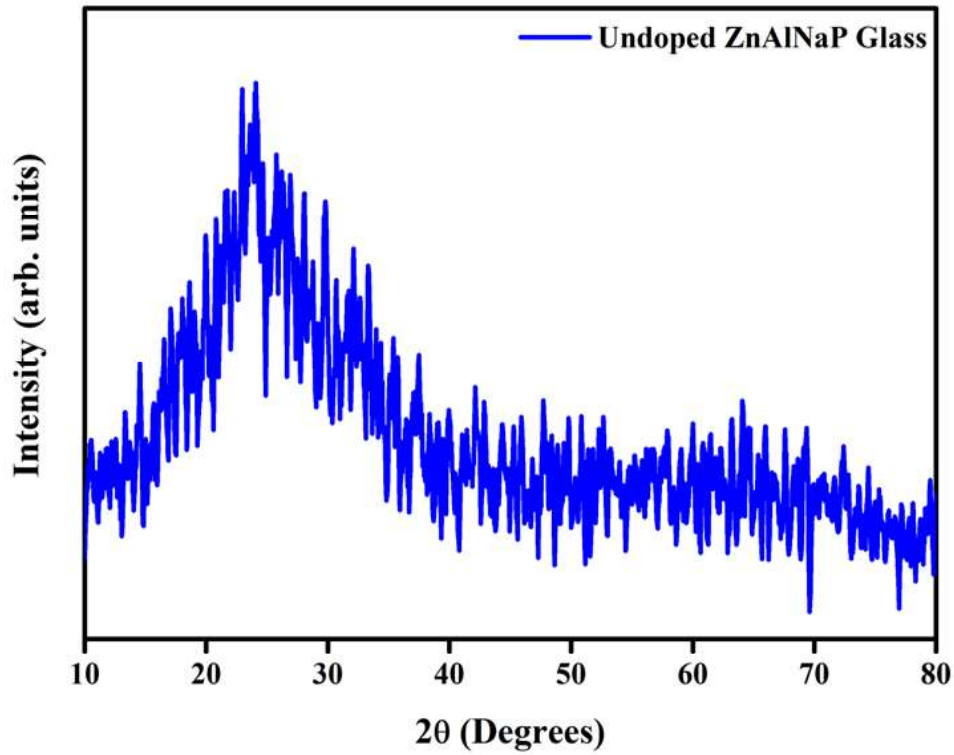


Fig. 13. XRD spectrum of the un-doped ZnAlNaP glass.

4.1.2. FT-IR spectral analysis:

The FT-IR spectrum recorded conveys information of various functional-groups involved and the characteristic vibrational modes of the phosphorus atoms in different configurations with bridging and non-bridging oxygens in the as-prepared phosphate glass. The FT-IR spectrum of an un-doped AZNP glass for the spectral range 400 to 4000 cm^{-1} , depicted in Fig. 14. Table 2 represents the positions of various peaks and their related peak assignments. The recorded spectrum indicates the translucent nature of the as-prepared phosphate glass.

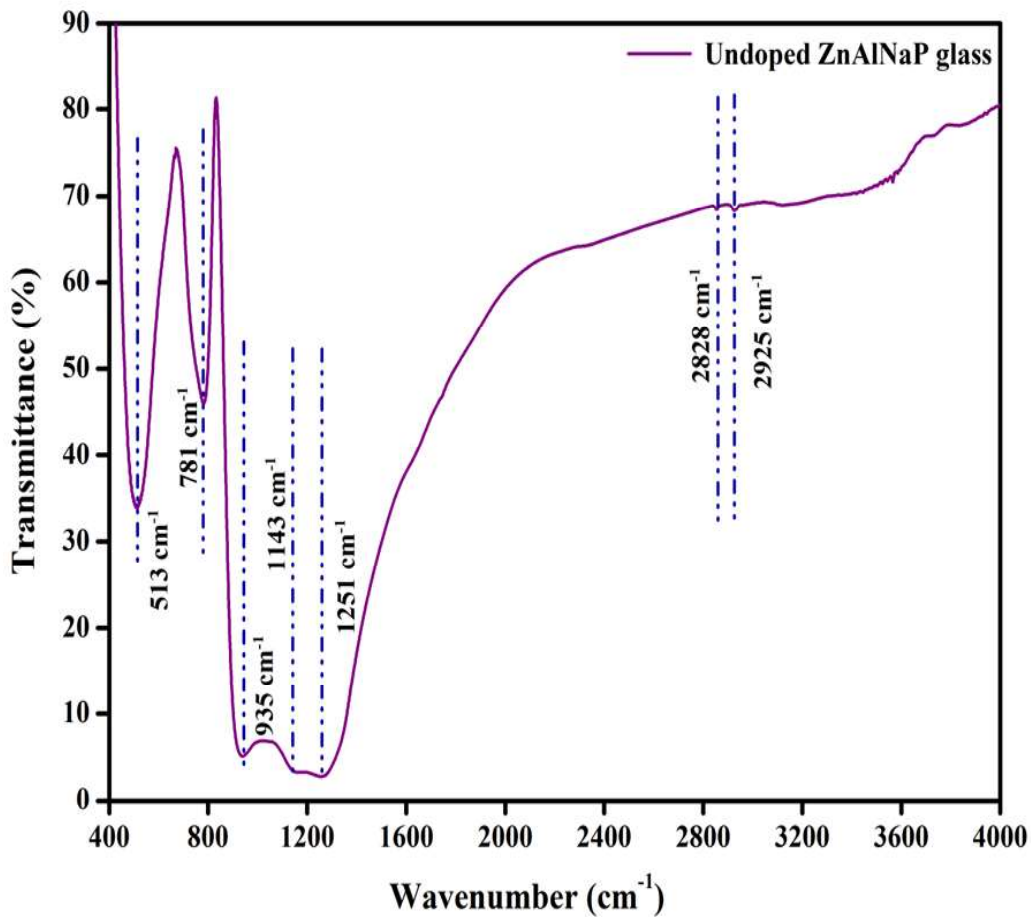


Fig. 14. FT-IR spectrum of undoped ZnAlNaP glass.

Table 2: Assignment of identified FT-IR bands for Dy³⁺ ions doped ZnAlNaP glasses.

Wavenumber (cm ⁻¹)	Assignments	References
513	harmonic P-O-P bending vibrations along with Zn-O vibrations	[1-3]
781	symmetric stretching vibration of P-O-P linkage corresponding to (PO ₄) ²⁻ tetrahedra (Q ¹ tetrahedra) with non-bridging oxygens (NBOs)	[4-7]
935	asymmetric stretching vibration of P-O-P linkage corresponding to (PO ₄) ¹⁻ tetrahedra (Q ² tetrahedra)	[8]
1143	asymmetric stretching vibration of (PO ₄) ³⁻ tetrahedra (Q ⁰ tetrahedra)	[8]
1251	asymmetric stretching vibrations of (PO ₄) ¹⁻ terminal group where two binding oxygens are bonded to phosphorus along with atoms of single NBOs	[9]
2828 & 2925	due to vibrations of P-O-H group inside the dissimilar sites	[9]

From Fig. 14, a total of seven infrared modes at 513, 781, 935, 1143, 1251, 2828 and 2925 cm⁻¹ have been identified. The first band near 513 cm⁻¹ could be attributed to harmonic P-O-P bending vibrations along with Zn-O vibrations [1-3]. The peak at 781 cm⁻¹ can be a symmetric stretching vibration of the P-O-P connection corresponding to non-bridging oxygen's (NBOs) in (PO₄)²⁻ tetrahedra (Q¹ tetrahedra) [4-7]. Similarly, the peak at 935 cm⁻¹ might be due to asymmetric stretching vibration of P-O-P linkage corresponding to (PO₄)¹⁻ tetrahedra (Q² tetrahedra). The vibrational peak marked at 1143 cm⁻¹ is the result of asymmetric stretching vibration of (PO₄)³⁻ tetrahedra (Q⁰ tetrahedra) [8]. The band seen around 1251 cm⁻¹ could be about asymmetric stretching vibrations of (PO₄)¹⁻ a terminal group where two binding oxygen's are bonded to phosphorus along with atoms of single NBOs. The two consecutive peaks at 2828 and 2925 cm⁻¹ may be due to vibrations of P-O-H group inside the different sites [9]. All the FT-IR bands have been designated according to the reported papers. The formula below can be used to calculate the OH content of a glass matrix:

$$\alpha_{OH} = \frac{\ln \frac{T_o}{T_D}}{l} \quad (3)$$

Where, T_o denotes the greatest transmission value, T_D denotes the glass transmission value at 3000 cm^{-1} and l denotes the thickness of the glass sample in question (i.e., un-doped sample in the present work). To achieve high quantum efficiency, the sample's OH content must be as low as possible. The OH concentration of the un-doped AZNP glass is 145 ppm, which is lower than other published glass samples like GeS_2 (175 ppm) [10]. Relatively less OH content obtained for the as prepared glass indicates favorable situation for radiative transitions instead of non-radiative transitions. This result supports the superior quality of the titled glasses and stood them as better choice for preparing visible various visible photonic devices with minimal radiative loss.

4.1.3. Raman spectral analysis:

The recorded Raman spectrum ($200\text{-}1400\text{ cm}^{-1}$) for ZnAlNaPDy1.0 glass is shown in Fig. 15. The Raman spectra of ZnAlNaPDy glass is used to study the existing P-O bonds and vibrational modes in our phosphate glass network. Commonly, phosphate glasses consist of Q^n groups of tetrahedral sites for connectivity (here n signifies the number of bridging oxygen atoms in each PO_4 unit). Three characteristic bands at 359 , 726 and 1195 cm^{-1} have been observed from Fig. 15.

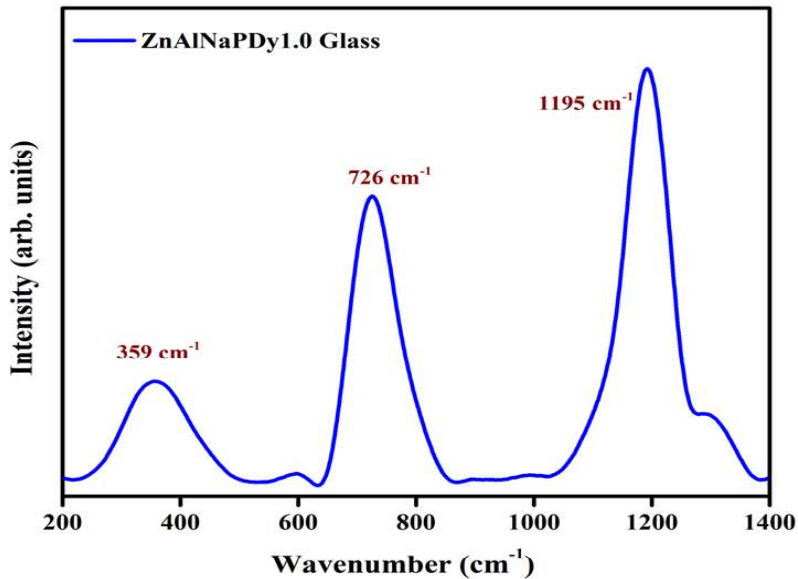


Fig. 15. Raman spectrum of 1.0 mol% Dy^{3+} doped ZnAlNaP glass.

Table 3 shows the major peak positions and their accompanying peak assignments. The most noticeable band is at 1195 cm^{-1} , which is a feature of symmetric stretching of an NBO in $(\text{PO}_4)^{1-}$

tetrahedra and could be the phonon energy for the as-prepared AZNP glass. The symmetric stretching of P-O-P connections in $(\text{PO}_4)^{1-}$ and $(\text{PO}_4)^{2-}$ tetrahedral units is attributed to the band at 726 cm^{-1} . The bending vibration of O-P-O chains in phosphate glass networks is associated with the band at 359 cm^{-1} [45–48].

Table 3: The assignments of Raman bands for Dy^{3+} ions doped ZnAlNaP glasses.

Wavenumber (cm^{-1})	Assignments	References
359	bending vibration of O-P-O chains in phosphate glass networks	[11,14]
726	symmetric stretching of P-O-P linkages in $(\text{PO}_4)^{1-}$ and $(\text{PO}_4)^{2-}$ tetrahedral units	[12-14]
1195	symmetric stretching of a NBO in $(\text{PO}_4)^{1-}$ tetrahedra	[12-14]

4.2. Thermal analysis using DSC-TGA

Fig. 16 shows the results of a DSC examination done on an un-doped ZnAlNaP glass sample with the temperature ranging between 33°C and 1200°C along with $10^\circ\text{C}/\text{min}$ heating rate. T_g , T_x , T_c and T_m are the glass transition temperature, onset crystallization temperature, peak crystallization temperature and melting temperature, respectively and the values of these parameters have been found to be equal to 156°C , 482°C , 875°C and 1043°C , respectively. Using these values, glass's thermal stability can be calculated from the formula [15,16]:

$$\Delta T = T_x - T_g \quad (4)$$

Higher values of ΔT aids glass formation by impeding the process of crystallization. Therefore, higher values of ΔT also suggest that the formed glass is relatively more thermally stable [17]. In the as-prepared un-doped ZnAlNaP glass, ΔT was found to be 326°C which is a much higher value as compared to lead aluminum borate glass (27°C) [18] and Zinc Fluoroborate tellurite glass (153°C) [17]. Glasses having ΔT values more than 100°C are regarded to be more thermally stable,

making them excellent for manufacturing optoelectronic devices, according to the published data [17].

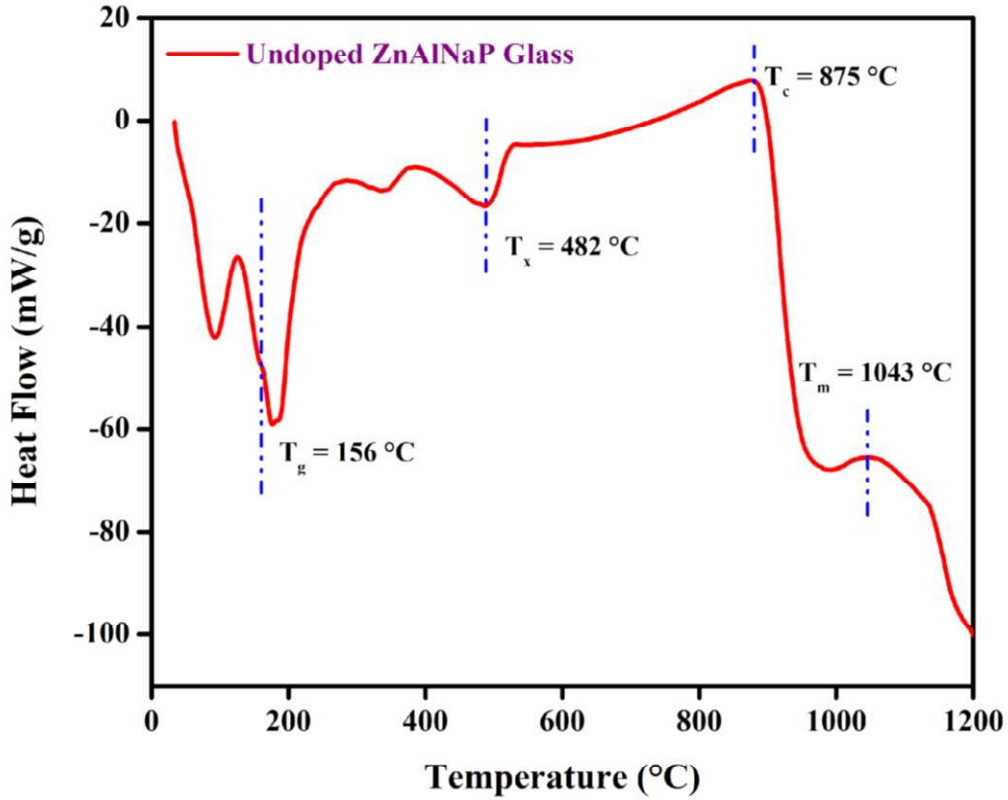


Fig. 16. DSC of the un-doped ZnAlNaP glass.

One of the other vital parameters to determine the glass's thermal stability is Hurby's parameter and is estimated from the following equation [16]:

$$K_H = \frac{T_x - T_g}{T_m - T_x} \quad (5)$$

Hurby's parameter ($K_H \geq 0.1$), has a larger value when the glass is more thermally stable [18]. The calculated K_H value for an un-doped ZnAlNaP glass is 0.5811, which is quite high and authenticate the thermal stability of the ZnAlNaP host glass.

Fig. 17 shows the TGA curve recorded for an un-doped ZnAlNaP glass, which shows a cumulative weight loss of 15.35 percent throughout a temperature range of 33°C to 1200°C. According to the

TGA curve, the loss in weight of the un-doped host glass with temperature involves in three different stages. The first stage of weight loss happens between 33°C and 129°C, the second stage occurs between 129°C and 462°C, and the third stage occurs between 462°C and 1200°C. The sample's total loss is 15.35 percent, and the sample's remaining mass is 84.65 percent. As shown in Fig. 17, the ZnAlNaP glass is thermally stable and has a lower mass loss percentage at higher temperatures.

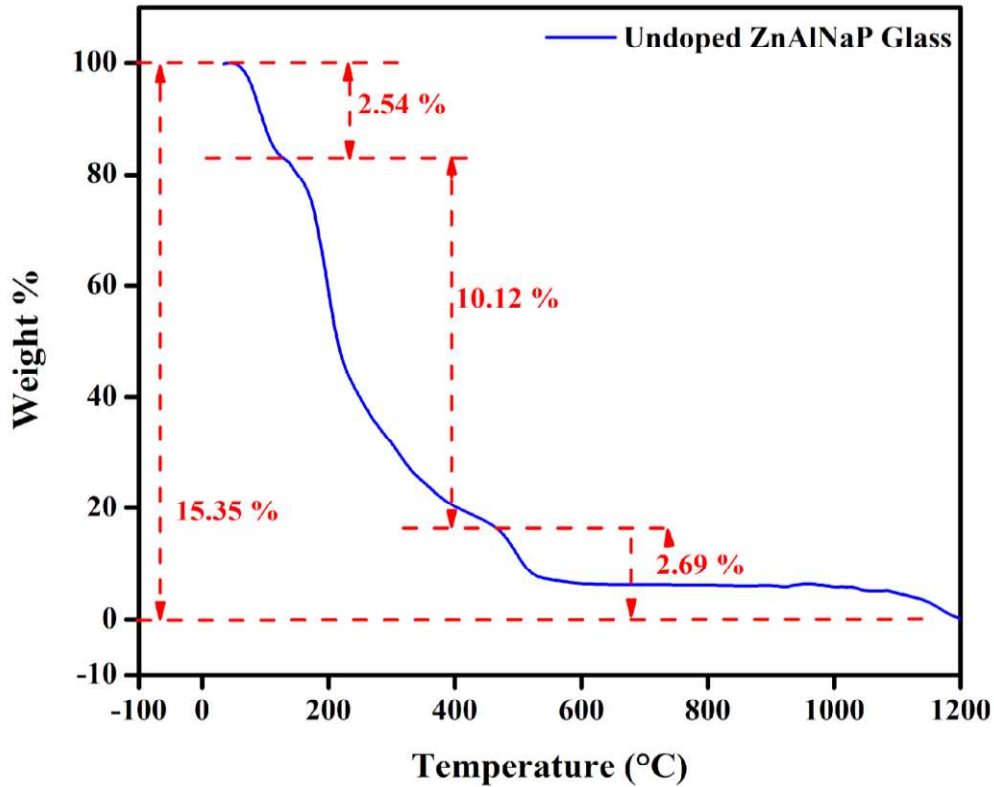


Fig. 17. TGA of the un-doped ZnAlNaP glass.

4.3. Absorption spectral study

The absorption spectra of ZnAlNaPDy glasses have been observed in wavelength range of 250-2000 nm, which covers the UV-Visible and NIR region of the electromagnetic spectrum. The humps present in the spectra clearly show the amount of absorbed light corresponding to the particular wavelength. But in the visible region, comparatively less intense bands are present. A total of 12 bands were observed, amid them five are in the UV region, two are in visible region

and five are in the NIR region. The bands in the UV region are observed at 224 nm, 325 nm, 350 nm and 387 nm, which resemble $^4D_{7/2}$, $^6P_{3/2}$, $^6P_{7/2}$ and $^4I_{13/2}$ energy levels. Whereas those in visible region are traced at 426 nm and 452 nm corresponding to $^4G_{11/2}$ and $^4I_{15/2}$. The bands present in NIR region are observed at 805 nm, 906 nm, 1097 nm and 1684 nm, which correspond to $^6F_{5/2}$, $^6F_{7/2}$, $^6H_{7/2}$, $^6F_{11/2}$ and $^6H_{11/2}$ energy levels, respectively [11,19,20]. Absorption spectra of Dy^{3+} doped ZnAlNaP glass samples are shown in Fig. 18. There were no shifts in band positions as the concentration of Dy^{3+} ions increased, but there was some variation in the corresponding intensities.

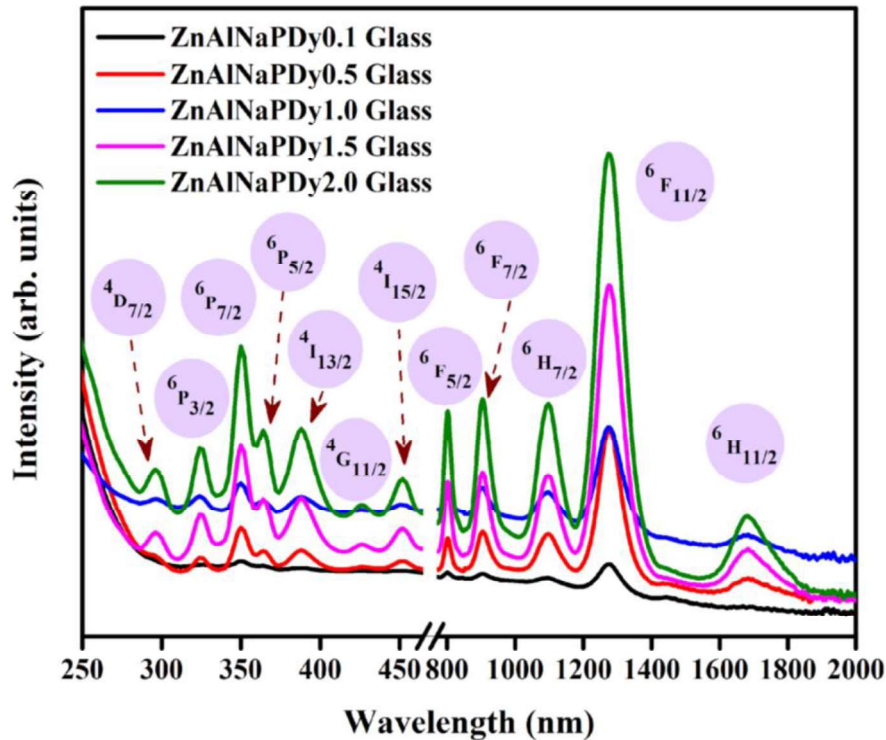


Fig. 18. Absorption spectra of Dy^{3+} doped ZnAlNaP glasses for different concentrations.

4.3.1. Nephelauxetic effect (β) and bonding parameters (δ):

The nephelauxetic effect is triggered by a partially filled f-shell, which aids in establishing the kind of link between both the RE ions and oxygen ligands in the host glass. Actually, the nephelauxetic effect causes the 4f orbital of the RE ions to distort when they are doped with the host glass. The energy level structure of RE ions is compressed, this could have possibly happened because of the overlapping oxygen and 4f-orbitals, perhaps causing a wavelength shift. We set the

terms Nephelauxetic ratio (β) and bonding parameters (δ) in this effect, which reveals the bond's nature existing among Dy^{3+} ions and the oxygen molecules contained in the host's matrix [21]. Nephelauxetic ratio is computed from the formula below:

$$\beta = \frac{\underline{\nu}_c}{\underline{\nu}_a} \quad (6)$$

Table 4: Nephelauxetic ratio (β), bonding parameter (δ), band gap (eV) and Urbach energy (eV) for Dy^{3+} ions doped ZnAlNaP glasses.

Sr. No.	Glass System	Nephelauxetic ratio	Bonding Parameters	Band Gap (eV)		Urbach Energy (eV)
		β	δ	Direct Band Gap	Indirect Band Gap	
1.	ZnAlNaPDy0.1 Glass	1.00367	-0.3652	4.70	3.80	0.47
2.	ZnAlNaPDy0.5 Glass	1.00294	-0.2929	4.66	3.78	0.42
3.	ZnAlNaPDy1.0 Glass	1.00396	-0.3946	4.63	3.67	0.43
4.	ZnAlNaPDy1.5 Glass	1.00293	-0.2929	4.43	3.28	0.64
5.	ZnAlNaPDy2.0 Glass	1.00319	-0.3183	4.33	2.90	1.19

where, $\underline{\nu}_c$ denotes the wavenumber related to a certain RE ion transition under consideration, $\underline{\nu}_a$ denotes the wavenumber of the same transition for an aqua ion. Table 4 shows expected β values to the corresponding glasses as the concentration of Dy^{3+} ions increase. The values of the bonding parameters (δ) can be computed using the equation below:

$$\delta = \frac{1-\beta}{\beta} \times 100 \quad (7)$$

where, $\underline{\beta}$ represents the average value of β . The field environment of the ligands surrounding the Rare Earth ions can have a great effect on the bonding parameter δ . The positive or negative values

of the bonding parameters signify the ionic and covalent behavior of bonding between Dy³⁺ ions and the oxygen ligands. Table 4 lists the estimated values of the bonding parameter for the as-prepared ZnAlNaPDy glass samples. The negative values signify ionic nature of the bond existing among the Dy³⁺ ions and the oxygen molecules [21].

4.3.2. Band gap energy and Urbach's energy:

For each sample, bandgap was calculated by the extrapolation of the linear region in the $\alpha h\nu$ plot (as shown in Fig. 19) between absorption coefficient ($\alpha h\nu$) and energy ($h\nu$), defined by the following equation [22]:

$$\alpha h\nu = C(h\nu - E_g)^n \quad (8)$$

where C is a constant, $h\nu$ is energy of photon, and exponent is denoted by n , which can vary depending on the situation, such as 1/2 for direct allowed, 2 for indirect allowed, 1/3 for indirect forbidden, and 3 for direct forbidden transitions. The evaluated values of direct and indirect band gap values for the as-prepared ZnAlNaPDy glass samples are listed in Table 4 and the respective graphs are shown in Fig. 19. The optical band gap E_g provides the information about the onset of the optical absorption and Urbach energy is a concept that is used to describe the energetic aberrations in the optical band gap. It is obtained by fitting the absorption coefficient (α) as a function of energy ($h\nu$) to the exponential function given by the formula underneath [57]:

$$\alpha = \alpha_0 \exp\left(\frac{h\nu}{\Delta E}\right) \quad (9)$$

where, ΔE is denotes the Urbach's energy and α_0 is a constant. The steepness of the beginning of absorption near the band gap is measured by this energy. A lower Urbach energy is indicated by a sharp onset of absorption. The calculated values of ΔE are tabulated in Table 4 and are observed to be in range of 0.42-1.19 eV. Urbach energies with lower values indicate that the associated glass system has less disorder.

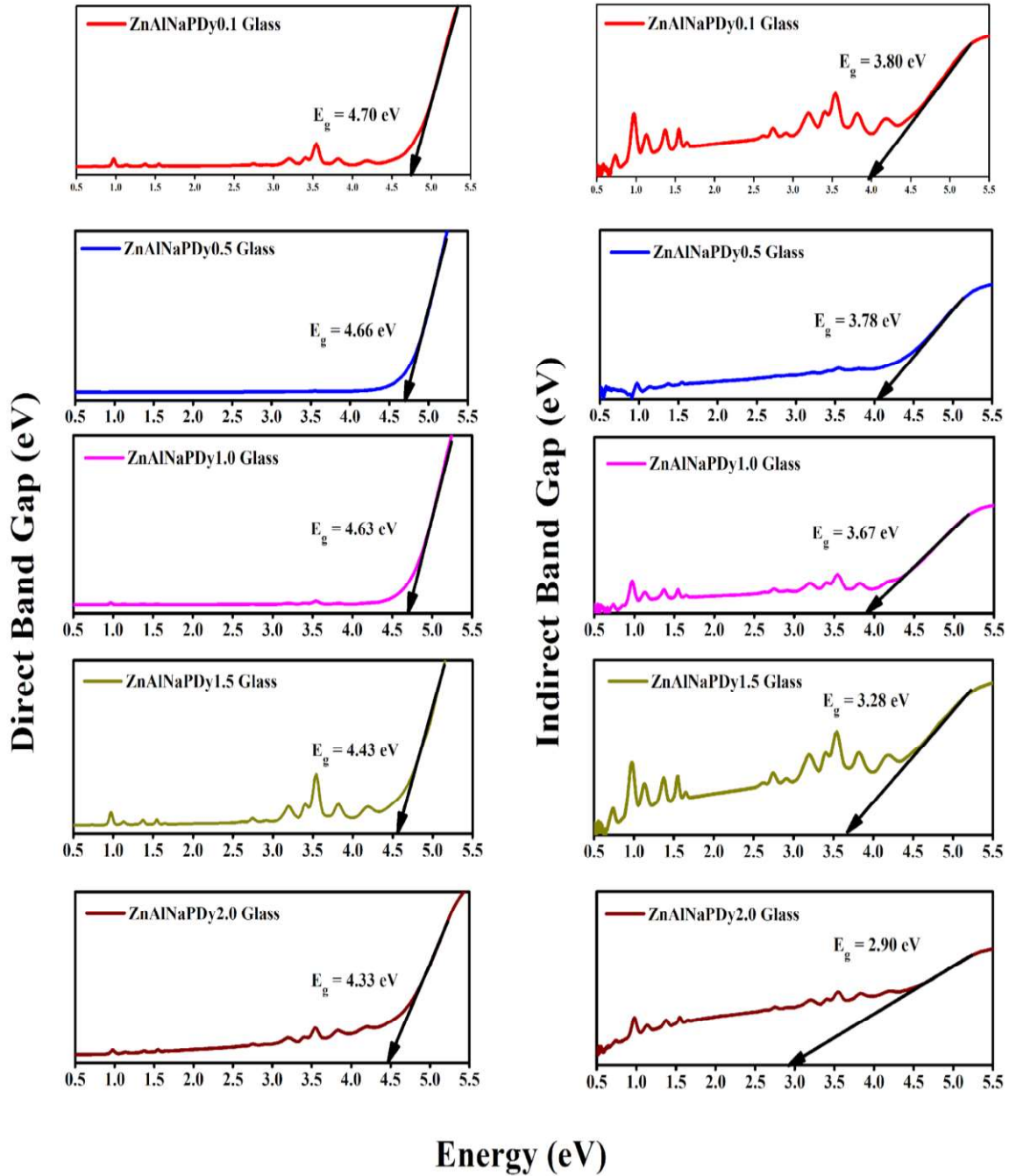


Fig. 19. Tauc plot for optical band gap of Dy^{3+} doped ZnAlNaP glasses for different concentrations.

4.3.3. Physical parameters:

The various physical parameters mentioned in the Table 5 are evaluated using the following formulae:

Linear refractive index (n_o): The linear refractive index of all studied glasses may be computed using the optical bandgap values in the following equation. [24,25]:

$$n_o = [6 \sqrt{\frac{5}{E_g}} - 2]^{1/2} \quad (10)$$

Dielectric constant (ϵ_o) [26]:

$$\epsilon_o = n_o^2 \quad (11)$$

Reflection Loss (R) [26]:

$$R = \left(\frac{n_o - 1}{n_o + 1} \right)^2 \quad (12)$$

Linear susceptibility $x^{(1)}$ [24,25]:

$$x^{(1)} = \left(\frac{n_o^2 - 1}{4\pi} \right) esu \quad (13)$$

Non-linear susceptibility $x^{(3)}$: Miller's rule is used to define third-order nonlinear susceptibility. [24,25]:

$$x^{(3)} = x^{(1)} \times 1.7 \times 10^{-10} esu$$

$$\text{or, } x^{(3)} = \left(\frac{n_o^2 - 1}{4\pi} \right) \times 1.7 \times 10^{-10} esu \quad (14)$$

Non-linear refractive index (n_2) [24,25]:

$$n_2 = \left(\frac{12\pi}{n_o} \right) x^{(3)} \quad (15)$$

In Fig. 20, all of the physical properties listed above are plotted versus the Dy^{3+} ion concentration in ZnAlNaP glasses. Because of the excitation energy, the optical band gap energy dropped as the Dy^{3+} ion concentration is increased. Because the refractive index is directly proportional to the concentration of Dy^{3+} ions, all other properties were shown to rise with the concentration of Dy^{3+} ions. The third order nonlinear susceptibility $x^{(3)}$ was observed to rise as the amount of Dy^{3+} ions increased. It could be owing to the glass network's strong polarization caused by Dy^{3+} ions in the ZnAlNaP glass.

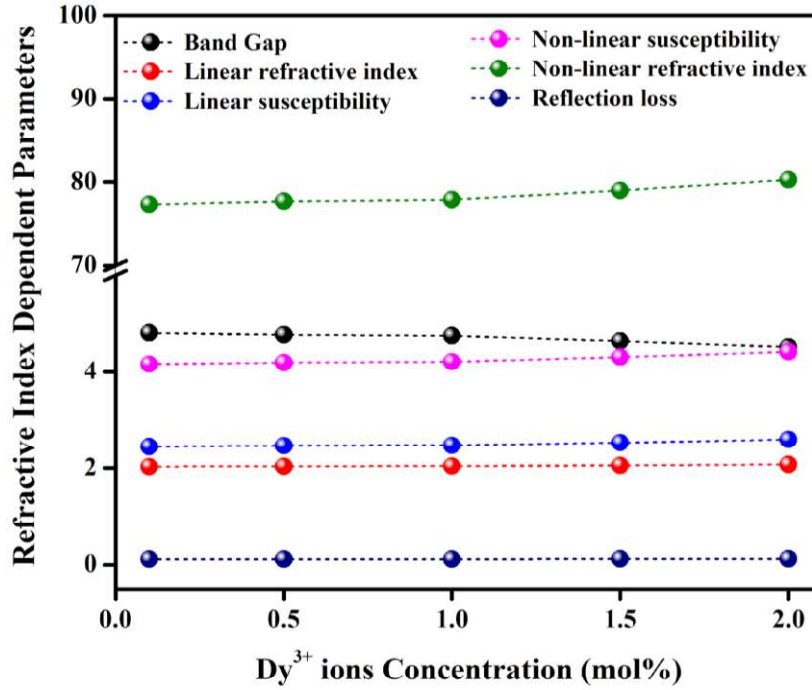


Fig. 20. Variation of physical parameters that are dependent on refractive index as a function of Dy³⁺ ion concentration in ZnAlNaP glasses.

Table 5: Physical properties of Dy³⁺ ions doped ZnAlNaP glasses.

Sr. No.	Physical properties	ZnAlNaPDy0.1 Glass	ZnAlNaPDy0.5 Glass	ZnAlNaPDy1.0 Glass	ZnAlNaPDy1.5 Glass	ZnAlNaPDy2.0 Glass
1.	Optical band gap (E _g) (eV)	4.81	4.77	4.75	4.64	4.52
2.	Linear refractive index (n ₀)	2.029	2.035	2.038	2.056	2.076
3.	Dielectric constant (ε ₀)	4.116	4.141	4.153	4.227	4.309
4.	Reflection loss (R)	0.115	0.116	0.117	0.119	0.122
5.	Linear susceptibility (χ ¹) [esu]	2.447	2.467	2.476	2.534	2.599
6.	Non-Linear susceptibility (χ ³) (×10 ⁻¹⁰ esu)	4.161	4.194	4.210	4.308	4.419
7.	Non-Linear refractive index, (n ₂) (×10 ⁻¹⁰ esu)	77.321	77.697	77.884	79.006	80.249

4.4. PL spectral analysis

To investigate the PL properties of the Dy^{3+} doped ZnAlNaP glasses, it is required to know the appropriate wavelengths of excitation and emission. One such graph of intensity versus wavelength for ZnAlNaPDy2.0 glass is shown in Fig. 21. In Fig. 21, the left half of the graph exhibits excitation spectrum in the wavelength region of 300-450 nm under the emission wavelength of 573 nm. Similarly, the PL emission spectrum for the same is shown on the right half of the graph for the wavelength range being 450-700 nm under the emission wavelength of 350 nm. It is commonly acknowledged that more atoms can be stimulated to a metastable state from the ground state when a sharp and intense excitation wavelength is used to excite a luminescent material. A relatively more intense emission peak observed in the visible PL emission spectrum at 573 nm was used as the emission wavelength to record PL excitation spectra. Similarly, the prominent PL excitation peak observed within the UV region at 350 nm, has been used as an excitation wavelength for recording the PL emission spectra.

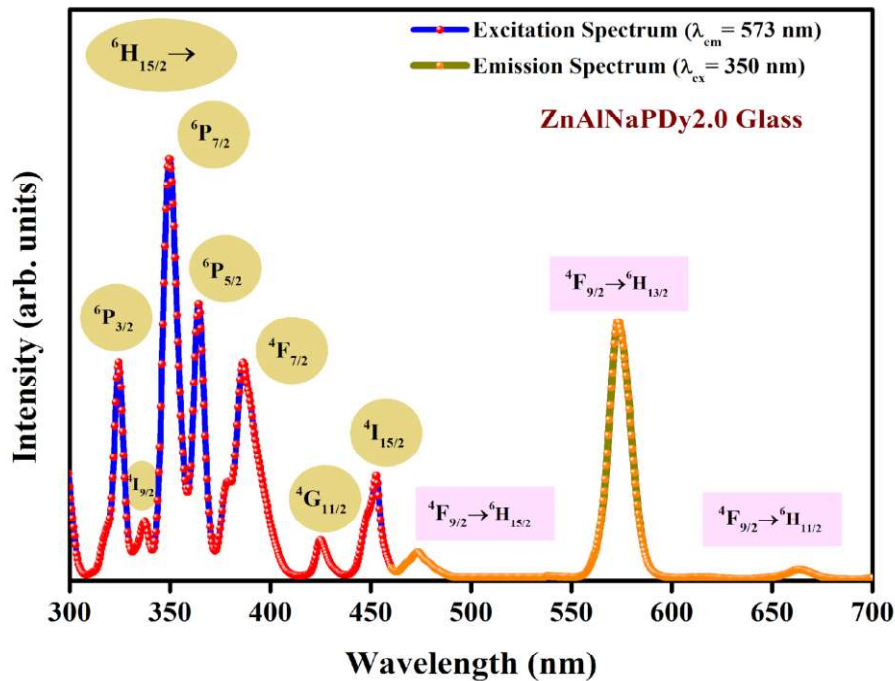


Fig. 21. PL Excitation and PL emission spectrum of 2.0 mol% Dy^{3+} ion doped ZnAlNaP glass recorded at $\lambda_{em} = 573 \text{ nm}$ and $\lambda_{ex} = 350 \text{ nm}$.

Seven major peaks were observed corresponding to 323 nm, 336 nm, 350 nm, 363 nm, 383 nm, 427 nm, 453 nm in the excitation spectrum region and three major peaks at 473 nm, 575 nm and 664 nm in the emission spectrum. The transitions corresponding to the peaks were labelled as ${}^6P_{3/2}$, ${}^4I_{9/2}$, ${}^6P_{7/2}$, ${}^6P_{5/2}$, ${}^4F_{7/2}$, ${}^4G_{11/2}$ and ${}^4I_{15/2}$ in the excitation region and ${}^4F_{9/2} \rightarrow {}^6H_{15/2}$ (Blue), ${}^4F_{9/2} \rightarrow {}^6H_{13/2}$ (yellow) and ${}^4F_{9/2} \rightarrow {}^6H_{11/2}$ (red) in the emission spectrum region [11,27]. In the current PL analysis, the blue emission transition (${}^4F_{9/2} \rightarrow {}^6H_{15/2}$) is magnetic-dipole (MD) in nature and the consecutive yellow emission transition (${}^4F_{9/2} \rightarrow {}^6H_{13/2}$) is electric-dipole (ED) ($\Delta L=2$, $\Delta J=2$) in nature [28,29]. The current research revealed that the magnetic dipole transition is unaffected by the atoms' local crystal environment in the as-prepared glass samples. The electric dipole transition is described as a hypersensitive emission, implying that its intensity is affected by the glass matrix's local surroundings. Furthermore, it was discovered that MD transitions dominate ED transitions in the current investigation, implying that Dy^{3+} ions are occupying high symmetry sites with an inversion center [30,31]. At 350 nm excitation wavelength, all the glass samples had a comparable profile of emission spectra, with no shift in emission bands (Fig. 22).

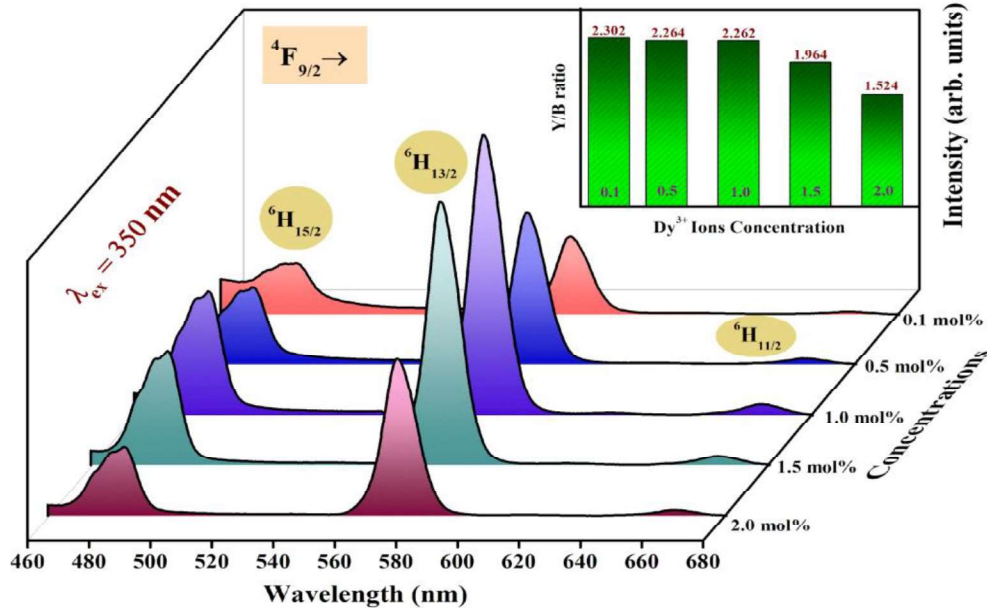


Fig. 22. PL emission spectra of Dy^{3+} ions doped ZnAlNaP glasses at $\lambda_{ex} = 350$ nm [The inset bar diagram shows Y/B ratio].

In addition, we can see in Fig. 22 that as we increase concentration of Dy^{3+} ions up to 1.0 mol percent, the emission intensity increases, then decrease. Quenching concentration via resonant energy transfer (RET) among Dy^{3+} ions can be read as this trend in intensity according to Dy^{3+} ions concentration, which also explains the energy level diagram's two cross-relaxation channels (CR1 and CR2). Fig. 23 depicts a schematic energy level diagram of as-prepared ZnAlNaPDy glasses and it describes energy transfer and types along possible cross-relaxation channels in the excitation and emission spectra, which is based on the down-conversion phenomenon because of the Dy^{3+} ions present in as-prepared ZnAlNaP glasses. As a result of the non-radiative transitions at the higher energy levels, the metastable state ($^4F_{9/2}$) becomes densely populated very quickly. As a result of the radiative transitions that occur from the metastable state, intense blue and yellow emission is produced.

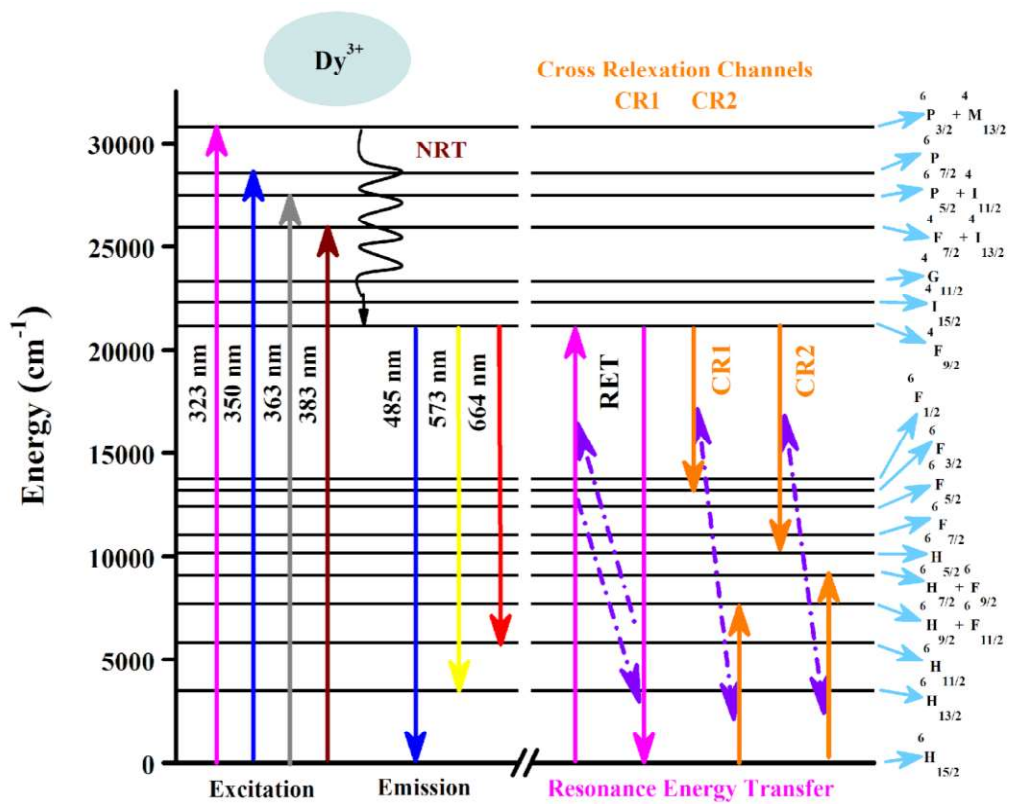


Fig. 23. Energy level diagram for Dy^{3+} doped ZnAlNaP glasses.

To investigate the non-symmetric characteristics of network surrounding Dy³⁺ ions within host glass's matrix, intensity ratios of yellow to blue (Y/B) have been evaluated for each Dy³⁺ ions doped ZnAlNaP glass sample. Table 8 shows the Y/B value calculated for each glass sample. The effect of Dy³⁺ ions on the local environment of the ZnAlNaP glass matrix, and therefore on the intensity of the hypersensitive (⁴F_{9/2} → ⁶H_{13/2}) transition, could explain the change in Y/B ratios. The Y/B ratio values decrease as the concentration of Dy³⁺ ions increase, as shown in the inset of Fig. 22. In addition, the Y/B ratio values for the prepared ZnAlNaP glass series is closer to 2, indicating that the bonds between Dy³⁺ and O²⁻ ions have a high covalence nature. These visible emission Y/B ratio data indicate that as-prepared Dy³⁺ doped ZnAlNaP glasses are capable of generating white light [32,33]. The Y/B ratios computed in the present work have been compared with some other reported studies [42, 34-36] and it was found that for the as-prepared glasses Y/B ratio is relatively high, shown in Table 6.

Table 6: Comparison of CIE color chromaticity co-ordinates and Y/B ratio of ZnAlNaPDy1.5 glass with some reported data.

Sr. No.	Glass System	CIE Chromaticity Coordinates	Y/B ratio	References
1.	ZnAlNaPDy1.5 Glass	(0.34, 0.37)	1.96	Present Work
2.	ZPABDy1.0 Glass	(0.31, 0.36)	0.74	[42]
3.	BCACDy0.5 Glass	(0.38, 0.41)	2.09	[34]
4.	AECBDy1.0 Glass	(0.29, 0.33)	0.88	[35]
5.	SLBDy1.0 Glass	(0.36,0.37)	1.11	[36]

4.5. PL decay analysis

The PL decay curves for the ⁴F_{9/2} → ⁶H_{13/2} transition observed for the as-prepared Dy³⁺ ions activated ZnAlNaP glasses at λ_{ex} = 350 nm, are shown in Fig. 24. It can be seen that all the decay curves have a single exponential fit and the normalized experimental decay curves have been fitted using the formula:

$$y = y_0 + A e^{-t/\tau_{exp}} \quad (16)$$

Here, ‘ y ’ and ‘ y_0 ’ represent the intensities at time ‘ t ’ and $t = 0$ respectively, A and τ_{exp} are the amplitude and experimental decay time of the spectra. The exponentially decaying curves could be due to the fast decay of the excited Dy^{3+} ions. Another possible reason for the single exponential nature of the decay curves could be the lesser effect of ligands on Dy^{3+} ions in the glass matrix [37]. The measured decay lifetimes for ZnAlNaPDy glasses as depicted in Table 8. It can be perceived that experimental decay time values are decreasing with increasing Dy^{3+} ions concentration.

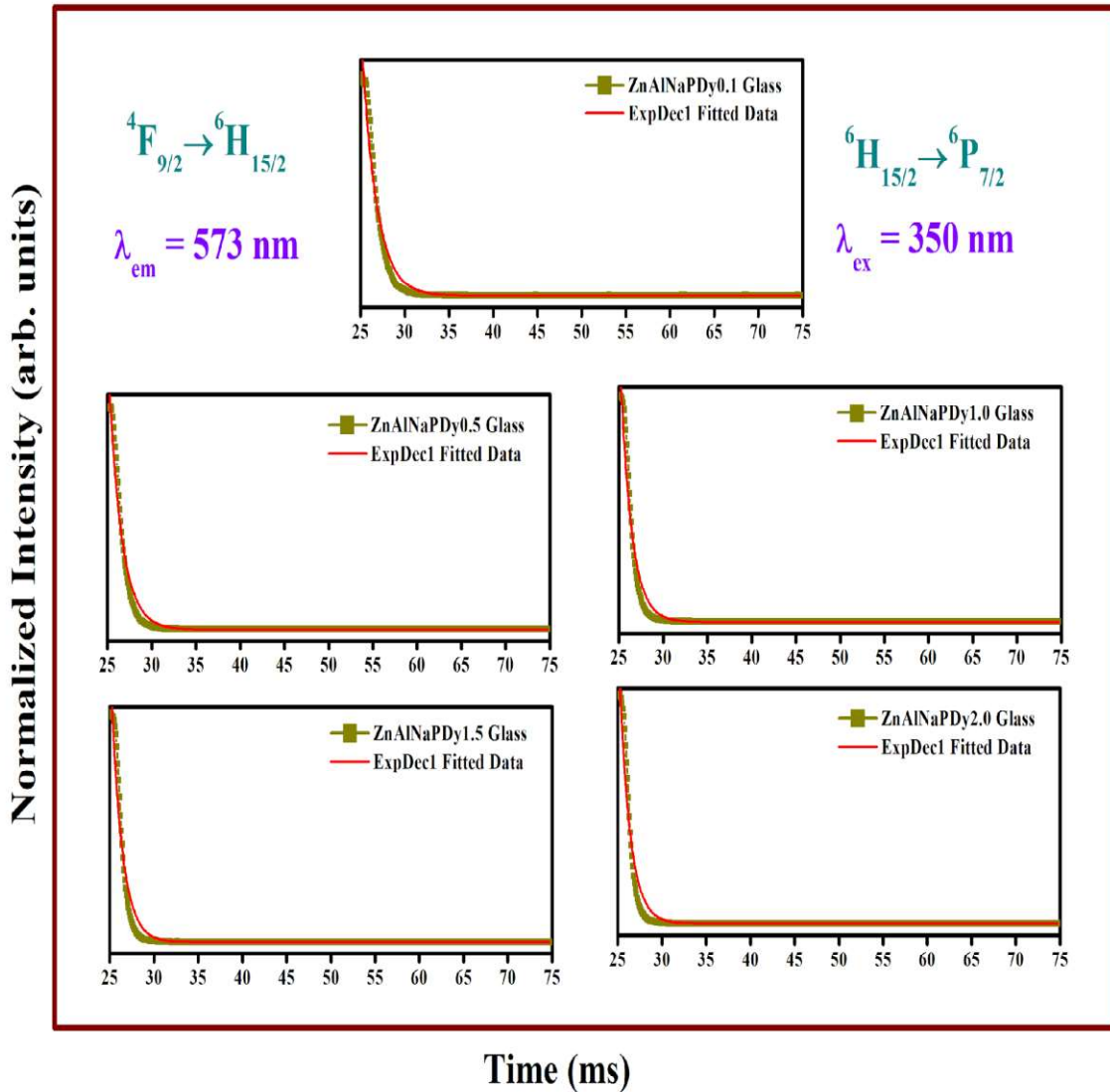


Fig. 24. Decay profile of Dy^{3+} ions in ZnAlNaP glasses for ${}^4F_{9/2} \rightarrow {}^6H_{13/2}$ (573 nm) transition and 350 nm excitation wavelength.

As we increase concentration of Dy³⁺ ions in the host glass matrix, number of Dy³⁺ ions reaching the metastable state will increase, and this automatically decreases the distance of separation between them. The distance of separation between the Dy ions reached to an optimum value leads to energy migration among the Dy ions through cross-relaxation mechanism leading to a decrease in the experimental lifetime (τ_{exp}) [20]. The τ_{exp} values measured for the titled glasses are compared with the corresponding values for other glasses in Table 7 [42,34,35,38]. As per the data appearing in Table 7, it can be seen that τ_{exp} values of the ZnAlNaP glasses are somewhat relatively higher than the other values reported for other glasses.

Table 7: Comparison of τ_{exp} of ZnAlNaPDy1.0 glass with some reported data.

Sr. No.	Glass System	τ_{exp} (ms)	References
1.	ZnAlNaPDy1.0 Glass	1.26	Present Work
2.	ZPABDy1.5 Glass	0.12	[42]
3.	BCACDy5.0 Glass	0.51	[35]
4.	AECBDy1.0 Glass	0.53	[35]
5.	PKMADy10.0 Glass	0.71	[38]
6.	PKMFADy10.0Glass	0.79	[38]

4.6. Colorimetric analysis

The CIE chromaticity coordinates were computed from the PL emission spectra to observe the emission color of the as-prepared ZnAlNaPDy glass series. The following equations can be used to calculate CIE-coordinates (x, y) using tristimulus X, Y and Z values.

$$x = \frac{X}{X+Y+Z} \quad (17)$$

$$y = \frac{Y}{X+Y+Z} \quad (18)$$

The Correlated Color Temperature (CCT) values of the samples were also calculated using the following formula [39]:

$$CCT = -449n^3 + 3525n^2 - 6823.2n + 5520.3 \quad (19)$$

where $n = \frac{x-x_e}{y-y_e}$ with $x_e = 0.332$ and $y_e = 0.186$, which are the coordinates of the epicenter of the CIE 1931 diagram [40]. The chromaticity coordinates values and their respective CCT values are represented in Table 8. The CCT values of ZnAlNaPDy1.5 were reported to be in the cool white region as shown in Fig. 25. The values of the CIE chromaticity coordinate of the present work have been compared with some other reported studies [34-36] and are listed in Table 6. As a result of the foregoing discussion, it can be concluded that the Dy³⁺ ions doped ZnAlNaP glasses are the optimum choice for the production of white light under n-UV excitation.

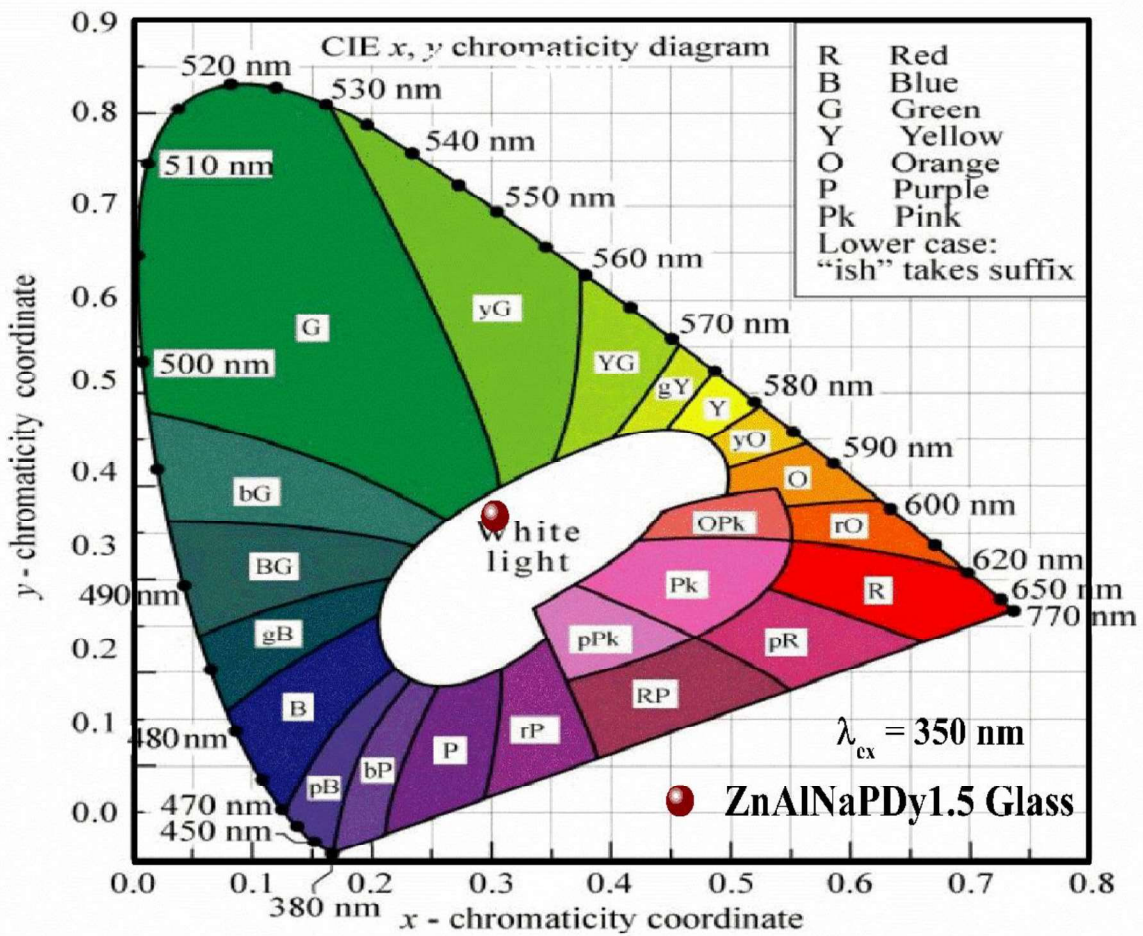


Fig. 25. CIE chromaticity diagram of Dy³⁺ doped ZnAlNaPDy1.5 glasses at $\lambda_{ex} = 350$ nm.

Table 8: CIE Co-ordinates, yellow to Blue (Y/B) intensity ratio and experimental lifetime (τ_{exp} (ms)) of Dy^{3+} ions doped ZnAlNaP glasses.

Sr. No.	Glass System	CIE Co-ordinates		CCT	Y/B Ratio	τ_{exp} (ms)
		CIE X	CIE Y			
1.	ZnAlNaPDy0.1 Glass	0.23	0.20	76006	2.30	1.68
2.	ZnAlNaPDy0.5 Glass	0.29	0.29	8768	2.26	1.46
3.	ZnAlNaPDy1.0 Glass	0.36	0.40	4703	2.26	1.26
4.	ZnAlNaPDy1.5 Glass	0.34	0.37	5214	1.96	1.23
5.	ZnAlNaPDy2.0 Glass	0.34	0.36	4963	1.52	1.19

4.7. Temperature-dependent PL (TD-PL) studies and activation-energy estimation

To investigate the thermal profile of the as-prepared ZnAlNaP glass samples, the optimized glass of the present series i.e., ZnAlNaPDy1.0 glass was taken under consideration and the temperature-dependent PL spectrum was recorded using FLMS15147 spectrometer with 350 nm excitation within the temperature range of 30°C (Room temperature) to 200°C. With increasing temperature, the PL emission intensity was observed to be decreasing for ZnAlNaPDy1.0 glass as shown in Fig. 26. The inset of Fig. 26 depicts variation of normalized intensity of ${}^4\text{F}_{9/2} \rightarrow {}^6\text{H}_{13/2}$ transition within the temperature range of 298-473 K by considering the intensity as 100% at 30°C. At 200°C, the emission intensity was 74.4 %, which decreased by 25.6 % only. The 74.4 % retention of the PL emission intensity at 200 °C signifies the thermal stability of as-prepared ZnAlNaP glasses doped with different Dy^{3+} ions concentration.

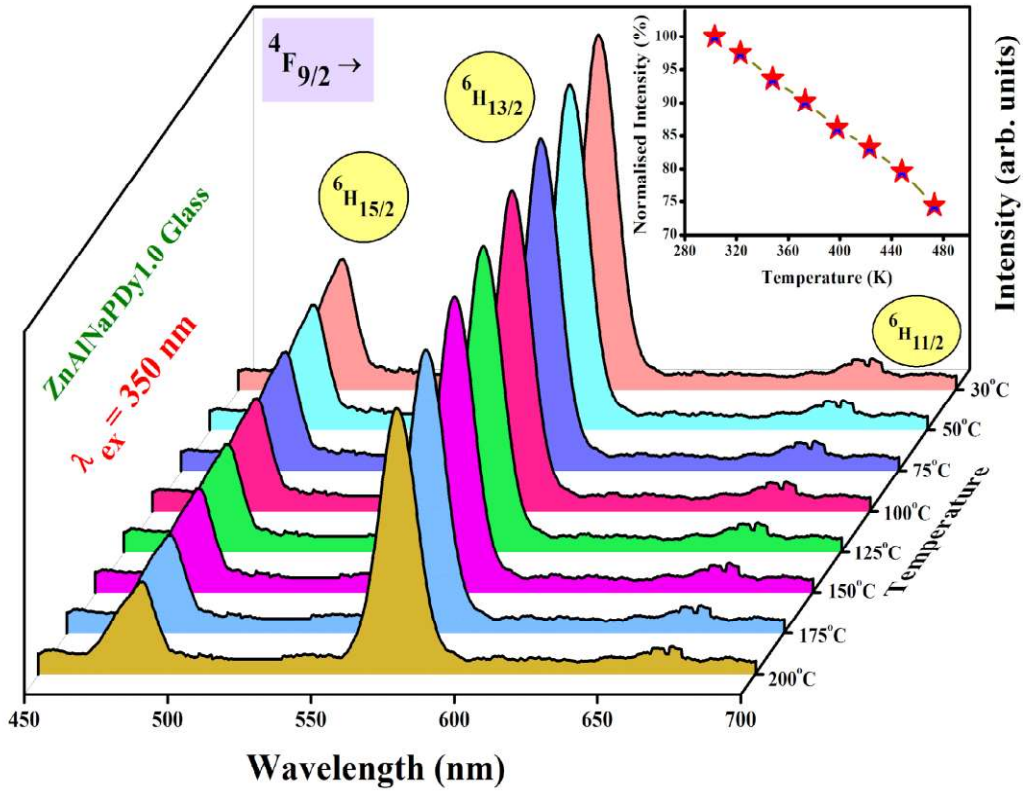


Fig. 26. Temperature dependent PL emission intensity variation of ZnAlNaPDy1.0 glass under 350 nm excitation wavelength [Inset shows variation of Normalized intensity with temperature (K)].

In addition, the activation energy (ΔE) of the glass sample was estimated using the Arrhenius equation, which describes the relationship between temperature and emission intensity [41]:

$$I_T = \frac{I_0}{1 + C \exp\left(-\frac{\Delta E}{K_B T}\right)} \quad (20)$$

Where I_0 and I_T are the emission intensities at room temperature and other temperatures in Kelvin respectively, C and K_B (8.617×10^{-5} eV/K) denotes the arbitrary constant and the Boltzmann constant, respectively. The slope of the linearly fitted graph plotted for $\ln((I_0/I_T)-1)$ versus $1/K_B T$, shown in Fig. 27, gives the desired value of the system's activation energy (ΔE). The estimated activation energy for ZnAlNaP glass doped with 1 mol% of Dy^{3+} ions was 0.212 eV which shows the good temperature stability of as-prepared Dy^{3+} doped AZNP glasses.

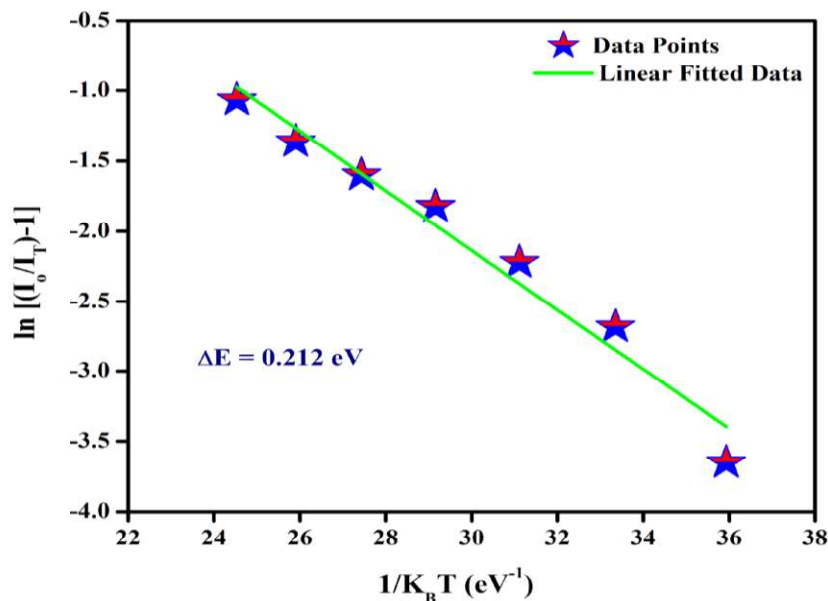


Fig. 27. Linear fitted curve of $\ln[(I_0/I_T)-1]$ versus $1/K_B T$.

References:

1. R.K. Brow, D.R. Tallant, S.T. Myers, C.C. Phifer, The short-range structure of zinc polyphosphate glass, *Journal of Non-Crystalline Solids*. 191 (1995) 45–55. [https://doi.org/10.1016/0022-3093\(95\)00289-8](https://doi.org/10.1016/0022-3093(95)00289-8).
2. J.J. Hudgens, S.W. Martin, Glass Transition and Infrared Spectra of Low-Alkali, Anhydrous Lithium Phosphate Glasses, *Journal of the American Ceramic Society*. 76 (1993) 1691–1696. <https://doi.org/10.1111/j.1151-2916.1993.tb06636.x>.
3. K. Meyer, Characterization of the structure of binary zinc ultraphosphate glasses by infrared and Raman spectroscopy, *Journal of Non-Crystalline Solids*. 209 (1997) 227–239. [https://doi.org/10.1016/S0022-3093\(96\)00563-7](https://doi.org/10.1016/S0022-3093(96)00563-7).
4. R.C. Lucacel, A.O. Hulpus, V. Simon, I. Ardelean, Structural characterization of phosphate glasses doped with silver, *Journal of Non-Crystalline Solids*. 355 (2009) 425–429. <https://doi.org/10.1016/J.JNONCRY SOL.2008.12.012>.
5. L. Montagne, G. Palavit, G. Mairesse, ³¹P MAS NMR and FT IR analysis of (5R_x/2)Na₂O.xBi₂O₃.(5R_x/2)P₂O₅ glasses, *Physics and Chemistry of Glasses*. 37 (1996) 206–211.
6. V. Sudarsan, R. Mishra, S.K. Kulshreshtha, Thermal and structural studies on TeO₂ substituted (PbO)_{0.5}(P₂O₅)_{0.5} glasses, *Journal of Non-Crystalline Solids*. 342 (2004) 160–165. <https://doi.org/10.1016/J.JNONCRY SOL.2004.07.014>.

7. P.Y. Shih, H.M. Shiu, Properties and structural investigations of UV-transmitting vitreous strontium zinc metaphosphate, *Materials Chemistry and Physics*. 106 (2007) 222–226. <https://doi.org/10.1016/J.MATCHEMPHYS.2007.05.038>.
8. A.M. Efimov, V.G. Pogareva, Water-related IR absorption spectra for some phosphate and silicate glasses, *Journal of Non-Crystalline Solids*. 275 (2000) 189–198. [https://doi.org/10.1016/S0022-3093\(00\)00250-7](https://doi.org/10.1016/S0022-3093(00)00250-7).
9. C. Shivakumara, R. Saraf, P. Halappa, White luminescence in Dy³⁺ doped BiOCl phosphors and their Judd–Ofelt analysis, *Dyes and Pigments*. 126 (2016) 154–164. <https://doi.org/10.1016/J.DYEPIG.2015.10.032>.
10. B.B. Kale, A. Jha, S.K. Apte, P. v Adhyapak, D.P. Amalnerkar, Removal of OH impurities from GeS₂ by reactive atmosphere and its glass preparation, *Materials Chemistry and Physics*. 78 (2003) 330–336. [https://doi.org/10.1016/S0254-0584\(01\)00551-X](https://doi.org/10.1016/S0254-0584(01)00551-X).
11. R. Sharma, A.S. Rao, N. Deopa, M. Venkateswarlu, M. Jayasimhadri, D. Haranath, G. Vijaya Prakash, Spectroscopic study of Pr³⁺ ions doped Zinc Lead Tungsten Tellurite glasses for visible photonic device applications, *Optical Materials*. 78 (2018) 457–464. <https://doi.org/10.1016/J.OPTMAT.2018.02.054>.
12. G. le Saoût, P. Simon, F. Fayon, A. Blin, Y. Vaills, Raman and infrared structural investigation of (PbO)_x(ZnO)_(0.6-x)(P₂O₅)_{0.4} glasses, *Journal of Raman Spectroscopy*. 40 (2009) 522–526. <https://doi.org/https://doi.org/10.1002/jrs.2158>.
13. S.P. Valappil, D. Ready, E.A.A. Neel, D.M. Pickup, W. Chrzanowski, L.A. O’Dell, R.J. Newport, M.E. Smith, M. Wilson, J.C. Knowles, Antimicrobial Gallium-Doped Phosphate-Based Glasses, *Advanced Functional Materials*. 18 (2008) 732–741. <https://doi.org/https://doi.org/10.1002/adfm.200700931>.
14. A.K. Yadav, P. Singh, A review of the structures of oxide glasses by Raman spectroscopy, *RSC Adv*. 5 (2015) 67583–67609. <https://doi.org/10.1039/C5RA13043C>.
15. Sanju, Ravina, Anu, A. Kumar, V. Kumar, M.K. Sahu, S. Dahiya, N. Deopa, R. Punia, A.S. Rao, Physical, structural and optical characterization of Dy³⁺ doped ZnF₂-WO₂-B₂O₃-TeO₂ glasses for opto-communication applications, *Optical Materials*. 114 (2021) 110937. <https://doi.org/10.1016/J.OPTMAT.2021.110937>.
16. K. Jha, M. Jayasimhadri, Spectroscopic investigation on thermally stable Dy³⁺ doped zinc phosphate glasses for white light emitting diodes, *Journal of Alloys and Compounds*. 688 (2016) 833–840. <https://doi.org/10.1016/J.JALLCOM.2016.07.024>.
17. Ravina, Naveen, Sheetal, V. Kumar, S. Dahiya, N. Deopa, R. Punia, A.S. Rao, Judd-Ofelt itemization and influence of energy transfer on Sm³⁺ ions activated B₂O₃-ZnF₂-SrO-SiO₂ glasses for orange-red emitting devices, *Journal of Luminescence*. 229 (2021) 117651. <https://doi.org/10.1016/J.JLUMIN.2020.117651>.
18. N. Deopa, A.S. Rao, S. Mahamuda, M. Gupta, M. Jayasimhadri, D. Haranath, G.V. Prakash, Spectroscopic studies of Pr³⁺ doped lithium lead alumino borate glasses for

- visible reddish orange luminescent device applications, *Journal of Alloys and Compounds*. 708 (2017) 911–921. <https://doi.org/10.1016/J.JALLCOM.2017.03.020>.
19. S. Damodaraiah, V.R. Prasad, S. Babu, Y.C. Ratnakaram, Structural and luminescence properties of Dy³⁺ doped bismuth phosphate glasses for greenish yellow light applications, *Optical Materials*. 67 (2017) 14–24. <https://doi.org/10.1016/J.OPTMAT.2017.03.023>.
 20. N. Deopa, A.S. Rao, Photoluminescence and energy transfer studies of Dy³⁺ ions doped lithium lead alumino borate glasses for w-LED and laser applications, *Journal of Luminescence*. 192 (2017) 832–841. <https://doi.org/10.1016/J.JLUMIN.2017.07.052>.
 21. Chr.K. Jørgensen, The Nephelauxetic Series, in: *Progress in Inorganic Chemistry*, John Wiley & Sons, Ltd, 1962: pp. 73–124. <https://doi.org/https://doi.org/10.1002/9780470166055.ch2>.
 22. E.A. Davis, N.F. Mott, Conduction in non-crystalline systems V. Conductivity, optical absorption and photoconductivity in amorphous semiconductors, *The Philosophical Magazine: A Journal of Theoretical Experimental and Applied Physics*. 22 (1970) 903–922. <https://doi.org/10.1080/14786437008221061>.
 23. F. Urbach, The Long-Wavelength Edge of Photographic Sensitivity and of the Electronic Absorption of Solids, *Physical Review*. 92 (1953) 1324. <https://doi.org/10.1103/PhysRev.92.1324>.
 24. W.S. AbuShanab, E.B. Moustafa, A.H. Hammad, Dependence of the structure, optical, and dynamic properties of novel cadmium phosphate glass on vanadium content, *Journal of Materials Research and Technology*. 9 (2020) 14178–14189. <https://doi.org/10.1016/J.JMRT.2020.10.007>.
 25. M.S. Shams, S.Y. Marzouk, A.M. El-Refaey, S.H. Abdel-Hafez, I.O. Olarinoye, Y.S. Rammah, Fabrication, linear/nonlinear optical properties, Judd–Ofelt parameters and gamma-ray attenuation capacity of Er₂O₃ doped P₂O₅–ZnO–CdO glasses, *Journal of Materials Research and Technology*. 15 (2021) 5540–5553. <https://doi.org/10.1016/J.JMRT.2021.10.134>.
 26. F. Ahmadi, R. Hussin, S.K. Ghoshal, Physical and structural properties of dysprosium ion doped phosphate glasses, *Optik*. 227 (2021) 166000. <https://doi.org/10.1016/J.IJLEO.2020.166000>.
 27. H.A. Othman, G.M. Arzumanyan, D. Möncke, The influence of different alkaline earth oxides on the structural and optical properties of undoped, Ce-doped, Sm-doped, and Sm/Ce co-doped lithium alumino-phosphate glasses, *Optical Materials*. 62 (2016) 689–696. <https://doi.org/10.1016/J.OPTMAT.2016.10.051>.
 28. Y. Tian, B. Chen, B. Tian, R. Hua, J. Sun, L. Cheng, H. Zhong, X. Li, J. Zhang, Y. Zheng, T. Yu, L. Huang, Q. Meng, Concentration-dependent luminescence and energy transfer of flower-like Y₂(MoO₄)₃:Dy³⁺ phosphor, *Journal of Alloys and Compounds*. 509 (2011) 6096–6101. <https://doi.org/10.1016/J.JALLCOM.2011.03.034>.

29. M. Jayasimhadri, K. Jang, H.S. Lee, B. Chen, S.-S. Yi, J.-H. Jeong, White light generation from Dy³⁺-doped ZnO–B₂O₃–P₂O₅ glasses, *Journal of Applied Physics*. 106 (2009) 13105. <https://doi.org/10.1063/1.3159899>.
30. E. Pavitra, G.S.R. Raju, W. Park, J.S. Yu, Concentration and penetration depth dependent tunable emissions from Eu³⁺ co-doped SrY₂O₄:Dy³⁺ nanocrystalline phosphor, *New J. Chem.* 38 (2014) 163–169. <https://doi.org/10.1039/C3NJ00987D>.
31. S. Kaur, A.S. Rao, M. Jayasimhadri, Spectroscopic and photoluminescence characteristics of Sm³⁺ doped calcium aluminozincate phosphor for applications in w-LED, *Ceramics International*. 43 (2017) 7401–7407. <https://doi.org/10.1016/J.CERAMINT.2017.02.129>.
32. A.M. Babu, B.C. Jamalaih, J.S. Kumar, T. Sasikala, L.R. Moorthy, Spectroscopic and photoluminescence properties of Dy³⁺-doped lead tungsten tellurite glasses for laser materials, *Journal of Alloys and Compounds*. 509 (2011) 457–462. <https://doi.org/10.1016/J.JALLCOM.2010.09.058>.
33. M.S. Rao, V. Sudarsan, M.G. Brik, Y. Gandhi, K. Bhargavi, M. Piasecki, I. v Kityk, N. Veeraiiah, De-quenching influence of aluminum ions on Y/B ratio of Dy³⁺ ions in lead silicate glass matrix, *Journal of Alloys and Compounds*. 575 (2013) 375–381. <https://doi.org/10.1016/J.JALLCOM.2013.05.098>.
34. N. Deopa, S. Saini, S. Kaur, A. Prasad, A.S. Rao, Spectroscopic investigations on Dy³⁺ ions doped zinc lead alumino borate glasses for photonic device applications, *Journal of Rare Earths*. 37 (2019) 52–59. <https://doi.org/10.1016/J.JRE.2018.04.013>.
35. R.A. Talewar, S. Mahamuda, K. Swapna, A.S. Rao, Near UV based Dy³⁺ ions doped alkaline-earth chloro borate glasses for white LED's and visible lasers, *Optics & Laser Technology*. 119 (2019) 105646. <https://doi.org/10.1016/J.OPTLASTEC.2019.105646>.
36. I. Kashif, A. Ratep, Judd–Ofelt and luminescence study of Dysprosium-doped lithium borosilicate glasses for lasers and w-LEDs, *Boletín de La Sociedad Española de Cerámica y Vidrio*. (2021). <https://doi.org/10.1016/J.BSECV.2021.06.001>.
37. J. Azkargorta, I. Iparraguirre, R. Balda, J. Fernández, On the origin of bichromatic laser emission in Nd³⁺-doped fluoride glasses, *Opt. Express*. 16 (2008) 11894–11906. <https://doi.org/10.1364/OE.16.011894>.
38. K.U. Kumar, C.S. Rao, C.K. Jayasankar, S.S. Babu, J.L. Lucio, M.A.V. H., M.A.M. Gamez, Optical properties of Dy³⁺ -doped P₂O₅ - K₂O–MgO/MgF₂–Al₂O₃ glasses, *Physics Procedia*. 13 (2011) 70–73. <https://doi.org/10.1016/J.PHPRO.2011.02.017>.
39. C.S. McCamy, Correlated color temperature as an explicit function of chromaticity coordinates, *Color Research & Application*. 17 (1992) 142–144. <https://doi.org/https://doi.org/10.1002/col.5080170211>.
40. N. Deopa, A.S. Rao, Spectroscopic studies of single near ultraviolet pumped Tb³⁺ doped Lithium Lead Alumino Borate glasses for green lasers and tricolour w-LEDs, *Journal of Luminescence*. 194 (2018) 56–63. <https://doi.org/10.1016/J.JLUMIN.2017.09.057>.

41. R. Bajaj, A.S. Rao, G.V. Prakash, Linear and nonlinear photoluminescence from thermally stable KYF₄:Eu³⁺ cubic nanocrystals, *Journal of Alloys and Compounds*. 885 (2021) 160893. <https://doi.org/10.1016/J.JALLCOM.2021.160893>.
42. T.A. Lodi, N.F. Dantas, T.S. Goncalves, A.S.S. de Camargo, F. Pedrochi, A. Steimacher, Dy³⁺ doped calcium boroaluminate glasses and Blue Led for smart white light generation, *Journal of Luminescence*. 207 (2019) 378–385. <https://doi.org/10.1016/J.JLUMIN.2018.11.045>.

Chapter 5: Summary & Future Scope

Summary

To conclude, ZnAlNaP glasses doped with different Dy³⁺ ions concentrations were made using melt-quench process and investigated using XRD, FT-IR, Raman, DSC-TGA, absorption, PL excitation & emission, and TDPL analysis in the current study. The measured XRD spectrum validated the ZnAlNaPDy glasses' non-crystalline phase. The presence of distinct functional groups was confirmed by the FT-IR spectrum produced for the un-doped ZnAlNaP glass. Different vibrational modes can be seen in the Raman spectra of ZnAlNaPDy1.0 glass.

The thermal stability and total loss in weight of the host glass are revealed by DSC and TGA analysis, respectively. The total mass loss for an un-doped ZnAlNaP glass was determined to be 15.35 %, confirming its stability at relatively high temperatures. The optical band gap energy was calculated using absorption spectrum characteristics recorded for the as-prepared glasses and the Tauc plot. The PL emission were detected for the titled glasses (under 350 nm excitation), with two enhanced peaks in the blue and yellow regions at 484 and 573 nm, respectively. Due to RET amid Dy³⁺ ions, concentration quenching for the ZnAlNaP glasses is found to be at 1 mol % of Dy³⁺ ions. As the concentration of Dy³⁺ ions increase, the experimental lifetime values for as-prepared ZnAlNaP glasses measured from decay profiles pertaining to the ⁴F_{9/2}→⁶H_{13/2} transition at λ_{ex} = 350 nm excitation decrease, which could be ascribed to cross-relaxation processes taking place amongst the trivalent dysprosium ions.

The CIE chromaticity coordinates and CCT values reported for ZnAlNaP glasses represent the emission of the cold white light region. The thermal behavior of ZnAlNaPDy glasses revealed by TD-PL analysis shows that at 200 °C, the aforementioned glasses retain 74.4 % of the PL emission intensity, suggesting that the ZnAlNaPDy glasses are thermally stable. The as-prepared Dy³⁺ ions doped ZnAlNaP glasses can exhibit luminescence that can be used to produce white light, implying that they are appropriate for developing w-LEDs based on the aforementioned results.

Future Scope

- RE doped glasses play a vital role in manufacturing optical devices like optical fibres amplifiers and have also found great utilizations in lasers, pharmaceuticals, photovoltaic

devices, telecommunications, and civil military applications like as IR detectors, IR fairings, nuclear imaging and surveillance.

- The above-mentioned applications of RE doped glasses are possible only if it is chemically & thermally stable, has relatively minimal phonon energies, better RE ion solubility and excellent transparency. The structure and ligand field environment of the host glass affects the bandwidths of emission transitions and decides the luminescence adequacy of a doped RE ion. Thus, it is quite important to choose a host material with relatively lower phonon energies [1]. We will try to alter the host glass composition of the titled glasses with suitable elements and try to attain glasses having relatively less phonon energies than the titled glasses and study their PL characteristics.
- Quite recently it was observed that, the PL efficiency of the glasses doped with certain rare earth/transition metal ions can be enhanced by converting them in to glassy ceramics. We have the plans to convert the glasses investigated in the present dissertation work into glassy ceramics by heat treating them at an appropriate temperature and time. The glasses heat treated for longer durations converts them in to glassy ceramics by producing micro/nano crystals due to nucleation process. Such nano/micro crystals produced due to nucleation process in fact converts glasses into a glassy ceramics and helps in enhancing the PL characteristics of the host glass.

References:

1. <https://www.sciencedirect.com/science/article/abs/pii/0022508883901637>

*****THE END*****

PAPER NAME

Final plag file thesis.docx

WORD COUNT

7888 Words

CHARACTER COUNT

41898 Characters

PAGE COUNT

24 Pages

FILE SIZE

55.2KB

SUBMISSION DATE

May 10, 2022 12:22 PM GMT+5:30

REPORT DATE

May 10, 2022 12:23 PM GMT+5:30

● 9% Overall Similarity

The combined total of all matches, including overlapping sources, for each database.

- 4% Internet database
- Crossref database
- 5% Submitted Works database
- 5% Publications database
- Crossref Posted Content database

● Excluded from Similarity Report

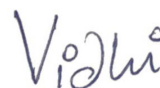
- Bibliographic material
- Cited material
- Quoted material
- Small Matches (Less than 10 words)



Prof. A.S. Rao
(Project Supervisor)



Ankita
2K20/MSCPHY/04



Vidhi
2K20/MSCPHY/33

Chapter 1: Introduction

1.1 Light Emitting Diodes

Since the beginning of mankind, people have always tried to invent, innovate, and discover new things that can benefit human civilization. Therefore, it should not come as a surprise, but at the same time, we can admit these commendable advancements made by researchers, which are useful for lighting applications in day-to-day life. One of the most remarkable innovations of the twentieth century was light-emitting diodes (LEDs). These devices are a great source of artificial lighting and at the same time eco-friendly.

Today, white- LEDs (w-LEDs) have become fourth-generation solid-state lighting (SSL) gadgets due to the wide range of benefits, such as power saving, higher dependability, brilliant productivity, life span, luminous efficiency and earth-friendly. The w-LEDs are now made with optical excitation sources that have a single or many layers of phosphors [1,2]. The concentration of epoxy resin placed on the phosphor has a significant impact on the emission of phosphor converted (pc) w-LEDs. The sealant used in pc w-LEDs gets degraded at high temperatures, which considerably affects its characteristics such as luminous efficiency and color rendering index [3–6].

The research in rare earth (RE) doped luminescent materials has taken a quantum leap due to impressive advancements in SSL technologies. RE doped glasses have proven to be more advantageous than phosphors due to their unique properties including broader non-homogeneous bandwidths, large doping capacity, and improved thermal stability. RE doped glasses are used in optical devices such as fibre optic amplifiers, lasers, pharmaceuticals, photovoltaics, telecommunications, and civil-military purposes for instance infrared detectors, infrared fairings, nuclear imaging and surveillance [7–11]. The above-mentioned applications of RE doped glasses are possible only if it is chemically & thermally stable, has relatively minimal phonon energies, have better RE³⁺ solubility with excellent transparency. The host glass's structure and ligand field environment affect the bandwidths of emission bands and decides the photoluminescence (PL) adequacy of RE³⁺. Thus, selecting a host material with relatively lower phonon energies is very important [6,12].

Phosphate glasses, in contrast to commonly used glass formers such as silicate, borate, and others, are known to have good mechanical and thermal stability, excellent transparency, better

RE^{3+} solubility, low melting point (compared to silicate glass), eco-friendly and isotropic refractive index [13–17]. Nonetheless, pure phosphorus pentoxide (P_2O_5), a chemically unstable oxide is a compound that comes in the category of glass formers. P_2O_5 is immensely hygroscopic in nature when it comes to moisture-induced hydrolysis of the P–O–P bonds. As a result, its usage as a substitute for silicate glasses is frequently limited to a narrow range of technological applications. Despite this, the high solubility of P_2O_5 glasses makes them useful in synthesizing bioactive materials [18–21].

The morphology of glass is decided by two main components, the network former and the network modifier. Network formers are considered to be an integral component in the construction of any glass matrix. It can be a metal oxide and one such case is that of Al_2O_3 which we have also used in the composition of our glass. Al_2O_3 conjugation in phosphate glass can act as a network former as well as a network modifier. Al_2O_3 increases the crosslinks with PO_4 tetrahedra in the glass. It gives the phosphate glass moisture resistance and thermal stability, as well as a lower thermal coefficient of expansion, which makes it suitable for ion exchange planar waveguide devices. Aluminium oxide in phosphate glass can improve the host glass's physical and chemical stability [22–24].

The addition of network modifiers in the host matrix modifies its internal structure and simultaneously builds an integrated environment for the RE^{3+} , allowing them to maintain a high luminescence efficiency [25]. The glass modifiers that we have used in our study are zinc oxide (ZnO) and sodium oxide (Na_2O). We can improve the noble features of phosphate glass by adding divalent metal oxides like zinc oxide (ZnO) to it, such as lower glass transition temperatures and higher chemical stability. Furthermore, glasses containing ZnO are less hygroscopic and toxic, making them more efficient for developing optoelectronic devices [6,12,24,26]. In glasses, alkaline metal oxides like sodium oxide (Na_2O) can influence and regulate their optical properties. Adding Na_2O to the phosphate glass matrix as a network modifier promotes the formation of non-branching oxygen atoms. Also, it improves the solubility of RE ions, making it suitable for higher concentration of dopants in the glass and also useful for short-length optical amplifiers [27,28].

Doping RE^{3+} in phosphate glasses has several advantages, including lower propagation losses, a high number of intra-configuration transition channels for RE^{3+} , an isotropic refractive index, and the ability to produce them more easily. The outer 5s and 5p shells shield the RE^{3+} surroundings, affecting the 4f-4f transitions in RE^{3+} , resulting in intense and narrow emissions

[3]. From the existing seventeen RE ions, Dy^{3+} ions when used as a dopant in glass, makes it quite suitable for producing white light due to two major bands of emission corresponding to the $^4\text{F}_{9/2} \rightarrow ^6\text{H}_{15/2}$ transition which is a magnetic dipole and $^4\text{F}_{9/2} \rightarrow ^6\text{H}_{13/2}$ transition which is an electric dipole pertaining to 480-500 nm and 580-600 nm ascribing to the blue and yellow part of the visible spectrum, respectively [29,30]. The yellow band is more susceptible to the nature of the host's material and is heavily dependent on it, whereas the blue band is less susceptible to the host material. As a result, Dy^{3+} doped glasses with an acceptable yellow and blue transitions ratio can create white light [31].

Apart from being a single-phase white light source, Dy^{3+} doped glasses have a wide range of applications, including luminescence lamps that are free of mercury and light generating materials when mixed RE ions are added. All of the aforementioned advantages of the constituent chemical species like P_2O_5 , Al_2O_3 , ZnO , Na_2O and Dy_2O_3 gave us an incentive to prepare a series of phosphate glasses by name zinc alumino sodium phosphate (ZnAlNaP) glasses.

1.2 Literature review

H. George et. al. conducted spectroscopic investigation by evaluating the CCT values for the Dy^{3+} doped NaBiSrP glasses which lie in the neutral white zone under n-UV excitation [32]. The structural, thermal and optical studies of Dy^{3+} doped $\text{B}_2\text{O}_3\text{-WO}_3\text{-ZnO-Li}_2\text{O-Na}_2\text{O}$ glasses were performed by G. Lakshminarayana et al [33]. The PL studies performed on the aforementioned glasses show strong peaks at blue and yellow emission bands when observed using UV excitation and the Y/B values show relatively higher values, making this combination a suitable candidate for white light generation [33]. The optical and radiative properties of dysprosium doped sodium aluminum phosphate (NAP) glasses were investigated by A. Amarnath Reddy et al [34]. The Y/B ratios found in visible emission imply the prominent nature of covalency and asymmetry effects in the aforementioned glasses, and the Y/B intensity ratios observed in visible emission showing the ease of producing white light in the Dy^{3+} doped NAP glass [34].

All of above-mentioned researchers motivated us to work in this field utilizing Dy^{3+} doped phosphate glasses that can be suitably significant for white light applications in photonic devices. In the present work, we have investigated the glassy nature, structural aspects, thermal stability and spectroscopic features of the as-prepared glasses using various characterization techniques

like XRD, FT-IR, Raman, DSC-TGA, optical absorption, PL (excitation, emission and decay) and temperature dependent PL (TD-PL).

Chapter 2: Theoretical Framework

2.1 Photoluminescence of materials:

Luminescent materials are substances that, in addition to black-body emission, transform an incident energy source into electromagnetic wave output in the ultraviolet (UV), visible, or infrared regions of the spectra. Luminescence can be classified on the basis of the simulation that is provided and the Table 1 given below summarizes it [1].

2.2 Difference between fluorescence, phosphorescence and chemiluminescence:

- Photoluminescence is classified into fluorescence and phosphorescence. If the substance's glow is triggered by light, then it is photoluminescence, whereas if the glow is caused by a chemical reaction, then it is chemiluminescence.
- Fluorescence and phosphorescence are both caused by a substance's capacity to absorb the light and subsequently release the light with a longer wavelength and consequently less energy.
- The basic difference between these two phenomena is the time taken to complete the process. In the case of fluorescence, the emission occurs immediately, so it can be observed only when the light source is kept on (for example, UV lights); however, in the case of phosphorescence, the absorbed light energy can be stored for a period of time and then released later, as a result, even after the light source has been switched off, there is an afterglow.
- To conclude, if it fades away quickly, it is fluorescence; if it lasts longer, it is phosphorescence. It's chemiluminescence if it requires some type of activation.

- A good example of it can be considered if we imagine a scenario at the nightclub: ⁷Teeth, eyes and fabric glowing under the black light are considered fluorescent, the emergency exit sign is phosphorescent and the glow sticks are chemiluminescent [1].

2.3 Rare earth (RE) materials:

- There are 17 RE elements in periodic table. Scandium, Yttrium and some 15 other lanthanide series elements come under this category.
- Since, all RE elements are metals, therefore they are sometimes known as the "Rare Earth metals".
- They are also called "Rare Earth oxides" since most of them are available in the market as oxide compounds.
- Rare earth elements are commonly employed as catalysts, phosphors, and polishing agents. In air pollution management, illuminated screens in electronic devices, and a variety of other applications rare earth elements are commonly used [2].
- Actually, rare earth elements are not "rare" as the name suggests. For example, the two least abundant rare earth elements are Thulium and Lutetium but each of them has an average crustal abundance approximately 200 times more than that of the gold. Although these metals are not rare but are quite tough to mine as it is uncommon to obtain these metals in enough concentrations for economical extraction.
- Yttrium, cerium, lanthanum and neodymium come under the category of the most abundant rare earth elements. The average crustal abundances for these elements are similar to some of the most frequently used industrial metals for instance chromium (Cr), nickel (Ni), zinc (Zn), and lead (Pb) etc. But again, they can rarely be found in extractable concentrations [2].

2.4 Rare earth elements in glass synthesis:

- Researchers have been studying rare earth oxides for a long time now, especially how the addition of rare earth oxides can change the properties of the glass. It was for the first time in the 1800s that Drossbach, a German scientist patented his work of manufacturing a mixture of rare earth oxides to decolorize the glass. It is said to be cerium is firstly commercially used

although it is in their raw form combining with other RE oxides. Later in 1912, Crookes from England discovered cerium's excellent properties for ultraviolet absorption without giving any color hence making it quite useful in making protective eyeglasses.

- Some of the most commonly used Rare Earth Elements in glass are erbium, ytterbium, and neodymium. Some of the uses are: Erbium-doped silica fiber is widely used for optical communication; ytterbium-doped silica fiber is used in manufacturing some engineering materials, and neodymium-doped is useful in making glass lasers. Addition of rare earth oxides in glass have the ability to change the fluorescent properties of the glass [3].

2.5 White LEDs:

- One of the most remarkable innovations of the twentieth century was that of the light-emitting diodes (LEDs). These devices are a great source of artificial lighting and at the same time eco-friendly. Today, white- LEDs or w-LEDs have become fourth generation solid-state lighting (SSL) gadgets due to the wide range of benefits that they offer, such as power saving, higher dependability, brilliant productivity, life span, luminous efficiency and earth friendly.
- At present, w-LEDs are fabricated using optical excitation sources with a coating of one or many phosphors. In the case of phosphor converted (pc) w-LEDs, the resulting emitted light is immensely affected due to concentration of epoxy-resin coated on phosphor. The sealant used in pc w-LEDs, gets degraded at high temperatures which in turn considerably affect its characteristics such as, luminous efficiency and color rendering index.
- The research in the field of rare earth (RE) doped luminescent materials have taken a quantum leap due to impressive advancements in SSL technologies. Owing to their peculiar qualities such as high doping capacity, broad inhomogeneous bandwidths and better thermal stability, rare earth doped glasses have proved to be more advantageous over phosphors [4].

Chapter 3: Experimental Techniques

3.1 Materials & Methods:

A. Preparation: The most common methods to prepare a glass are melt quenching method, Chemical

vapor deposition and sol-gel method. Out of these three techniques, melt quenching has been the most popular and quite feasible so far in the research field. The key feature of this melt quenching technique is that it is widely applicable to prepare all kinds of compositions of glasses like borate, phosphate, silicate, oxide or non-oxide systems. We have all kinds of options available as dopants and co-dopants to give a variety to our glass system which becomes quite easy using this technique. There are minor chances of the sample being prone to some kind of impurities but that can be avoided using the crucibles made of noble metals like Gold, Platinum, etc. [1].

B. Melt-quenching Technique: We have prepared a phosphate glass for our research work and the Rare Earth ion that has been used as a dopant is Dysprosium (Dy^{3+}). The high purity analytical grade oxides or salts were taken as precursors. Powders such as zinc oxide (ZnO), sodium oxide (Na_2O), aluminum oxide (Al_2O_3), di-ammonium hydrogen orthophosphate ($(NH_4)_2HPO_4$) and the dopant dysprosium oxide (Dy_2O_3) were weighed in required quantities using a high-accuracy electronic balance. Then using acetone as the dispersing medium, the components were then grinded in an agate mortar for about 45 minutes until the mixture was a soft powder. The so-obtained fine powder was then transferred to a silica crucible and a constant heat of 1270 °C was applied in a programmable furnace for two hours. Thereafter, the as obtained melt was cast into a coin shaped glass by pressing it between two pre-heated brass plates. This process is known as quenching and since the melt was quenched into a coin shape, this is why we call it the melt quenching technique. The coin shaped glasses were then immediately transferred to an annealing furnace at 350 °C for 2 hours to eradicate the internal stresses, air bubbles and to maintain the stability of the internal glass structure [1, 6].

Using a Bruker D8 Advance Diffractometer with nickel filtered Cu-K α radiation ($\lambda = 1.5406 \text{ \AA}$) and diffraction angles ranging from $10^\circ \leq 2\theta \leq 80^\circ$, the XRD spectrum of an un-doped ZnAlNaP glass sample was obtained. Perkin Elmer's Frontier Spectrometer ($450\text{--}4000 \text{ cm}^{-1}$) was used to measure the FT-IR spectrum of the identical sample utilizing the KBr-disk method. Raman spectroscopy was performed using a Renishaw model Invia Reflex Raman microscope. The optical absorption studies were done using a Jasco V-770 Spectrophotometer. A JASCO made (FP-8300) spectrofluorophotometer (resolution of 1.0 nm) with a Xenon flash lamp as an excitation source was used to make the spectral recordings of PL excitation, PL emission and PL decay. All

measurements were recorded at an ambient temperature. TDPL studies were conducted on FLMS15147 Spectrometer.

3.2 Characterization Techniques:

a. **XRD:** Diffraction of light refers to the bending of light around the corners of an obstacle. It is the required condition for diffraction to occur. The size of the obstacle needs to be almost equivalent to the frequency of light being used. X-ray, as other EM rays, can also be diffracted, but for the diffraction of X-ray the size of the obstacle ought to be a couple of angstroms (approx. 1 \AA), which is approximately the frequency of X-rays. The reason behind this is that the atomic spacing in the Crystal is almost a few \AA . The constructive interference of monochromatic x-rays is the basic principle of XRD. X-rays are directed towards the sample under investigation, and sample's crystal structure causes the X-rays to spread in a variety of directions. It is recorded by a detector and further amplified to be analyzed on a monitor screen [7].

Bragg's Law:

This law implies that if an x-ray is incident at an angle of incidence (θ) onto a crystal surface, then that x-ray reflects at the same angle of scattering (θ). If the path difference (d) is a whole number (n) multiple of wavelength (λ) then an interference pattern can be seen.

Bragg's Law is:

$$n \lambda = 2d \sin(\theta) \quad (1)$$

here, λ is the incident wavelength of x-rays, d is the spacing between the crystal layers (i.e., path difference), θ is the angle of incidence & n is the diffraction order.

X-Ray Diffraction (XRD) Methods

There are several XRD methods:

1. Laue's Photographic Method
2. Bragg's X-Ray Spectrometer Method
3. Rotating Crystal Method

4. Powder Crystal Method

Since we have used powder method, so elaborating on that:

The sample to be tested is homogenized and ground into a fine powder. The powdered sample is then struck on a hair and mounted vertically in the axis of a cylindrical camera with a piece of gum.

A monochromatic beam is permitted to fall on it, various possibilities exist. A few particles may emerge from the random alignment of tiny crystals. For each set, there is the probability of reflections in different orders. In addition, another proportion of grains will have a different set of planes in the appropriate positions for reflections to occur [3].

- b. ABSORPTION:** Absorption spectroscopy of a glass sample is carried out using the radiations lying in the UV-Visible region of Electromagnetic spectrum. The amount of light absorbed by a particular glass sample is observed in the phenomenon. When the radiation of a particular wavelength falls on the glass sample, the electrons in the outermost shells of the compound participate and get excited to the first excited state of the material. The light from a source (usually tungsten lamp or deuterium) after passing through a monochromator falls on the beam splitter and a series of mirrors. Thereafter, the light finally falls on the sample holder where the glass sample is placed. The absorption data corresponding to a particular wavelength range of that particular sample is obtained on a computer screen connected to the spectrophotometer. This data shows how much light of a particular wavelength is absorbed by the sample. The measurements are carried out using a reference sample for which the absorption data is already known. It is to be noted that this process involves relative measurements and not direct measurements. This phenomenon is used to determine the optical properties of the glass sample like optical band gap, refractive index and other such properties [5].
- c. PHOTOLUMINESCENCE (PL) SPECTROSCOPY:** PL spectroscopy is a type of light-emitting spectroscopy in which the emission of light arises due to a process called photo-excitation. As the light is directed to the sample, the electrons inside the material go to the excited regions (excitation). After releasing energy in non-radiative forms, the electron goes down to an intermediate level called the conduction band. Thereafter, when electrons flow from the conduction band to their ground states, energy can be released in the form of light (called radiative relaxation). This phenomenon is shown in fig. 9. The experimental setup is quite

similar to that of Absorption spectroscopy except for the monochromator near the source. PL spectroscopy is beneficial to estimate the electronic structure and assets of the compound as it provides the peak light intensity that objects can emit at a certain wavelength [1].

- d. FT-IR:** FT-IR Spectroscopy (fourier-transform infrared spectroscopy) is a characterization technique that is concerned with the vibration of molecules. The source, interferometer, and detector are the three important parts of an FT-IR Spectroscopy (fig. 10).

The source energy is directed onto the sample through an interferometer. All source radiation must reach the sample during each scan. The light is then split into two directions at right angles by passing through a beam splitter. One of these beams is divided and sent to a fixed mirror before returning to beam-splitter. Another beam is channeled at a movable mirror. Furthermore, both of these two beams will recombine at the beam-splitter, although difference in path lengths will cause constructive and destructive interference, resulting in interference pattern. The sample is next passed through the earlier recombined beam, which absorbs all of the distinct wavelength's characteristic of its spectrum. The detector records the change in energy and time corresponding to many wavelengths for same time. A laser beam is imposed throughout the procedure to give a reference for instrument operation.

Now, one could think that recording a spectrum in terms of energy vs time is strange, unless one considers the correlation between time and frequency: they are reciprocal. Using the Fourier transform (FT) function, an I-vs-t spectrum can be transformed to an I-vs- ν spectrum. The FT can be given by the expression:

here, $A(\tau)$ are the frequency domain & $X(k)$ are the time domain points and N are the total points in the spectrum.

Because each functional group has its own distinct vibrational energy that may be utilized to identify a molecule by combining all of the functional groups, FTIR microscopy is an excellent tool for identifying samples, characterization of multilayer films, and particle analysis. Because each functional group is made up of distinct atoms with variable bond strengths, each of these functional groups, and categories of functional groups, has its own set of vibrations. Because

each molecule's collection of vibrational energy bands is distinct, these peaks can be utilized to identify the functional groups involved utilizing literature analyses of large sample datasets [8].

- e. **RAMAN SPECTROSCOPY:** Raman spectroscopy is a method for measuring the vibrational energy modes of a material by means of diffused light. CV Raman, an Indian physicist, was the first to see Raman spectra in 1928, along with his research partner KS Krishnan. Raman spectroscopy may offer both chemical and structural information, as well as material identification via Raman fingerprints. By detecting the Raman Scattering of a material, Raman spectroscopy retrieves this information. Whenever light is scattered by a molecule, the photon's electromagnetic oscillatory field results in the polarization of the electron cloud, leaving the molecule in a high-energy state with the photon energy imparted to it. This results in the production of a virtual state of the molecule, which is an extremely short-lived combination between a photon and a molecule. Like scattered light, this virtual state is unstable, and the photon is expelled almost instantly.

The energy of a molecule does not vary after interacting with a photon in the most of the scattering and energy, & therefore the wavelength, of the scattering photon is equal to incident photon. This is known as elastic scattering Rayleigh scattering ($\lambda_{\text{scatter}} = \lambda_{\text{laser}}$) and is the most common mechanism.

But to observe Raman scattering, we need to use certain kinds of filters in order to let in only that wavelength which satisfies the conditions for Raman Scattering. The conditions imposed on the wavelength to observe Raman Scattering is that the wavelength of the scattered photon should be either greater than or less than that of the laser used. Former is the case when we get to observe the Stokes Raman Scattering ($\lambda_{\text{scatter}} > \lambda_{\text{laser}}$) and latter is the case when we get to observe the Anti-Stokes Raman Scattering ($\lambda_{\text{scatter}} < \lambda_{\text{laser}}$) [4].

Chapter 4: Spectroscopic Characterization of Dy³⁺ ions doped

Phosphate glasses for epoxy free white LED applications

25 4.1 Structural analysis

4.1.1. XRD spectrum:

Fig. 13 shows the XRD spectrum obtained for an un-doped ZnAlNaP glass in the $10^\circ \leq 2\theta \leq 80^\circ$ spectral region. The existence of a large hump in the recorded XRD spectrum in absence of intense peaks indicates the non-crystalline behavior of the as-prepared glass, which is a sign of long-range structural instability.

34 4.1.2. FT-IR spectral analysis:

The FT-IR spectrum recorded conveys information of various functional-groups involved and the characteristic vibrational modes of the phosphorus atoms in different configurations with bridging and non-bridging oxygens in the as-prepared phosphate glass. The FT-IR spectrum of an un-doped AZNP glass for the spectral range 400 to 4000 cm^{-1} , depicted in Fig. 14. Table 2 represents the positions of various peaks and their related peak assignments. The recorded spectrum indicates the translucent nature of the as-prepared phosphate glass.

From Fig. 14, a total of seven infrared modes at 513, 781, 935, 1143, 1251, 2828 and 2925 cm^{-1} have been identified. The first band near 513 cm^{-1} could be attributed to harmonic P-O-P bending vibrations along with Zn-O vibrations [1-3]. The peak at 781 cm^{-1} can be a symmetric stretching vibration of the P-O-P connection corresponding to non-bridging oxygen's (NBOs) in $(\text{PO}_4)^{2-}$ tetrahedra (Q^1 tetrahedra) [4-7]. Similarly, the peak at 935 cm^{-1} might be due to asymmetric stretching vibration of P-O-P linkage corresponding to $(\text{PO}_4)^{1-}$ tetrahedra (Q^2 tetrahedra). The vibrational peak marked at 1143 cm^{-1} is the result of asymmetric stretching vibration of $(\text{PO}_4)^{3-}$

tetrahedra (Q^0 tetrahedra) [8]. The band seen around 1251 cm^{-1} could be about asymmetric stretching vibrations of $(\text{PO}_4)^{1-}$ a terminal group where two binding oxygen's are bonded to phosphorus along with atoms of single NBOs. The two consecutive peaks at 2828 and 2925 cm^{-1} may be due to vibrations of P-O-H group inside the different sites [9]. All the FT-IR bands have been designated according to the reported papers. The formula below can be used to calculate the OH content of a glass matrix:

$$\alpha_{OH} = \frac{\ln \frac{T_o}{T_D}}{l} \quad (3)$$

Where, T_o denotes the greatest transmission value, T_D denotes the glass transmission value at 3000 cm^{-1} and l denotes the thickness of the glass sample in question (i.e., un-doped sample in the present work). To achieve high quantum efficiency, the sample's OH content must be as low as possible. The OH concentration of the un-doped AZNP glass is 145 ppm, which is lower than other published glass samples like GeS_2 (175 ppm) [10]. Relatively less OH content obtained for the as prepared glass indicates favorable situation for radiative transitions instead of non-radiative transitions. This result supports the superior quality of the titled glasses and stood them as better choice for preparing visible various visible photonic devices with minimal radiative loss.

4.1.3. Raman spectral analysis:

The recorded Raman spectrum ($200\text{--}1400\text{ cm}^{-1}$) for $\text{ZnAlNaPDy}1.0$ glass is shown in Fig. 15. The Raman spectra of ZnAlNaPDy glass is used to study the existing P-O bonds and vibrational modes in our phosphate glass network. Commonly, phosphate glasses consist of Q^n groups of tetrahedral sites for connectivity (here n signifies the number of bridging oxygen atoms in each PO_4 unit). Three characteristic bands at 359 , 726 and 1195 cm^{-1} have been observed from Fig. 15.

Table 3 shows the major peak positions and their accompanying peak assignments. The most noticeable band is at 1195 cm^{-1} , which is a feature of symmetric stretching of an NBO in $(\text{PO}_4)^{1-}$ tetrahedra and could be the phonon energy for the as-prepared AZNP glass. The symmetric stretching of P-O-P connections in $(\text{PO}_4)^{1-}$ and $(\text{PO}_4)^{2-}$ tetrahedral units is attributed to the band at 726 cm^{-1} . The bending vibration of O-P-O chains in phosphate glass networks is associated with the band at 359 cm^{-1} [45–48].

4.2. Thermal analysis using DSC-TGA

Fig. 16 shows the results of a DSC examination done on an un-doped ZnAlNaP glass sample with the temperature ranging between 33°C and 1200°C along with 10°C/min heating rate. T_g , T_x , T_c and T_m are the glass transition temperature, onset crystallization temperature, peak crystallization temperature and melting temperature, respectively and the values of these parameters have been found to be equal to 156°C, 482°C, 875°C and 1043°C, respectively. Using these values, glass's thermal stability can be calculated from the formula [15,16]:

$$\Delta T = T_x - T_g \quad (4)$$

Higher values of ΔT aids glass formation by impeding the process of crystallization. Therefore, higher values of ΔT also suggest that the formed glass is relatively more thermally stable [17]. In the as-prepared un-doped ZnAlNaP glass, ΔT was found to be 326°C which is a much higher value as compared to lead aluminum borate glass (27°C) [18] and Zinc Fluoroborate tellurite glass (153°C) [17]. Glasses having ΔT values more than 100°C are regarded to be more thermally stable, making them excellent for manufacturing optoelectronic devices, according to the published data [17].

One of the other vital parameters to determine the glass's thermal stability is Hurby's parameter and is estimated from the following equation [16]:

$$K_H = \frac{T_x - T_g}{T_m - T_x} \quad (5)$$

Hurby's parameter ($K_H \geq 0.1$), has a larger value when the glass is more thermally stable [18]. The calculated K_H value for an un-doped ZnAlNaP glass is 0.5811, which is quite high and authenticate the thermal stability of the ZnAlNaP host glass.

Fig. 17 shows the TGA curve recorded for an un-doped ZnAlNaP glass, which shows a cumulative weight loss of 15.35 percent throughout a temperature range of 33°C to 1200°C. According to the TGA curve, the loss in weight of the un-doped host glass with temperature involves in three different stages. The first stage of weight loss happens between 33°C and 129°C, the second stage occurs between 129°C and 462°C, and the third stage occurs between 462°C and 1200°C. The

sample's total loss is 15.35 percent, and the sample's remaining mass is 84.65 percent. As shown in Fig. 17, the ZnAlNaP glass is thermally stable and has a lower mass loss percentage at higher temperatures.

4.3. Absorption spectral study

The absorption spectra of ZnAlNaPDy glasses have been observed in wavelength range of 250-2000 nm, which covers the UV-Visible and NIR region of the electromagnetic spectrum. The humps present in the spectra clearly show the amount of absorbed light corresponding to the particular wavelength. But in the visible region, comparatively less intense bands are present. A total of 12 bands were observed, amid them five are in the UV region, two are in visible region and five are in the NIR region. The bands in the UV region are observed at 224 nm, 325 nm, 350 nm and 387 nm, which resemble $^4D_{7/2}$, $^6P_{3/2}$, $^6P_{7/2}$ and $^4I_{13/2}$ energy levels. Whereas those in visible region are traced at 426 nm and 452 nm corresponding to $^4G_{11/2}$ and $^4I_{15/2}$. The bands present in NIR region are observed at 805 nm, 906 nm, 1097 nm and 1684 nm, which correspond to $^6F_{5/2}$, $^6F_{7/2}$, $^6H_{7/2}$, $^6F_{11/2}$ and $^6H_{11/2}$ energy levels, respectively [11,19,20]. Absorption spectra of Dy³⁺ doped ZnAlNaP glass samples are shown in Fig. 18. There were no shifts in band positions as the concentration of Dy³⁺ ions increased, but there was some variation in the corresponding intensities.

4.3.1. Nephelauxetic effect (β) and bonding parameters (δ):

The nephelauxetic effect is triggered by a partially filled f-shell, which aids in establishing the kind of link between both the RE ions and oxygen ligands in the host glass. Actually, the nephelauxetic effect causes the 4f orbital of the RE ions to distort when they are doped with the host glass. The energy level structure of RE ions is compressed, this could have possibly happened because of the overlapping oxygen and 4f-orbitals, perhaps causing a wavelength shift. We set the terms Nephelauxetic ratio (β) and bonding parameters (δ) in this effect, which reveals the bond's nature existing among Dy³⁺ ions and the oxygen molecules contained in the host's matrix [21]. Nephelauxetic ratio is computed from the formula below:

$$\beta = \frac{\nu_c}{\nu_a} \quad (6)$$

where, $\underline{\nu}_c$ denotes the wavenumber related to a certain RE ion transition under consideration, $\underline{\nu}_a$ denotes the wavenumber of the same transition for an aqua ion. Table 4 shows expected β values to the corresponding glasses as the concentration of Dy^{3+} ions increase. The values of the bonding parameters (δ) can be computed using the equation below:

$$\delta = \frac{1-\beta}{\beta} \times 100 \quad (7)$$

where, $\underline{\beta}$ represents the average value of β . The field environment of the ligands surrounding the Rare Earth ions can have a great effect on the bonding parameter δ . The positive or negative values of the bonding parameters signify the ionic and covalent behavior of bonding between Dy^{3+} ions and the oxygen ligands. Table 4 lists the estimated values of the bonding parameter for the as-prepared ZnAlNaPDy glass samples. The negative values signify ionic nature of the bond existing among the Dy^{3+} ions and the oxygen molecules [21].

4.3.2. Band gap energy and Urbach's energy:

For each sample, bandgap was calculated by the extrapolation of the linear region in the $\ln(\alpha h\nu)$ plot (as shown in Fig. 19) between absorption coefficient ($\alpha h\nu$) and energy ($h\nu$), defined by the following equation [22]:

$$\alpha h\nu = C(h\nu - E_g)^n \quad (8)$$

where C is a constant, $h\nu$ is energy of photon, and exponent is denoted by n , which can vary depending on the situation, such as 1/2 for direct allowed, 2 for indirect allowed, 1/3 for indirect forbidden, and 3 for direct forbidden transitions. The evaluated values of direct and indirect band gap values for the as-prepared ZnAlNaPDy glass samples are listed in Table 4 and the respective graphs are shown in Fig. 19. The optical band gap E_g provides the information about the onset of the optical absorption and Urbach energy is a concept that is used to describe the energetic aberrations in the optical band gap. It is obtained by fitting the absorption coefficient (α) as a function of energy ($h\nu$) to the exponential function given by the formula underneath [57]:

$$\alpha = \alpha_0 \exp\left(\frac{h\nu}{\Delta E}\right) \quad (9)$$

where, ΔE is denotes the Urbach's energy and α_0 is a constant. The steepness of the beginning of absorption near the band gap is measured by this energy. A lower Urbach energy is indicated by a sharp onset of absorption. The calculated values of ΔE are tabulated in Table 4 and are observed to be in range of 0.42-1.19 eV. Urbach energies with lower values indicate that the associated glass system has less disorder.

4.3.3. Physical parameters:

The various physical parameters mentioned in the Table 5 are evaluated using the following formulae:

Linear refractive index (n_o): The linear refractive index of all studied glasses may be computed using the optical bandgap values in the following equation. [24,25]:

$$n_o = [6 \sqrt{\frac{5}{E_g}} - 2]^{1/2} \quad (10)$$

Dielectric constant (ϵ_o) [26]:

$$\epsilon_o = n_o^2 \quad (11)$$

Reflection Loss (R) [26]:

$$R = \left(\frac{n_o - 1}{n_o + 1} \right)^2 \quad (12)$$

Linear susceptibility $x^{(1)}$ [24,25]:

$$x^{(1)} = \left(\frac{n_o^2 - 1}{4\pi} \right) esu \quad (13)$$

Non-linear susceptibility $x^{(3)}$: Miller's rule is used to define third-order nonlinear susceptibility. [24,25]:

$$x^{(3)} = x^{(1)} \times 1.7 \times 10^{-10} esu$$

$$\text{or, } x^{(3)} = \left(\frac{n_o^2 - 1}{4\pi} \right) \times 1.7 \times 10^{-10} esu \quad (14)$$

Non-linear refractive index (n_2) [24,25]:

$$n_2 = \left(\frac{12\pi}{n_0} \right) \chi^{(3)} \quad (15)$$

In Fig. 20, all of the physical properties listed above are plotted versus the Dy³⁺ ion concentration in ZnAlNaP glasses. Because of the excitation energy, the optical band gap energy dropped as the Dy³⁺ ion concentration is increased. Because the refractive index is directly proportional to the concentration of Dy³⁺ ions, all other properties were shown to rise with the concentration of Dy³⁺ ions. The third order nonlinear susceptibility $\chi^{(3)}$ was observed to rise as the amount of Dy³⁺ ions increased. It could be owing to the glass network's strong polarization caused by Dy³⁺ ions in the ZnAlNaP glass.

4.4. PL spectral analysis

To investigate the PL properties of the Dy³⁺ doped ZnAlNaP glasses, it is required to know the appropriate wavelengths of excitation and emission. One such graph of intensity versus wavelength for ZnAlNaPDy2.0 glass is shown in Fig. 21. In Fig. 21, the left half of the graph exhibits excitation spectrum in the wavelength region of 300-450 nm under the emission wavelength of 573 nm. Similarly, the PL emission spectrum for the same is shown on the right half of the graph for the wavelength range being 450-700 nm under the emission wavelength of 350 nm. It is commonly acknowledged that more atoms can be stimulated to a metastable state from the ground state when a sharp and intense excitation wavelength is used to excite a luminescent material. A relatively more intense emission peak observed in the visible PL emission spectrum at 573 nm was used as the emission wavelength to record PL excitation spectra. Similarly, the prominent PL excitation peak observed within the UV region at 350 nm, has been used as an excitation wavelength for recording the PL emission spectra.

Seven major peaks were observed corresponding to 323 nm, 336 nm, 350 nm, 363 nm, 383 nm, 427 nm, 453 nm in the excitation spectrum region and three major peaks at 473 nm, 575 nm and 664 nm in the emission spectrum. The transitions corresponding to the peaks were labelled as ²⁰ $^6P_{3/2}$, ⁴ $^1I_{9/2}$, ⁶ $^1P_{7/2}$, ⁶ $^1P_{5/2}$, ⁴ $^1F_{7/2}$, ⁴ $^1G_{11/2}$ and ⁴ $^1I_{15/2}$ in the excitation region and ⁵ $^4F_{9/2} \rightarrow ^6H_{15/2}$ (Blue), ⁴ $^1F_{9/2} \rightarrow ^6H_{13/2}$ (yellow) and ⁴ $^1F_{9/2} \rightarrow ^6H_{11/2}$ (red) in the emission spectrum region [11,27]. In the current PL analysis, the blue emission transition (⁹ $^4F_{9/2} \rightarrow ^6H_{15/2}$) is magnetic-dipole (MD) in nature and the consecutive yellow emission transition ($^4F_{9/2} \rightarrow ^6H_{13/2}$) is electric-dipole (ED) ($\Delta L=2, \Delta J=2$) in nature [28,29].

The current research revealed that the magnetic dipole transition is unaffected by the atoms' local crystal environment in the as-prepared glass samples. The electric dipole transition is described as a hypersensitive emission, implying that its intensity is affected by the glass matrix's local surroundings. Furthermore, it was discovered that MD transitions dominate ED transitions in the current investigation, implying that Dy^{3+} ions are occupying high symmetry sites with an inversion center [30,31]. At 350 nm excitation wavelength, all the glass samples had a comparable profile of emission spectra, with no shift in emission bands (Fig. 22).

In addition, we can see in Fig. 22 that as we increase concentration of Dy^{3+} ions up to 1.0 mol percent, the emission intensity increases, then decrease. Quenching concentration via resonant energy transfer (RET) among Dy^{3+} ions can be read as this trend in intensity according to Dy^{3+} ions concentration, which also explains the energy level diagram's two cross-relaxation channels (CR1 and CR2). Fig. 23 depicts a schematic energy level diagram of as-prepared ZnAlNaPDy glasses and it describes energy transfer and types along possible cross-relaxation channels in the excitation and emission spectra, which is based on the down-conversion phenomenon because of the Dy^{3+} ions present in as-prepared ZnAlNaP glasses. As a result of the non-radiative transitions at the higher energy levels, the metastable state ($^4F_{9/2}$) becomes densely populated very quickly. As a result of the radiative transitions that occur from the metastable state, intense blue and yellow emission is produced.

To investigate the non-symmetric characteristics of network surrounding Dy^{3+} ions within host glass's matrix, intensity ratios of yellow to blue (Y/B) have been evaluated for each Dy^{3+} ions doped ZnAlNaP glass sample. Table 8 shows the Y/B value calculated for each glass sample. The effect of Dy^{3+} ions on the local environment of the ZnAlNaP glass matrix, and therefore on the intensity of the hypersensitive ($^4F_{9/2} \rightarrow ^6H_{13/2}$) transition, could explain the change in Y/B ratios. The Y/B ratio values decrease as the concentration of Dy^{3+} ions increase, as shown in the inset of Fig. 22. In addition, the Y/B ratio values for the prepared ZnAlNaP glass series is closer to 2, indicating that the bonds between Dy^{3+} and O^{2-} ions have a high covalence nature. These visible emission Y/B ratio data indicate that as-prepared Dy^{3+} doped ZnAlNaP glasses are capable of generating white light [32,33]. The Y/B ratios computed in the present work have been compared

with some other reported studies [42, 34-36] and it was found that for the as-prepared glasses Y/B ratio is relatively high, shown in Table 6.

4.5. PL decay analysis

The PL decay curves for the ${}^4F_{9/2} \rightarrow {}^6H_{13/2}$ transition observed for the as-prepared Dy^{3+} ions activated ZnAlNaP glasses at $\lambda_{ex} = 350$ nm, are shown in Fig. 24. It can be seen that all the decay curves have a single exponential fit and the normalized experimental decay curves have been fitted using the formula:

$$y = y_0 + A e^{-t/\tau_{exp}} \quad (16)$$

Here, 'y' and 'y₀' represent the intensities at time 't' and $t = 0$ respectively, A and τ_{exp} are the amplitude and experimental decay time of the spectra. The exponentially decaying curves could be due to the fast decay of the excited Dy^{3+} ions. Another possible reason for the single exponential nature of the decay curves could be the lesser effect of ligands on Dy^{3+} ions in the glass matrix [37]. The measured decay lifetimes for ZnAlNaPDy glasses as depicted in Table 8. It can be perceived that experimental decay time values are decreasing with increasing Dy^{3+} ions concentration.

As we increase concentration of Dy^{3+} ions in the host glass matrix, number of Dy^{3+} ions reaching the metastable state will increase, and this automatically decreases the distance of separation between them. The distance of separation between the Dy ions reached to an optimum value leads to energy migration among the Dy ions through cross-relaxation mechanism leading to a decrease in the experimental lifetime (τ_{exp}) [20]. The τ_{exp} values measured for the titled glasses are compared with the corresponding values for other glasses in Table 7 [42,34,35,38]. As per the data appearing in Table 7, it can be seen that τ_{exp} values of the ZnAlNaP glasses are somewhat relatively higher than the other values reported for other glasses.

4.6. Colorimetric analysis

The CIE chromaticity coordinates were computed from the PL emission spectra to observe the emission color of the as-prepared ZnAlNaPDy glass series. The following equations can be used to calculate CIE-coordinates (x , y) using tristimulus X , Y and Z values.

$$x = \frac{X}{X+Y+Z} \quad (17)$$

$$y = \frac{Y}{X+Y+Z} \quad (18)$$

The Correlated Color Temperature (CCT) values of the samples were also calculated using the following formula [39]:

$$CCT = -449n^3 + 3525n^2 - 6823.2n + 5520.3 \quad (19)$$

where $n = \frac{x-x_e}{y-y_e}$ with $x_e = 0.332$ and $y_e = 0.186$, which are the coordinates of the epicenter of the CIE 1931 diagram [40]. The chromaticity coordinates values and their respective CCT values are represented in Table 8. The CCT values of ZnAlNaPDy1.5 were reported to be in the cool white region as shown in Fig. 25. The values of the CIE chromaticity coordinate of the present work have been compared with some other reported studies [34-36] and are listed in Table 6. As a result of the foregoing discussion, it can be concluded that the Dy³⁺ ions doped ZnAlNaP glasses are the optimum choice for the production of white light under n-UV excitation.

4.7. Temperature-dependent PL (TD-PL) studies and activation-energy estimation

To investigate the thermal profile of the as-prepared ZnAlNaP glass samples, the optimized glass of the present series i.e., ZnAlNaPDy1.0 glass was taken under consideration and the temperature-dependent PL spectrum was recorded using FLMS15147 spectrometer with 350 nm excitation within the temperature range of 30°C (Room temperature) to 200°C. With increasing temperature, the PL emission intensity was observed to be decreasing for ZnAlNaPDy1.0 glass as shown in Fig. 26. The inset of Fig. 26 depicts variation of normalized intensity of ⁴F_{9/2} → ⁶H_{13/2} transition within the temperature range of 298-473 K by considering the intensity as 100% at 30°C. At 200°C, the emission intensity was 74.4 %, which decreased by 25.6 % only. The 74.4 % retention of the PL

emission intensity at 200 °C signifies the thermal stability of as-prepared ZnAlNaP glasses doped with different Dy³⁺ ions concentration.

In addition, the activation energy (ΔE) of the glass sample was estimated using the Arrhenius equation, which describes the relationship between temperature and emission intensity [41]:

$$I_T = \frac{I_o}{1 + C \exp\left(-\frac{\Delta E}{K_B T}\right)} \quad (20)$$

Where I_o and I_T are the emission intensities at room temperature and other temperatures in Kelvin respectively, C and K_B (8.617×10^{-5} eV/K) denotes the arbitrary constant and the Boltzmann constant, respectively. The slope of the linearly fitted graph plotted for $\ln((I_o/I_T)-1)$ versus $1/K_B T$, shown in Fig. 27, gives the desired value of the system's activation energy (ΔE). The estimated activation energy for ZnAlNaP glass doped with 1 mol% of Dy³⁺ ions was 0.212 eV which shows the good temperature stability of as-prepared Dy³⁺ doped AZNP glasses.

Chapter 5: Summary & Future Scope

Summary

To conclude, ZnAlNaP³⁰ glasses doped with different Dy³⁺ ions concentrations were made using melt-quench process and investigated using XRD, FT-IR, Raman, DSC-TGA, absorption, PL excitation & emission, and TDPL analysis in the current study. The measured XRD spectrum validated the ZnAlNaPDy glasses' non-crystalline phase. The⁴² presence of distinct functional groups was confirmed by the FT-IR spectrum produced for the un-doped ZnAlNaP glass. Different vibrational modes can be seen in the Raman spectra of ZnAlNaPDy1.0 glass.

The thermal stability and total loss in weight of the host glass are revealed by DSC and TGA analysis, respectively. The total mass loss for an un-doped ZnAlNaP glass was determined to be 15.35 %, confirming its stability at relatively high temperatures. The optical band gap energy was calculated using absorption spectrum characteristics recorded for the as-prepared glasses and the Tauc plot. The PL emission were detected for the titled glasses (under 350 nm excitation), with two enhanced peaks⁵ in the blue and yellow regions at 484 and 573 nm, respectively. Due to RET amid Dy³⁺ ions, concentration quenching for the ZnAlNaP glasses is found to be at 1 mol % of Dy³⁺ ions. As the¹ concentration of Dy³⁺ ions increase, the experimental lifetime values for as-prepared ZnAlNaP glasses measured from decay profiles pertaining to the³⁸ $^4F_{9/2} \rightarrow ^6H_{13/2}$ transition at $\lambda_{ex} = 350$ nm excitation decrease, which could be ascribed to cross-relaxation processes taking place amongst the trivalent dysprosium ions.

The CIE chromaticity coordinates and CCT values reported for ZnAlNaP glasses represent the emission of the cold white light region. The thermal behavior of ZnAlNaPDy glasses revealed by TD-PL analysis shows that at 200 °C, the aforementioned glasses retain 74.4 % of the PL emission intensity, suggesting that the ZnAlNaPDy glasses are thermally stable. The as-prepared Dy³⁺ ions doped ZnAlNaP glasses can exhibit luminescence that can be used to produce white light, implying that they are appropriate for developing w-LEDs based on the aforementioned results.

Future Scope

- RE doped glasses play a vital role in manufacturing optical devices like optical fibres amplifiers and have also found great utilizations in lasers, pharmaceuticals, photovoltaic

devices, telecommunications,² and civil military applications like as IR detectors, IR fairings, nuclear imaging and surveillance.

- The above-mentioned applications of RE doped glasses are possible only if it is chemically & thermally stable, has relatively minimal phonon energies, better RE ion solubility and excellent transparency. The structure and ligand field environment of the host glass affects the bandwidths of² emission transitions and decides the luminescence adequacy of a doped RE ion. Thus, it is quite important to choose a host material with relatively lower phonon energies [1]. We will try to alter the host glass composition of the titled glasses with suitable elements and try to attain glasses having relatively less phonon energies than the titled glasses and study their PL characteristics.
- Quite recently it was observed that, the PL efficiency of the glasses doped with certain rare earth/transition metal ions can be enhanced by converting them in to glassy ceramics. We have the plans to convert the glasses investigated in the present dissertation work⁴ into glassy ceramics by heat treating them at an appropriate temperature and time. The glasses heat treated for longer durations converts them in to glassy ceramics by producing micro/nano crystals due to nucleation process. Such nano/micro crystals produced due to nucleation process in fact converts glasses into a glassy ceramics and helps in enhancing the PL characteristics of the host glass.

*****THE END*****

● **9% Overall Similarity**

Top sources found in the following databases:

- 4% Internet database
- Crossref database
- 5% Submitted Works database
- 5% Publications database
- Crossref Posted Content database

TOP SOURCES

The sources with the highest number of matches within the submission. Overlapping sources will not be displayed.

1	IIT Delhi on 2019-02-18 Submitted works	<1%
2	Rajat Bajaj, A.S. Rao, G. Vijaya Prakash. "Photoluminescence down-shi... Crossref	<1%
3	slideshare.net Internet	<1%
4	Delhi Technological University on 2019-01-31 Submitted works	<1%
5	iopscience.iop.org Internet	<1%
6	University of Abertay Dundee on 2021-12-13 Submitted works	<1%
7	enzolifesciences.com Internet	<1%
8	Mohd. Shkir, I.S. Yahia, S. AlFaify, M.M. Abutalib, Shabbir Muhammad. ... Crossref	<1%

9	Tian, Bining, Baojiu Chen, Yue Tian, Jiashi Sun, Xiangping Li, Jinsu Zha...	<1%
	Crossref	
10	Universiti Teknologi Malaysia on 2018-07-13	<1%
	Submitted works	
11	Universiti Teknologi Malaysia on 2017-01-29	<1%
	Submitted works	
12	University of Newcastle on 2019-11-11	<1%
	Submitted works	
13	Delhi Technological University on 2019-03-20	<1%
	Submitted works	
14	14impressions.in	<1%
	Internet	
15	osapublishing.org	<1%
	Internet	
16	pure.ed.ac.uk	<1%
	Internet	
17	rsc.org	<1%
	Internet	
18	K. Brahmachary, D. Rajesh, Y.C. Ratnakaram. "Luminescence propertie...	<1%
	Crossref	
19	L. Shamshad, N. Ali, Ataullah, J. Kaewkhao, G. Rooh, T. Ahmad, F. Zam...	<1%
	Crossref	
20	Yijia Liu, Gengxin Zhang, Junben Huang, Xiaoma Tao, Guihua Li, Gemei...	<1%
	Crossref	

- 21

Himamaheswara Rao V., Syam Prasad P., Mohan Babu M., Venkatesw...

Crossref

<1%
- 22

Trilok K. Pathak, Bennie Viljoen, Hendrik C. Swart, R. Edward Kroon. " L...

Crossref

<1%
- 23

mdpi.com

Internet

<1%
- 24

IIT Delhi on 2019-04-22

Submitted works

<1%
- 25

K. Siva Rama Krishna Reddy, K. Swapna, Sk. Mahamuda, M. Venkatesw...

Crossref

<1%
- 26

Rakshit Jain, Rachna Sinha, Mukesh K. Sahu, M. Jayasimhadri. "Synthe...

Crossref

<1%
- 27

Universiti Putra Malaysia on 2017-03-18

Submitted works

<1%
- 28

Yulei Zhao, Yihui Zhong, Huan Chang, Weizhen Liu, Zongliang Xiao, Yo...

Crossref

<1%
- 29

Masdar Institute of Science and Technology on 2018-07-23

Submitted works

<1%
- 30

P. Rekha Rani, M. Venkateswarlu, Sk Mahamuda, K. Swapna, Nisha De...

Crossref

<1%
- 31

University of Sheffield on 2015-06-29

Submitted works

<1%
- 32

Vijayakumar, R., G. Venkataiah, and K. Marimuthu. "Structural and lumi...

Crossref

<1%

33	aip.scitation.org	Internet	<1%
34	baadalsg.inflibnet.ac.in	Internet	<1%
35	eprints.utm.my	Internet	<1%
36	science.gov	Internet	<1%
37	C.R. Kesavulu, C.K. Jayasankar. "White light emission in Dy3+-doped le...	Crossref	<1%
38	G. Annadurai, S. Masilla Moses Kennedy, V. Sivakumar. " Synthesis of ...	Crossref	<1%
39	N. Jaidass, C. Krishna Moorthi, A. Mohan Babu, M. Reddi Babu. "Lumin...	Crossref	<1%
40	P. Sailaja, Sk. Mahamuda, Rupesh A. Talewar, K. Swapna, A.S. Rao. "Sp...	Crossref	<1%
41	Universiti Teknologi Malaysia on 2018-06-28	Submitted works	<1%
42	m.scirp.org	Internet	<1%

New Submission	Submission 7626	ICAPIE-2022	Conference	News	EasyChair
----------------	-----------------	-------------	------------	------	-----------

ICAPIE-2022 Submission 7626


If you want to **change any information** about your paper, use links in the upper right corner.

For all questions related to processing your submission you should contact the conference organizers. [Click here to see information about this conference.](#)

All **reviews sent to you** can be found at the bottom of this page.

[Update information](#)[Update authors](#)[Update file](#)[Withdraw](#)

Submission 7626

Title	Spectroscopic characterization of Dy ³⁺ ions doped phosphate glasses for epoxy-free white LED applications
Paper:	 (May 07, 16:50 GMT)
Author keywords	Phosphate Glasses Dysprosium Ions XRD Photoluminescence CIE Coordinates
Abstract	The present work illustrates a detailed spectroscopic analysis carried out on dysprosium ions doped Zinc Alumino Sodium Phosphate (ZnAlNaP) glasses with a chemical composition of (10-x) ZnO-20Al ₂ O ₃ -10Na ₂ O-60P ₂ O ₅ - xDy ₂ O ₃ (x = 0.1 to 2.0 mol%). The XRD spectrum recorded for an un-doped ZnAlNaP glass demonstrates a broad hump confirming its non-crystalline nature. To understand the applicability of the titled glasses for epoxy-free solid-state lighting devices, photoluminescence (excitation, emission, and decay) spectra were recorded and analysed. The PL emission recorded under 350 nm excitation show two significant bands, 4F _{9/2} → 6H _{15/2} (blue) and 4F _{9/2} → 6H _{13/2} (yellow) at 484 nm and 573 nm respectively. Temperature-dependent photoluminescence studies conducted on 1.0 mol % of the Dy ³⁺ ions in ZnAlNaP glasses revealed activation energy of 0.212 eV with a percentage of loss 25.6 % in PL intensity. The CIE-chromaticity coordinates and color correlated temperature (CCT) were evaluated from the photoluminescence spectral characteristics. All the spectroscopic investigations conducted on the titled glasses finally reveal the superior nature of the titled glasses for their usage in fabricating epoxy-free white light-emitting diodes and other related optoelectronic devices.
Submitted	May 07, 16:50 GMT
Last update	May 07, 16:50 GMT

Authors

first name	last name	email	country	affiliation	Web page	corresponding?
Vidhi	Kundu	vidhikundu9@gmail.com	India	Delhi Technological University	http://dtu.ac.in/	
Ankita	Wadhwa	ankitawadhwa70@gmail.com	India	Delhi Technological University	http://dtu.ac.in/	
Rao	A.S.	drsallam@gmail.com	India	Delhi Technological University	http://dtu.ac.in/	✓



PAYMENT RECEIPT

Paid Successfully

₹9,000 

Rupees Nine Thousand Only

 TECHNOSCIENCE

To: Razorpay

UPI ID: razorpay@icici



From: ANKITA WADHWA

Punjab National Bank



UPI Ref No: 213041082347

05:39 PM, 10 May 2022



100% SECURE PAYMENTS

TECHNOSCIENCE

ICAPIE-2022

Program Name

Seventh International Conference on Advanced Production and Industrial Engineering (ICAPIE) - 2022)

Conference Dates:

June 11-12, 2022

Name of the organizer

CAPIER, Delhi Technological University, Delhi in association with National Institute of Technology, Delhi

Contact Us:

✉ icapie.dtu@gmail.com



Terms & Conditions:

You agree to share information entered on this page with TECHNOSCIENCE (owner of this page) and Razorpay, adhering to applicable laws.



Powered by Razorpay



₹ 9000.00

Payment Successful!

Share Your Experience

Payment ID: pay_JTWGR3dMNaV51A
A confirmation email has been sent to you



Vidhi Kundu <vidhikundu9@gmail.com>

Acceptance for Paper ID - 7626 for ICAPIE 2022

2K20CH66 tanishqraj
<tanishqraj_pe20b16_22@dtu.ac.in>
To: vidhikundu9@gmail.com
Cc: icapie.dtu@gmail.com

Tue, May 10, 2022 at 10:23
PM

Dear author (s),

Thank you for your submission to ICAPIE-2022.

Please find attached the certificate that your paper is accepted for consideration for publication in Advances in Transdisciplinary Engineering (ATDE)/ International Journal of Electrical and Electronics Research (IJEER).

Kindly note that paper presentation during the conference, ICAPIE-2022 is a mandatory requirement for further processing pertaining to publication and the decision of the publisher will be final. Certificate of paper presentation will be issued after presentation in the conference.

Regards



certificate 7626.jpg
341K



CERTIFICATE

Dear Authors,

Authors: Vidhi Kundu, Ankita Wadhwa and Rao A.S.

Paper ID: PAPER ID- 7626

Paper Title: Spectroscopic characterization of Dy³⁺ ions doped phosphate glasses for epoxy-free white LED applications

This is to enlighten you that the aforementioned paper is accepted for consideration for publication in **Advances in Transdisciplinary Engineering (ATDE), a Scopus Indexed Publication of IOS Press/ International Journal of Electrical and Electronics Research (IJEER)**, a Scopus Indexed journal, subjected to presentation **during 7th International Conference on Advanced Production and Industrial Engineering ICAPIE'22** scheduled to be organized during **June 11-12, 2022**.

The team of CAPIER and ICAPIE'22 would like to congratulate you on your achievements.

A handwritten signature in black ink, appearing to be "R. Singari".

Prof Ranganath M Singari

Chair Person, ICAPIE'22

HoD, Department of Design,

Delhi Technological University, Delhi

Advances in Transdisciplinary Engineering

ISSN print 2352-751X

ISSN online 2352-7528

Subjects [Engineering](#)



[SIGN UP FOR NEWS](#)

[View Recent Titles](#)

[Aims and Scope](#)

[Book Series Editors](#)

Aims and Scope

Advances in Transdisciplinary Engineering (ATDE) is a peer-reviewed book series covering the developments in the key application areas in product quality, production efficiency and overall customer satisfaction.

ATDE will focus on theoretical, experimental and case history-based research, and its application in engineering practice.

The series will include proceedings and edited volumes of interest to researchers in academia, as well as professional engineers working in industry.

Abstracting/Indexing



Books from this Series

